CHEMICAL REVIEWS

Review

pubs.acs.org/CR

Optical Super-Resolution Imaging of Surface Reactions

Tao Chen,[†,‡] Bin Dong,[§] Kuangcai Chen,[§] Fei Zhao,[§] Xiaodong Cheng,[§] Changbei Ma,[∥] Seungah Lee,[⊥] Peng Zhang,[⊥] Seong Ho Kang,[*,⊥] Ji Won Ha,[*,#] Weilin Xu,[*,†] and Ning Fang[*,§]

[†]State Key Laboratory of Electroanalytical Chemistry and Jilin Province Key Laboratory of Low Carbon Chemical Power, Changchun Institute of Applied Chemistry, Chinese Academy of Science, 5625 Renmin Street, Changchun 130022, P.R. China

[‡]University of Chinese Academy of Science, Beijing, 100049, P. R. China

[§]Department of Chemistry, Georgia State University, Atlanta, Georgia 30303, United States

[∥]State Key Laboratory of Medical Genetics & School of Life Sciences, Central South University, Changsha 410013, China

[⊥]Department of Applied Chemistry and Institute of Natural Sciences, Kyung Hee University, Yongin-si, Gyeonggi-do 17104, Republic of Korea

[#]Department of Chemistry, University of Ulsan, 93 Dahak-Ro, Nam-Gu, Ulsan 44610, Republic of Korea

ABSTRACT: Optical super-resolution imaging has gained momentum in investigations of heterogeneous and homogeneous chemical reactions at the single-molecule level. Thanks to its exceptional spatial resolution and ability to monitor dynamic systems, much detailed information on single-molecule reaction/adsorption processes and single-particle catalytic processes has been revealed, including chemical kinetics and reaction dynamics; active-site distributions on single-particle surfaces; and size-, shape-, and facet-dependent catalytic activities of individual nanocatalysts. In this review, we provide an overview of recent advances in super-resolution chemical imaging of surface reactions.

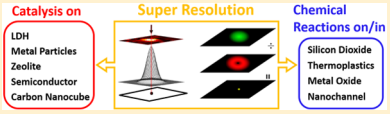

CONTENTS

1. INTRODUCTION

The 2014 Nobel Prize in Chemistry was awarded to Eric Betzig, Stefan W. Hell, and William E. Moerner for their contributions to the development of optical super-resolution microscopy. As a powerful tool for visualization, super-resolution optical microscopy has quickly seen a wide range of applications in biology. On the other hand, it was also discovered that this technique can be applied perfectly for the purpose of studying chemical systems,

Special Issue: Super-Resolution and Single-Molecule Imaging

Received: October 3, 2016

DOI: 10.1021/acs.chemrev.6b00673
Chem. Rev. XXXX, XXX, XXX−XXX

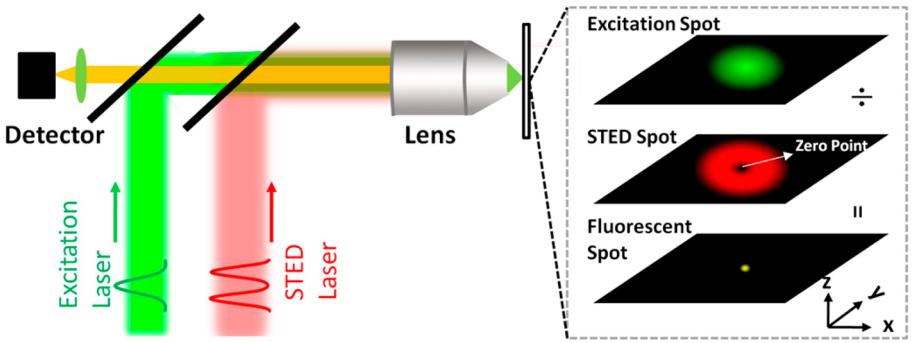

Figure 1. Principles of STED microscopy.

among which surface reactions on nanomaterials have emerged as perhaps the most prominent example of how the improved spatial resolution has led to new exploration and understanding of uncharted territories. In this review, we summarize these recent technical developments and applications.

Surface reactions on nanomaterials are important for many modern industrial processes because of the large variety of surface transformations involved, including (de)hydrogenation, redox, carbon-based bond coupling, and cleavage reactions.[1−8] Tremendous work had been done with traditional ensemble methods.[9−11] However, because of the inherent heterogeneity among nanoparticles in size, shape, morphology, surface composition, and so on, it is challenging to determine the precise structure−reactivity relationship from such ensemble measurements. For a deeper and more precise understanding of structure−reactivity relationships, it is highly desirable to study surface reactions in situ at the single-molecule/single-particle level in real time with sufficiently high spatiotemporal resolution. The newly developed optical super-resolution imaging techniques have proved to be highly effective for this goal.[12−17]

2. PRINCIPLES OF OPTICAL SUPER-RESOLUTION IMAGING

Because of the diffraction of light, the light rays from a single point source cannot be converged to an infinitely small point on the image plane by the lens systems of conventional optical microscopy systems. Instead, a blurred image with a relatively large contour is obtained. The three-dimensional (3D) intensity profile of the focused spot from a point source is called the point spread function (PSF). The spatial resolution of an optical microscopy technique, defined by the full width at half-maximum (fwhm) of the PSF, can be expressed approximately as $d_{xy} \approx 0.61\lambda/\mathrm{NA}$ in the lateral directions, where λ is the wavelength of the light and NA as the numerical aperture of the objective lens. When imaged under visible light, an imaging system's spatial resolution is typically ∼200 nm.[18]

The spatial resolution in conventional optical microscopy becomes an obstacle for studying nanoscale objects with structural features smaller than the wavelength of light. To break this diffraction limit of light, a variety of optical high-resolution techniques have been developed.[19−24] For instance, as one of the earliest approaches, near-field scanning optical microscopy (NSOM) can achieve a spatial resolution of 20−50 nm by placing the excitation light source (an optical fiber or a metal tip) very close to the sample.[19] However, the requirement of physical proximity to the sample restricts the application of NSOM. On the other hand, far-field techniques that do not require physical proximity have also been developed to increase the spatial resolution, such as confocal microscopy,[20] which employs a focused laser beam for excitation and a pinhole for detection; multiphoton microscopy,[21] which reduces the size of the effective excitation PSF; 4Pi and I^{5}M microscopies,[22,23] which increase the NA by using two opposing objective lenses; and structured illumination microscopy (SIM),[24] which applies a patterned illumination field. These far-field techniques can achieve a resolution of ∼100 nm. Although this represents a significant improvement, the diffraction of light still fundamentally limits the resolution of these methods.[25] To truly overcome this physical barrier, other techniques have been developed[26−34] and immediately attracted attention from various fields in both biology and nanoscience. Many reviews have discussed these techniques in detail.[25,35−40] However, not all of these techniques are equally effective for studying surface reactivity on nanomaterials, so in this review, we will mainly discuss the techniques that have proven to be useful in this field.

2.1. Super-Resolution Imaging with Spatially Patterned Excitation

Special excitation patterns are employed in this type of method to overcome the diffraction limit of light. In stimulated emission depletion (STED) microscopy,[26,41] two lasers are used for different purposes (Figure 1): One, with a Gaussian intensity profile, is used for fluorescence excitation, and the other (called the STED laser), with a doughnut-shaped intensity profile, is used for the suppression of the fluorescence signals from fluorophores located off the excitation center (or in the "depletion donut") by the mechanism of stimulated emission. This results in a tiny, subdiffraction-limited fluorescence spot around the focal point. It is clear that the decrease in spatial extent of the effective spot or PSF in a STED microscope is associated with a fundamental increase of the passband of the effective transfer function of the microscope. This was the first method to provide conceptually unlimited spatial resolution. Ground-state depletion (GSD) microscopy,[27] an implementation of reversible saturable optical fluorescence transitions (RESOLFT) microscopy,[28] follows a similar strategy of using a depletion laser to suppress the fluorophores located off the excitation center. Similarly, based on the concept of utilizing saturable processes, saturated structured illumination microscopy (SSIM) can achieve a lateral resolution of tens of nanometers.[42] These super-resolution imaging methods with scanning have been used extensively for imaging stained samples, but have rarely been used for surface catalysis because of their scanning-induced low efficiency of data collection.

DOI: 10.1021/acs.chemrev.6b00673
Chem. Rev. XXXX, XXX, XXX−XXX

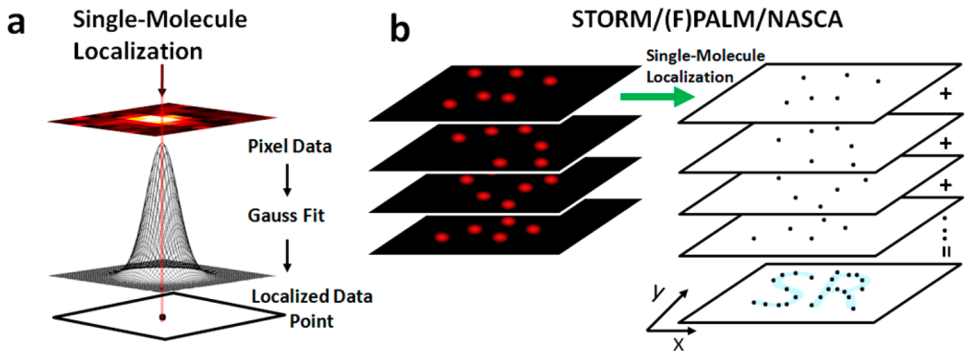

Figure 2. Principles of super-resolution fluorescence localization microscopy imaging.

2.2. Super-Resolution Imaging Based on Single-Molecule Localization

The spatial location of an emitter, such as a single fluorescent protein, fluorescent nanoparticle, or any other tiny diffraction-limited emitter, can be precisely determined with nanometer precision by fitting the fluorescence intensity profile with a PSF [usually approximated as a two-dimensional (2D) Gaussian function] (Figure 2a).[43,44] The precision with which the emitter's position can be found is mainly dependent on the number of collected photons.

Locating isolated individual fluorophores can easily be done by PSF fitting; however, when imaging a high-density fluorescently labeled sample, resolving the crowded fluorophores individually becomes difficult because of the overlap of the fluorescence PSFs from multiple fluorophores. To overcome this limitation, a new strategy was implemented that uses photoswitchable fluorophores that can undergo transitions between a dark state and a fluorescent state. In this way, at a given moment, only a very small fraction of the fluorophores can be excited to fluoresce, so that the precise location of these discrete probes can be determined by PSF fitting. Based on a captured time sequence of fluorescence images, the positions of a sufficiently large number of activated fluorophores can be determined precisely to reconstruct the image of a sample with super-resolution (Figure 2b). Three groups independently developed this super-resolution localization microscopy with different fluorescent probes. These methods are named stochastic optical reconstruction microscopy (STORM),[29] photoactivated localization microscopy (PALM),[30] and fluorescence photoactivation localization microscopy (FPALM).[31]

The stochastic switchable nature of fluorophores also enables other analysis methods for reconstructing super-resolution images, such as super-resolution optical fluctuation imaging (SOFI),[32] in which the autocorrelation and cross-correlation functions of the camera pixels in a time series can be calculated for a sample labeled with independently fluctuating fluorophores to result in an improved spatial resolution.

The overlapping of fluorescence signals on densely labeled samples does not usually arise in nanocatalysis systems when fluorogenic catalytic reactions occur successively with the formation of products one at a time. In such nanocatalysis systems, the locations where the individual fluorescent product molecules are observed can be precisely determined by fitting the intensity profile with the PSF and taken as the catalytic sites on the surface of the catalyst at different moments in time. By accumulating a large number of locations of product molecules, the catalytic active zones can be reconstructed with high precision. This super-resolution approach based on the localization of single product molecules has been used extensively in catalytic systems to map the active sites of different catalysts with sizes ranging from 100 nm to 50 μm. This method is called nanometer accuracy by stochastic catalytic reactions (NASCA) microscopy[45] and is recognized by many as the standard approach in super-resolution imaging studies of surface nanocatalysis.[12]

3. SUPER-RESOLUTION IMAGING OF SINGLE-PARTICLE CATALYSIS

Nanoscale and microscale catalysts for various chemical transformations[2−8] have been studied extensively.[1,2,11,46] The surface of a heterogeneous catalyst is one of the key factors determining its catalytic reactivity. However, despite more than 100 years of efforts to understand surface reactivity, the characterization of nano-/microscale catalytic reactivity remains highly challenging because of the ubiquitous heterogeneity among nanoparticles,[47] the dependence of catalytic activity on the surface atomic arrangement,[10,48−50] and the effects of structural dynamics (morphology changes and surface restructuring).[9,51−53] Various approaches have been implemented to address these challenges over the years, as surveyed in another review.[54] More recently, super-resolution imaging of catalytic events at the single-molecule/single-particle level has gathered considerable recognition as arguably the most direct and effective way to tackle these challenges.[12−14,16,17,55−64]

A crucial step is to design fluorogenic catalytic reactions, in which nonfluorescent or weakly fluorescent substrate molecules are catalyzed by a catalyst to produce highly fluorescent product molecules or the emission peaks of the fluorescent molecules shift after the catalytic transformation. The positions where individual product molecules form can be estimated with high accuracy and precision by super-resolution mapping, and they are usually assigned as the corresponding catalytic or reactive sites/regions on the surface of individual nanocatalysts. In this way, through the accumulation of a large number of turnover events, the activity maps can be reconstructed on the surface of individual nanocatalysts. Furthermore, if the reconstructed activity maps can be correlated with corresponding scanning electron microscopy (SEM) or transmission electron microscopy (TEM) images of the same nanocatalysts before and after the reaction processes, then information about the structure−reactivity relationship can be revealed more accurately at the single-particle level. Table 1 summarizes the fluorogenic catalytic reactions and catalysts reported in the literature. We discuss them in detail by classifying the catalysts into different types of surfaces on which the reactions occur.

DOI: 10.1021/acs.chemrev.6b00673
Chem. Rev. XXXX, XXX, XXX−XXX

Table 1. List of Fluorophores and Catalysts Used in Super-Resolution Imaging Studies of Catalytic Reactions

Substrate 1	Substrate 2	Product	Catalysts	Resolution (nm)	Reference
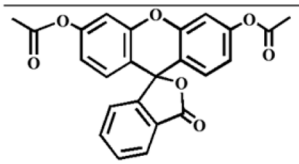	R'OH or H_2O	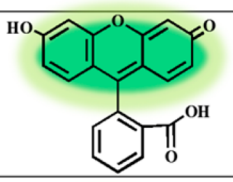	[Li^+-Al^{3+}] LDH	n/a	70
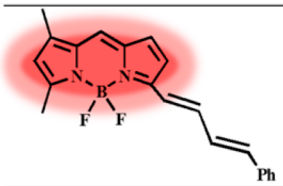	tert-butylhydroperoxide	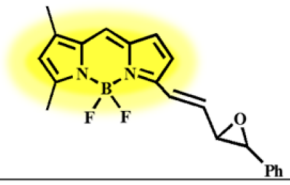	Ti-MCM-41	20	107
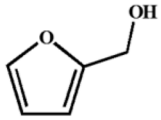	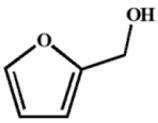	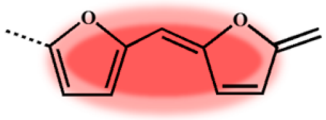	ZSM-22 ZSM-5 H-ZSM-5 ZSM-5/FCC Mordenite	10 10 ~17 n/a 10-50	45 45 111 110 108,109
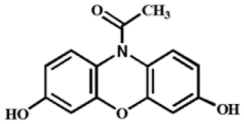	H_2O_2 H_2O_2 Photogenerated h^+ [a] Photogenerated h^+ [a] H_2O_2 H_2O_2	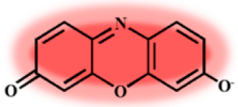	Au nanorod Sb-TiO_2 TiO_2 nanorod Au-CdS nanorod Au nanoparticle Pt nanoparticles	20-40	158,163 160 227,233 224 157 178
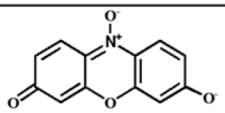	Photogenerated e^- NH_2OH HCl NH_2OH HCl Electron		TiO_2 nanorod Au nanoplate Au nanoparticle Carbon nanotube		227 159,160 157 248
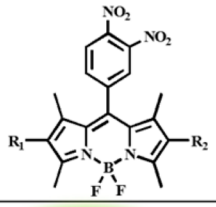	Photogenerated e^-	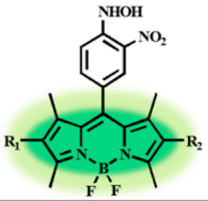	TiO_2 (R_1=R_2=H)	n/a	205
	Photogenerated e^-		Au-TiO_2 (R_1=R_2=SO_3Na)	~10	211
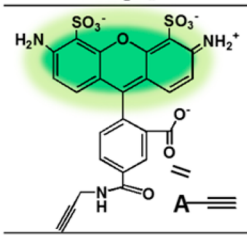	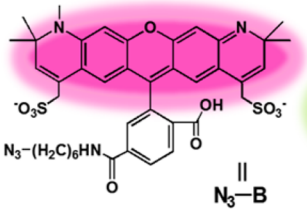	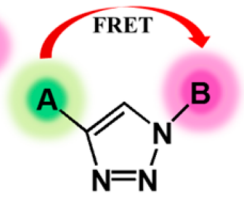	Cu/C	n/a	175
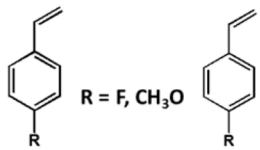	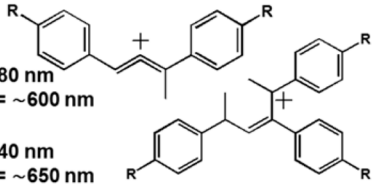	Product-1 λem (F) = ~580 nm λem (CH_3O) = ~600 nm Product-2 λem (F) = ~640 nm λem (CH_3O) = ~650 nm	H-ZSM-5	~20	112

[a]Amplex Red is oxidized by the $OH^•$ species, which is generated from the photogenerated hole (h^+) reacted with adsorbed H_2O/OH^- following an indirect mechanism.

3.1. Layered Double Hydroxides (LDHs)

Layered double hydroxides (LDHs) are versatile materials and are used widely in fundamental and applied studies.[65−69] Because of the large size and easily identifiable crystal faces of [Li^+−Al^{3+}] LDH crystals, crystal-face-induced differences in local catalytic activity were observed directly.[70] This LDH catalyst catalyzes the hydrolysis of nonfluorescent fluorescein ester to fluorescent fluorescein in aqueous solution or alcohol solvent. This process can be monitored on the basis of the strong luminescent properties of the product at the single-turnover level. By superlocalizing the individual turnover events, Roeffaers et al.[70] determined the distribution of the product molecules, and thus of the active sites, and they calculated the local catalytic rates simply by counting the numbers of turnovers. As shown in Figure 3, the

DOI: 10.1021/acs.chemrev.6b00673
Chem. Rev. XXXX, XXX, XXX−XXX

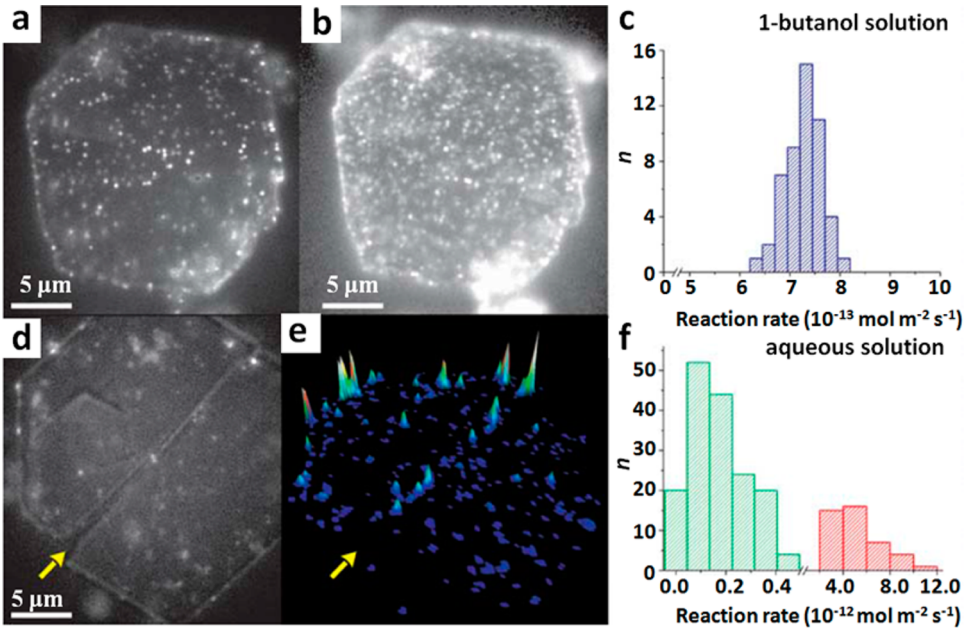

Figure 3. (a,b) Fluorescence wide-field images of a catalytic reaction in 1-butanol at ester concentrations of (a) 40 and (b) 700 nM. (c) Reaction rate distribution on a crystal face. (d) Fluorescence wide-field image in aqueous solution at a 600 nM ester concentration. (e) Reconstructed activity map of the crystal shown in panel d. (f) Reaction rate distributions on different faces of individual LDH crystals: red, (1010) faces; green, (0001) faces. Reprinted with permission from ref 70. Copyright 2006 Nature Publishing Group.

fluorescent product molecules were distributed homogeneously over the entire outer crystal surface in an alcohol solution at a formation rate proportional to the substrate concentration (Figure 3a,b), and no activity differences were observed between the basal plane and lateral faces (Figure 3c). By contrast, in aqueous solution, the fluorescent product molecules were mainly located at the lateral faces (Figure 3d,e), suggesting higher activities at these faces than on the basal plane (Figure 3f). Furthermore, the diffusion of the product molecules over the surface was also observed. All of the information acquired in this work is relevant to the rational design of high-efficiency industrial catalysts. It was expected by the authors that the developed technique will be able to provide deeper insight into heterogeneous nanocatalysis.[70] Indeed, since the original study, this approach has been widely used in the field of nanocatalysis.[55−57]

3.2. Zeolites

Zeolites are a class of solid acid materials with pores of molecular dimensions that are commonly used in the fields of petroleum refining, petrochemical industry, adsorbents, and ion exchange.[71] As catalysts, because of the their unique combination of acidic and shape-selective properties, zeolites have been widely used in fluid catalytic cracking (FCC), methanol-to-olefins, isomerization, and alkylation processes.[71−75] Because of this wide range of industrial applications, the pursuit of novel zeolites with desired framework structures has never stopped. However, the rational design of zeolitic materials is hampered by difficulties in tuning the number, distribution, and nature of acid sites. To address these issues, a deeper understanding of single zeolite particles is needed. Several excellent reviews have been published that summarize the studies of zeolites by various microscopic and spectroscopic characterization techniques.[16,47,57,76] Many studies of zeolites using fluorescence-based techniques but without the super-resolution capability have been reported, including molecular interactions in zeolite crystals,[77,78] mapping of mesoporous defects with the distribution of fluorescent dyes,[79−84] formation of emissive carbonaceous deposites,[85−90] chemical transformations inside individual catalytic particles,[91−105] and acidity distributions.[106]

3.2.1. Two-Dimensional Super-Resolution Imaging on Zeolites. Unlike other heterogeneous catalysts, on which the catalytic reactions occur at the outer surface of the catalysts, zeolites have 3D structures with complex nanoporous networks. Because of these complex structures, it is difficult to quantify intraparticle diffusion limitations in traditional ensemble experiments. By observing the catalytic transformation of a red fluorescent boron dipyrromethene (BODIPY) derivative to a yellow fluorescent product molecule within individual Ti-MCM-41 particles,[64,107] Roeffaers and co-workers monitored the product molecules selectively by NASCA microscopy with nanometer localization precision. The catalytic efficiencies in different parts of individual particles were revealed by the active-site distributions. Interestingly, it was found that the product molecules were formed only in the periphery (~300 nm, Figure 4, indicated by the green double-ended arrows) of the catalysts. Further calculations showed that only part of the volume (30−40%) of the catalyst was catalytically active for the reaction. In this way, the parameters of the Thiele modulus and effectiveness factor were determined at the single-particle level for the first time to allow the identification of the intraparticle diffusion limitations in heterogeneous catalysis.

On the other hand, for a nondiffusion-limited catalytic reaction where the substrate molecules are small enough to diffuse freely through the zeolites, active-site mapping can be achieved for the entire volume of the catalyst. Furfuryl alcohol is just such a small substrate molecule, whose oligomerization reaction catalyzed by zeolites can form highly fluorescent product. Figure 5 presents the typical mapping of turnover events on individual ZSM-22 zeolite particles with furfuryl alcohol as the substrate.[45] The width of the super-resolution images from precise localization of individual catalytic product molecules was close to the actual width of the needle-like ZSM-22 crystallites (100 nm). Similar

DOI: 10.1021/acs.chemrev.6b00673
Chem. Rev. XXXX, XXX, XXX−XXX

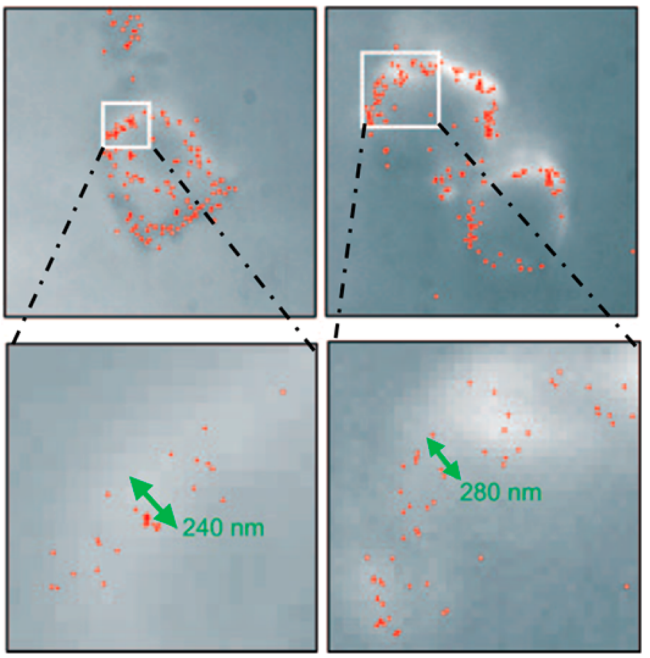

Figure 4. Typical individual turnover measurements on Ti-MCM-41 particles. Bottom: Enlargements of the parts of the images indicated in the top panel. Reprinted with permission from ref 107. Copyright 2010 Wiley-VCH.

experiments and analysis were also carried out on the larger-sized ZSM-5 crystals.[45] The heterogeneity of the catalytic activity on individual particles was clearly revealed (Figure 5c,d), attesting to the true power of super-resolution imaging in nanoscale reactivity mapping.

The same group later evaluated the effects of the dealumination of mordenite zeolites on the acid site distribution, reactivity, strength, and accessibility by combining stimulated Raman scattering (SRS) microscopy with NASCA microscopy (Figure 6).[108] The heterogeneous reactivities among different particles or even within individual crystals were confirmed by the sensitive and spatially resolved SRS imaging in combination with nitrile probes. In another follow-up study, the effects of the hierarchical porous structure (an extraframework structure of meso- and macropores over the inner molecular-sized micropores) of the dealuminated mordenite crystals were revealed by NASCA microscopy.[109] In contrast to the common belief that the extensive surface macroporosity could facilitate molecular transport and improve accessibility to the inner micropores and therefore enhance catalytic activity in the micropores, the super-resolution reaction map showed enhanced reactivity only in the narrow zones around meso- and macropores, suggesting that the substrate molecules could efficiently reach only the active sites in the micropores surrounding the extraframework structure. The desired distribution of the reactivity throughout the entire hierarchical porous zeolite did not actually occur.

3.2.2. Depth Profiling with Super-Resolution Imaging on Zeolites. For larger microparticles, fluorescent molecules on different focal planes can be located with superlocalization microscopy by adjusting the focal depths. Based on this concept, the fluid catalytic cracking (FCC) process on individual large spherical clay particles (50−100 μm in diameter) was studied with acidic zeolite (ZSM-5) embedded in the clay matrix to catalyze the oligomerization of furfuryl alcohol (Figure 7a).[110] In this work, NASCA microscopy and SOFI were combined to

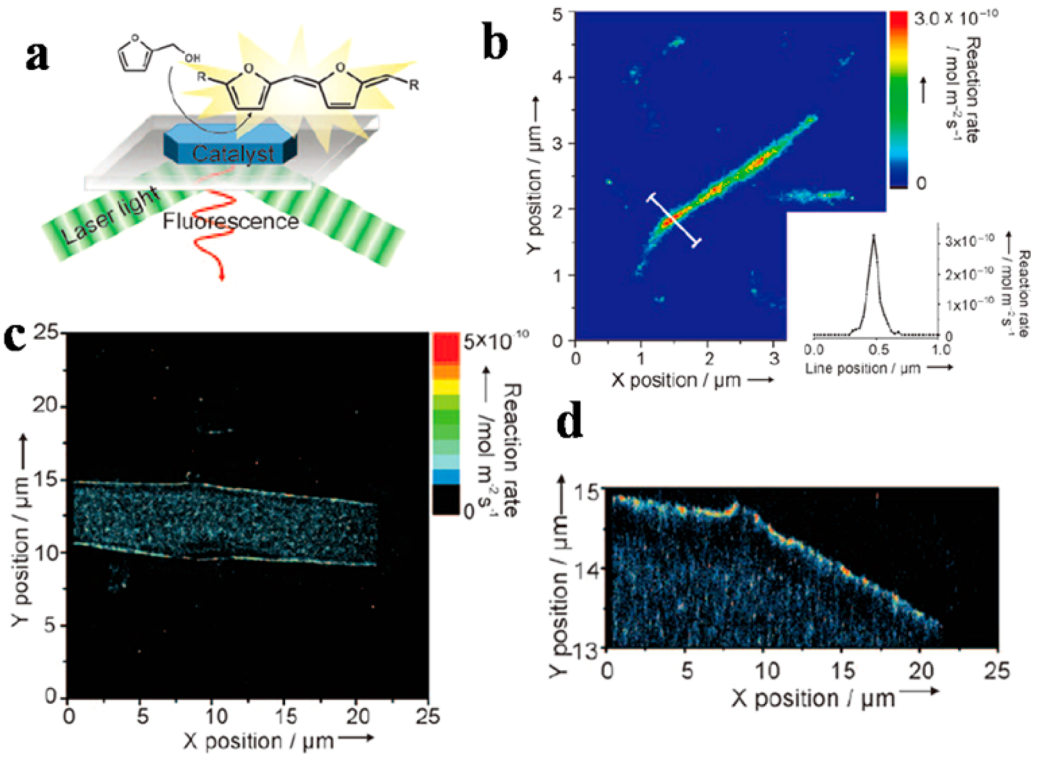

Figure 5. (a) Concept of NASCA microscopy. (b−d) Reaction maps of the oligomerization of furfuryl alcohol catalyzed by (b) ZSM-22 crystallites and (c,d) ZSM-5 crystals (panel d shows an enlargement of part of the image in panel c). The inset in panel b displays the local reaction rate along the white line. Reprinted with permission from ref 45. Copyright 2009 Wiley-VCH.

DOI: 10.1021/acs.chemrev.6b00673
Chem. Rev. XXXX, XXX, XXX−XXX

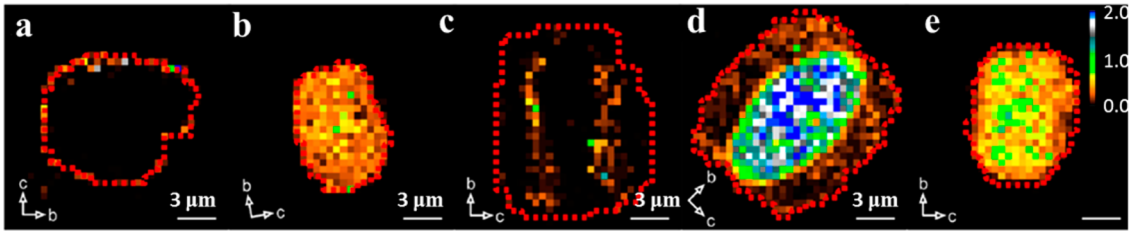

Figure 6. Furfuryl alcohol oligomerization reaction maps on mordenite zeolites. (a) Nondealuminated mordenite (SP-MOR) displayed catalytic activity only at the outer surface of the crystal. (b) Strongly dealuminated mordenite (SD-MOR) showed a rather homogeneous activity throughout the entire crystal volume. (c–e) More complex activity distributions were detected on mildly dealuminated mordenite (MD-MOR) at different stages of dealumination. Reprinted with permission from ref 108. Copyright 2014 American Chemical Society.

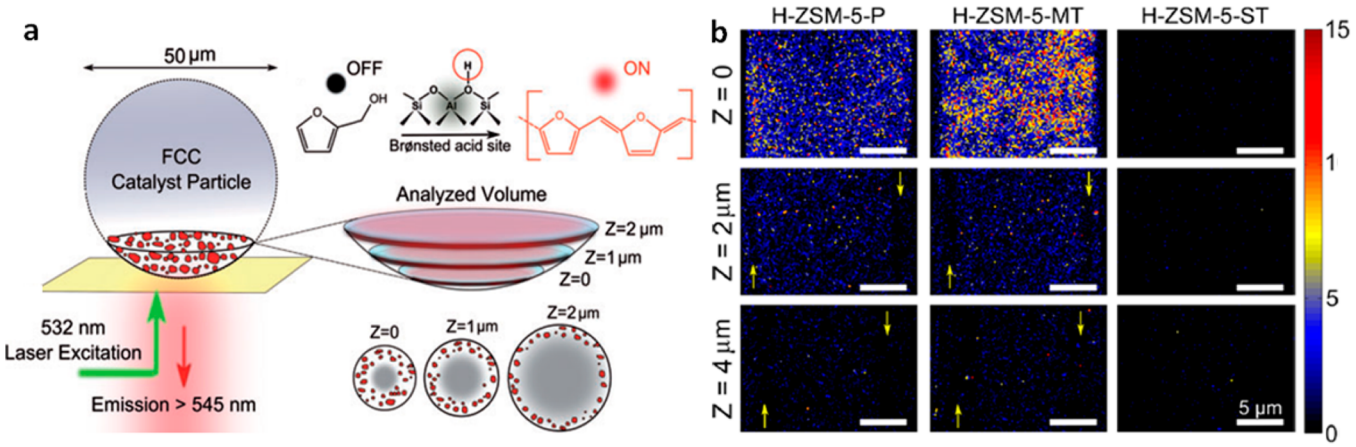

Figure 7. (a) Observation of the spatiotemporal gradients of reactivity on an FCC particle by wide-field fluorescence microscopy. Reprinted with permission from ref 110. Copyright 2015 Wiley-VCH. (b) Reactivity mapping of individual H-ZSM-5-P (parent zeolite), H-ZSM-5-MT (mild treatment), and H-ZSM-5-ST (strong treatment) crystals. Yellow arrows indicate the regions with lower reactivity due to a different crystallographic orientation of the subunits. Color bar: turnovers per 200 × 200 nm^2. Reprinted with permission from ref 111. Copyright 2015 American Chemical Society.

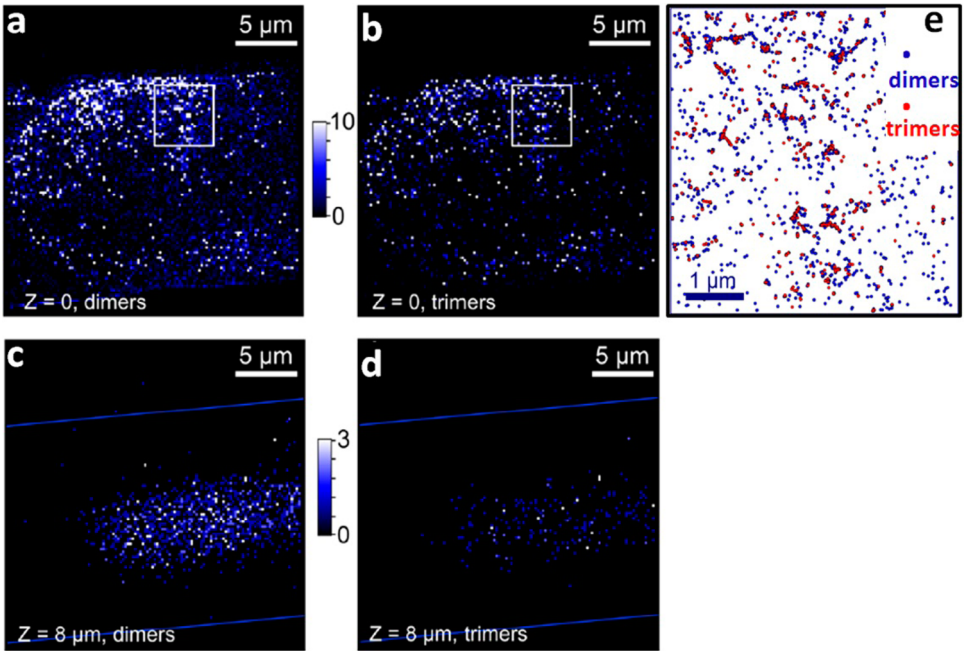

Figure 8. Super-resolution imaging of different products of the solvent-free oligomerization of 4-methoxystyrene on a zeolite H-ZSM-5 crystal. Accumulated maps of (a) dimeric and (b) trimeric products at (a,b) the outer surface of the crystal and of (c) dimeric and (d) trimeric products at (c,d) $Z = 8\ \mu m$. (e) Scatter plot of the dimeric (blue) and trimeric (red) species from the region indicated by white squares in panels a and b. Reprinted with permission from ref 112. Copyright 2016 American Chemical Society.

DOI: 10.1021/acs.chemrev.6b00673
Chem. Rev. XXXX, XXX, XXX–XXX

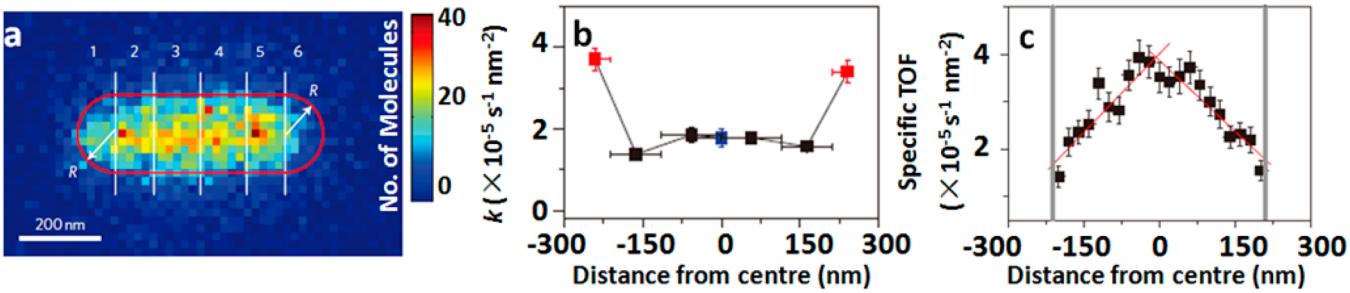

Figure 9. (a) Typical 2D distribution of product formed on a single Au nanorod. The red line indicates the outline of this rod based on the SEM image. (b) Specific catalytic rate constant (k) for each segment indicated in panel a. (c) Specific turnover frequency along the same nanorod. Reprinted with permission from ref 158. Copyright 2012 Nature Publishing Group.

reveal the 3D dispersion of submicrometer zeolite ZSM-5 domains. This experiment provided new insights into the dispersion and catalytic activity of zeolite ZSM-5 aggregates, including significant intraparticle heterogeneities in Brønsted reactivity, that were unattainable with the traditional confocal fluorescence microscopy approach.[76,98−104]

Another related study revealed the spatiotemporal gradients in the reactivity of zeolite H-ZSM-5 and quantified the effects of steaming post-treatments on the catalytic performance of individual crystals.[111] Figure 7b clearly illustrates the effects of steaming on reactivity at different focal depths. After mild steaming at 500 °C, the surface porosity of H-ZSM-5-MT was altered by dealumination and notably enhanced accessibility and reactivity; however, mild steaming also caused a highly heterogeneous distribution of accessible acid sites at the macroscopic level. Strong steaming at 700 °C led to a significant loss of Brønsted acidity and a 2-orders-of-magnitude-lower average turnover frequency on H-ZSM-5-ST. These results were further confirmed by the sputter depth profiling of Al in time-of-flight secondary-ion mass spectrometry (TOF-SIMS). It should be noted that this 3D imaging method with a large step size in the z direction is applicable only to large particles with sizes of micrometers.

Recently, the 3D imaging technique was also used to study the proton-transfer process of the fluorogenic oligomerization of styrene derivatives catalyzed by Brønsted acid sites on single zeolite H-ZSM-5 crystals.[112] Through a comparison of the survival times of fluorescent products formed at the surface (Z = 0) and in the middle (Z = 8 μm) of the parent zeolite crystal, the dimeric species (survival time of <0.7 s) and trimeric species (survival time of >0.7 s) could be distinguished and resolved spatially (Figure 8). The dimeric species were located both at the surface and in the middle of the zeolite crystals (Figure 8a,c), whereas the trimeric species were predominantly formed close to the outer surface (Figure 8b,d). The super-resolution map (Figure 8e) shows that the trimeric species appeared in agglomerates and in close proximity to each other, whereas the dimeric species distributed more evenly. This difference in distributions indicates that the accessibility of the Brønsted acid sites can largely determine the local reaction rates and product selectivity. Furthermore, the effects of solvent polarity and para substituent on the oligomerization reaction on zeolite H-ZSM-5 crystals were also studied. This study established an approach to investigating the effects of the host (microstructure of zeolite) and guest (solvent and substitute) on the reactivity of zeolite crystals.

3.3. Metal Nanoparticles

It is well-known that metal nanoparticles can catalyze many important chemical processes in industry.[2] Their catalytic activity is largely determined by their surface structures, which are mainly governed by their size, shape, composition, porosity (hollow vs solid), and supports.[10,48,49,113−115] Advances in surface science have led to a large amount of knowledge about the catalytic sites for a wide range of chemical reactions.[6,9,116−122] Measurements at the single-particle level are especially notable and include techniques such as electron and X-ray microscopy,[123−126] scanning probe microscopy,[126,127] and surface plasmon resonance microscopy and spectroscopy,[128−131] as well as the detection of the collision-induced transient currents on microelectrodes[132−136] and the use of single particles as electrodes.[137−140] Single-molecule fluorescence microscopy has also been employed extensively to study metal nanocatalysis to reveal surface catalytic properties,[141−148] size-dependent effects,[149,150] electro-induced deactivation,[151] activities of different type of surface atoms,[152] polymer aggregation mechanism,[153] heterogeneous and homogeneous catalytic behaviors,[154−156] and so on.

3.3.1. Mapping Active Sites on Individual Au Nanoparticles. Gold nanoparticles of different shapes and sizes have been widely used in imaging studies.[141,149,157−160] Advances in nanomaterial synthesis have resulted in various shapes of Au nanoparticles with well-defined surface facets, thus making it possible to study the site-dependent catalytic activity by the super-resolution imaging methods. Using a Au-catalyzed fluorogenic oxidation reaction of nonfluorescent Amplex Red to fluorescent resorufin by H_2O_2, Chen and co-workers studied the reactivity patterns of individual Au nanorods coated with a mesoporous silica shell.[158] As shown in Figure 9a, the superposition of every fluorescent product molecule allowed the active sites on a single Au@SiO_2 nanorod to be mapped with a high spatial resolution of ~40 nm. By varying the substrate concentration, the authors found that the specific catalytic rate constants of different segments on the single Au@SiO_2 nanorod followed the Langmuir−Hinshelwood mechanism (Figure 9b).[161] The entire nanoparticle was found to be active, but the distribution of specific activity was found to be inhomogeneous along each rod: The ends of the rods were more active than their side facets. The high specific activity of the ends was attributed to the unsaturated coordination there. However, even for the same surface facets, the specific catalytic activity was not constant but rather exhibited a linear gradient from the center of the rod toward the two ends (Figure 9c). This gradual activity decay was attributed to the gradient in the defect density from the center toward the two ends. In accordance with the seeded growth of Au nanorods, the centers of the rods grew the fastest, thus leading to

DOI: 10.1021/acs.chemrev.6b00673
Chem. Rev. XXXX, XXX, XXX−XXX

the highest defect densities.[162] Interestingly, a hidden surface reaction intermediate was later revealed through the same type of super-resolution imaging experiments on Au@SiO_2 nanorods.[163]

Based on another Au-catalyzed fluorogenic reduction reaction of nonfluorescent resazurin to fluorescent resorufin by NH_2OH, Chen and co-workers made similar observations on individual Au nanoplates coated with a 43-nm-thick mesoporous silica shell (Figure 10a).[159] By localizing the individual product molecules precisely, they were able to map the outlines of the individual Au nanoprisms (Figure 10b). Furthermore, by dividing the surfaces of the nanoprisms into different parts (plane surfaces, edges, and corners) (Figure 10b), they determined site-specific activities. The specific activity of the corners was found to be the highest, whereas that of the planar surface was the lowest (Figure 10c). Furthermore, for the (111) flat facets on the same Au@SiO_2 nanoplate, a radial activity gradient from the center toward the periphery was observed (Figure 10d). This observation was interpreted in terms of the percentage of low-coordination surface sites available in different regions, which generally follows the trend corners > edges > flat surfaces.[159]

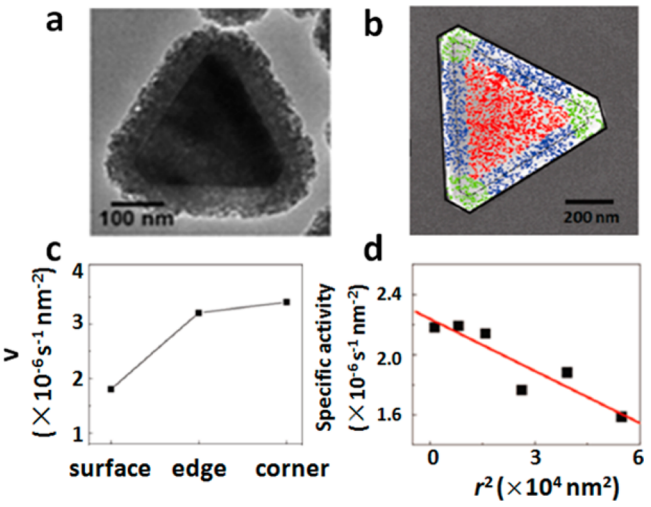

Figure 10. (a) TEM image of triangular Au@SiO_2. (b) Mapping of multiple product molecules (points) onto the SEM image of a single Au@SiO_2 nanoplate. The product molecules in different regions are colored differently: red, flat surfaces; blue, edges; and green, corners. (c) Specific activities (v) of different parts (surface, edges, and corners) on the nanoplate shown in panel b. (d) Distribution of the specific activities along the surface of the nanoplate, where r is the distance from the nanoplate center to the midpoint of the segment along the center–corner vector. Reprinted with permission from ref 159. Copyright 2013 American Chemical Society.

More recently, reactivity patterns on bare Au nanoplates without a SiO_2 shell were mapped by Xu and co-workers using the same Au-catalyzed fluorogenic reduction reaction (Figure 11a).[160] Their results were consistent with the previous observations that the gradient in catalytic activity is in accordance with the growth-induced distribution of defects.

In any case, the gradual radial decay of activity found in these studies suggests that knowledge about the surface facets alone is insufficient to predict the catalytic reactivity of a nanocatalyst and that the defects and unsaturated coordination of surface atoms must also be considered. The surface effects found by super-resolution imaging complicate the development of high-activity catalysts, as it is still difficult to experimentally determine the surface structures of nanocatalysts.[164,165] On the other hand, the surface defects introduced by synthesis might be a good sign for achieving higher efficiency in the application of nanocatalysis.

Temporal fluctuations of catalytic activity have been observed on nanocatalysts or electrodes in situ at both the ensemble and single-particle levels.[51,141,142,166−168] They have often been interpreted as possible catalysis-induced surface reconstructions.[51,141,168] Although evidence has been found for surface restructuring during catalysis,[9,52,53,168−170] its effects on fluctuations in catalytic activity are still not clearly understood. Recently, the spatial changes in the catalytic activities of single-nanoparticle catalysts over time were elucidated by Xu and co-workers using time-lapse super-resolution mapping.[160] The spatiotemporal variations in surface reactivity on individual (both Au and TiO_2) nanocatalysts (Figure 11b,c) revealed an interesting correlation between the reactivity and stability of the active sites. The corners and ends with more low-coordination sites were more reactive at earlier times, but their stability was lower than that of the flat surfaces. Over longer reaction times, the most stable sites of the flat surfaces eventually dominated the total apparent reactivity of single nanocatalysts. Interestingly, spontaneous activity recovery was also observed on some active sites after deactivation, probably as a result of adsorbate desorption. The spatiotemporal super-resolution discrimination of different active sites could lead to a

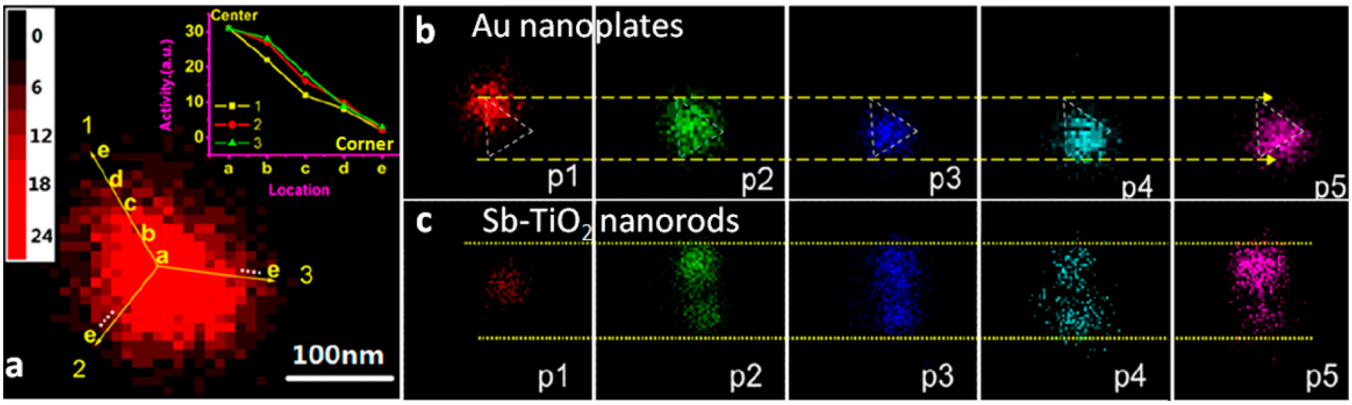

Figure 11. (a) Two-dimensional mapping of product molecules formed on a single Au nanoplate. Inset: Activity decay from the center of the plate to the corners. (b,c) Time-sequential 2D mappings of product molecules on (b) Au nanoplates and (c) Sb-TiO_2 nanorods. Reprinted with permission from ref 160. Copyright 2015 National Academy of Sciences.

DOI: 10.1021/acs.chemrev.6b00673
Chem. Rev. XXXX, XXX, XXX−XXX

comprehensive understanding of such reactivity patterns and help in the design of more efficient nanocatalysts.

3.3.2. Scalable Parallel Screening of Gold Nanoparticles. The observed activity heterogeneity among individual nanoparticles in the aforementioned single-particle nanocatalysis studies was initially interpreted in terms of the size and shape differences between nanoparticles;[142,143] however, this interpretation was inconclusive and could not explain all of the observations at the single-particle level. The parallel screening of the catalytic activities of large numbers of individual nanoparticles is imperative for drawing conclusions with statistical significance. For this purpose, Chen and co-workers combined the super-resolution imaging approach with SEM images of the same samples to directly correlate the activities of hundreds of nanoparticles with their individual sizes and shapes.[157]

Figure 12a presents a super-resolution catalytic reaction map of a sample containing mixed pseudospherical Au@SiO_2 nanoparticles (21@42 nm and 102@22 nm). As shown in Figure 12a,b, the individual nanoparticles, even within aggregates, were all clearly resolved. More importantly, the activities of individual nanoparticles could be quantified in terms of the numbers of product molecules counted and directly correlated with their sizes and shapes derived from the SEM images. It was found that, statistically, the larger particles did exhibit higher activity; however, there were clearly many exceptions: Even for nanoparticles of the same size, the catalytic activities could be significantly different (Figure 12, particle 1 vs. particle 2). These findings suggest that variations in nanoparticle size and shape are not the only factors determining the activity heterogeneity. Other factors, such as surface defect density (discussed above) and catalytic microenvironment, can play important roles. Obviously, these results can guide the design of high-efficiency nanocatalysts and accelerate the development of new catalysts.

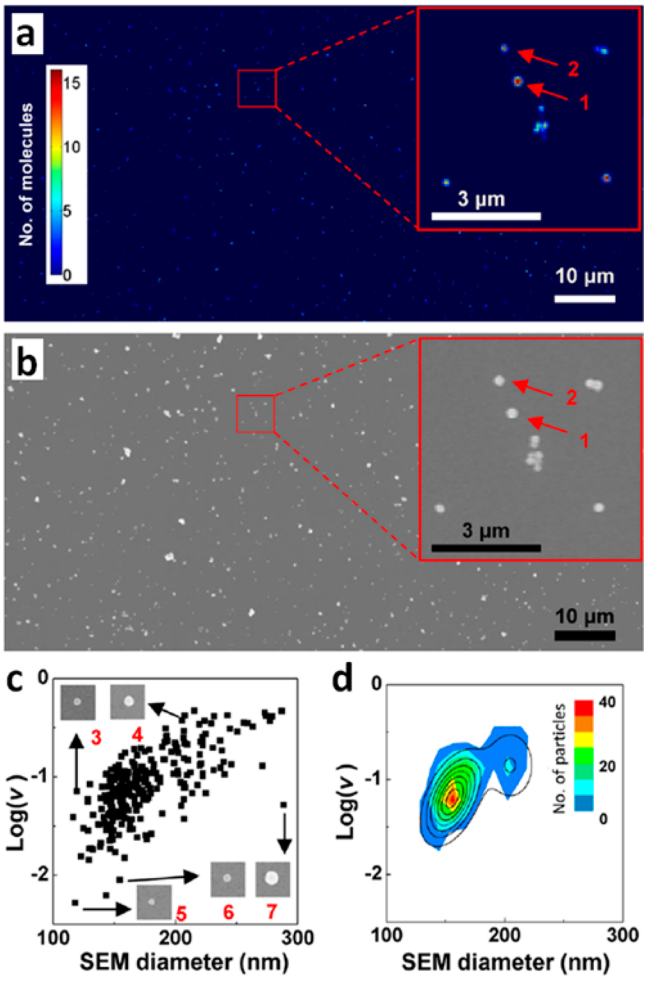

Figure 12. Activity screening of mixed pseudospherical (Au@mSiO_2) nanoparticles. (a) Parallel super-resolution mapping of multiple particles in single-molecule nanocatalysis. (b) SEM image of the area shown in panel a. (c) Scatter plot and (d) contour plot of individual nanoparticles versus their SEM diameters and turnover rates (v). Insets: SEM images of selected nanoparticles. Particle 3 shows high activities even though its size is among the smallest, whereas particle 7, which is large, shows relatively low activities. Reprinted with permission from ref 157. Copyright 2013 American Chemical Society.

3.3.3. Supported Nanocatalysts. In industrial applications, metal nanoparticles can be supported on carbon, metal oxide, clay, or other materials to improve their efficiency and stability and to make it easier to separate them from the product solution.[171−174] The optical super-resolution imaging method has also been used to study the nanocatalysis of supported nanocatalysts at the single-particle level. For example, Scaiano and co-workers studied the "click" reaction sites on a copper-in-charcoal material (Cu/C).[175] Based on a Cu click-activated fluorescence resonance energy transfer (FRET) system reported previously,[155] they confirmed the heterogeneous click reactivity between a donor-labeled alkyne and an acceptor-labeled azide. They found that, despite the high catalytic activity of Cu/C, no particles with multiple catalytic sites could be detected; at most 10% of the charcoal particles had a single catalytic site; and the observed active sites represented only ∼0.003% of the whole surface.[175] All of these findings suggest that there is still plenty of room for improving this already excellent catalyst.

It is more challenging to determine the distributions of active components or sites on supports with complex 3D structures because of the limitations of the existing techniques, especially under operando conditions.[176,177] Recently, with a multilayer nanocatalyst in which Pt nanoparticles were sandwiched between a SiO_2 core and a porous SiO_2 shell (SiO_2@Pt@mSiO_2) (Figure 13a,b) as a model platform, Fang and co-workers developed the first geometry-assisted 3D super-resolution imaging method to map the catalytic activity on single core−shell model nanocatalysts probed by a fluorogenic catalytic reaction.[178] In this method, 2D maps were obtained first with super-resolution localization microscopy. Then, based on the Pythagorean theorem, the ideal spherical shape of the nanocatalyst, and the diameter of the nanocatalyst measured by SEM, the 2D maps were converted into 3D maps of fluorescent product molecules on the surfaces of individual spherical nanocatalysts. The fluorescence intensities of individual product molecules were recorded to determine whether the individual product molecules were formed on the top or bottom of the nanocatalyst. In principle, this 3D mapping method could be used to study other structures with well-defined geometries.

3.4. Semiconductors as Photo(electro)catalysts

Semiconductors, such as TiO_2, ZnO, and CdS, have been intensively studied as photocatalysts because of their important roles in solar energy conversion.[179,180] Because of the unique electronic properties of semiconductors, with no electronic states lying between the conduction band (CB) and the valence band (VB), the electrons in the VB can be excited by suitable photons to the CB and generate electron (e^-)−hole (h^+) pairs. The holes

DOI: 10.1021/acs.chemrev.6b00673
Chem. Rev. XXXX, XXX, XXX−XXX

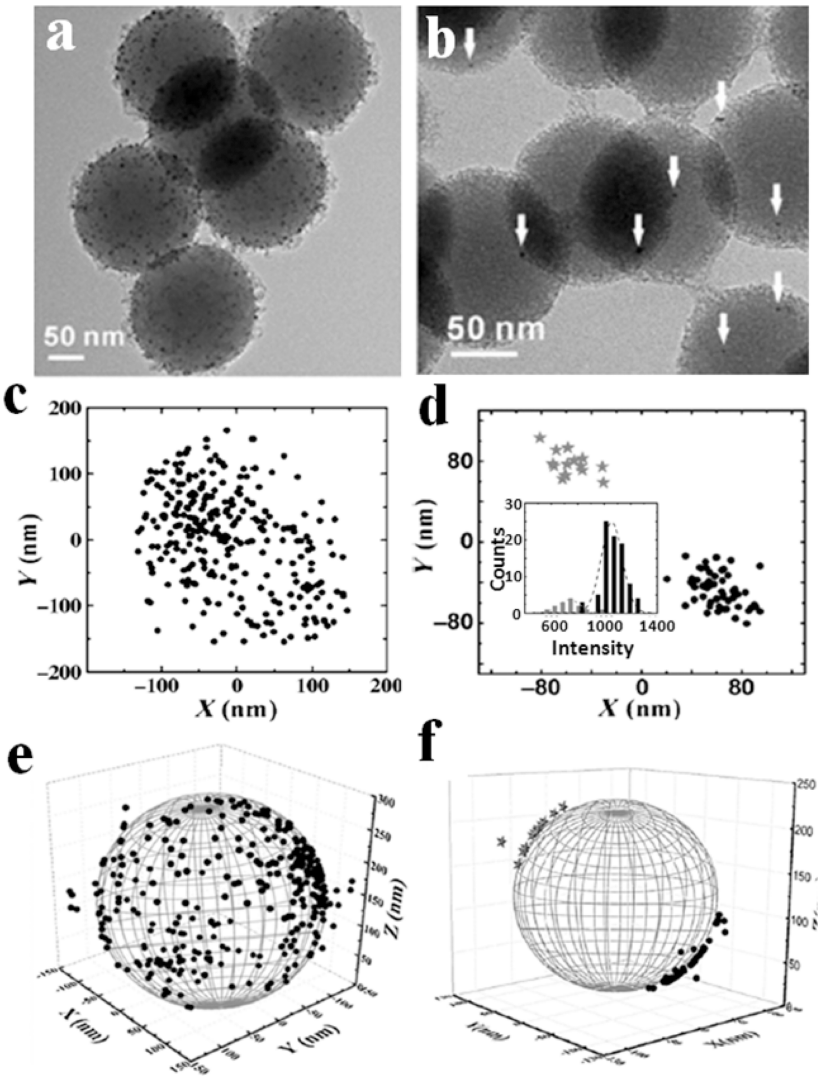

Figure 13. (a,c,e) Three-dimensional super-resolution mapping on a nanocatalyst with high Pt loading. (a) TEM image of the spherical nanocatalysts. (c) Two-dimensional mapping of product molecules on a nanocatalyst. (e) Three-dimensional super-resolution map generated by projecting the 2D coordinates of product molecules onto the spherical surface. (b,d,f) Three-dimensional super-resolution mapping on a nanocatalyst with low Pt loading. Inset of panel d: Fluorescence intensity distributions of two groups of particles. Reprinted with permission from ref 178. Copyright 2014 Wiley-VCH.

and electrons are immediately captured within picoseconds by some trap sites.[181] Figure 14 illustrates the primary steps in the

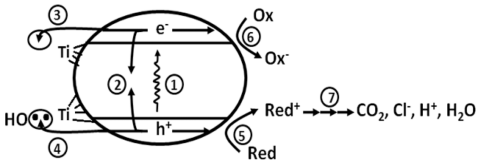

Figure 14. Primary steps in the mechanism of photocatalysis. Adapted with permission from ref 182. Copyright 2014 American Chemical Society.

mechanism of photocatalysis (using TiO_2 as an example): (1) formation of h^+–e^- pairs by photon absorption, (2) h^+–e^- recombination, (3) trapping of a CB electron at a Ti(IV) site to yield Ti(III), (4) trapping of a VB hole at a surface titanol group, (5) initiation of an oxidative pathway by a VB hole, (6) initiation of a reductive pathway by a CB electron, and (7) further processes.[182] In this mechanism, only the photogenerated charges that reach the semiconductor surface are available for photocatalytic reactions (step 5 and 6). The h^+ and e^- charge carriers can directly oxidize or reduce the substrate (S), or they can react with O_2 and OH^- to form all kinds of reactive oxygen species (ROS), including singlet oxygen ($^1O_2$), superoxide ($O_2^{\bullet-}$), hydroperoxyl radical ($HO_2^{\bullet}$), hydroxyl radical ($^{\bullet}OH$), and hydrogen peroxide (H_2O_2).

The redox processes of the substrate can be monitored directly through measurements of transient absorption,[183] and the ROS can be investigated by various methods,[56] including near-infrared spectroscopy, laser-induced fluorescence spectroscopy, and electron spin resonance spectroscopy. The emergence of single-molecule fluorescence technique has enabled scientists to reveal further details of the reaction mechanisms of ROS with appropriate fluorescent probes,[183−187] intramolecular charge transfer,[188,189] interfacial electron transfer (ET),[190−195] crystal surface reactivity,[196−199] and kinetics/dynamics of charge carriers.[200−203] The improved spatial resolution of optical super-resolution imaging techniques is crucial for taking another important step toward an understanding of the distributions, reactivities, and local nanoenvironments of active sites on individual nanocatalysts.

DOI: 10.1021/acs.chemrev.6b00673
Chem. Rev. XXXX, XXX, XXX−XXX

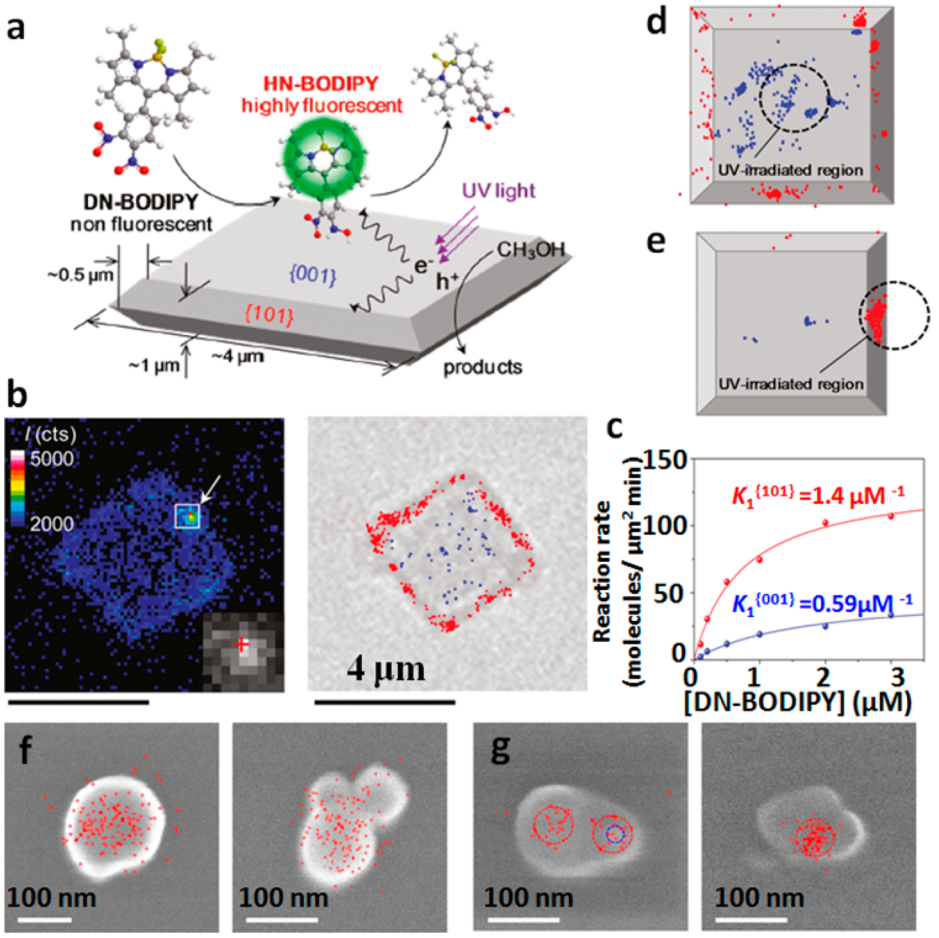

Figure 15. (a) Photocatalysis of a BODIPY derivative on TiO_2. (b) Fluorescence (left) and transmission (right) images of the same TiO_2 crystal. In the left image, the reactive site is indicated by an arrow. In the right image, the red and blue dots represent the locations of product molecules formed on the (101) and (001) facets, respectively, of the crystal. (c) Substrate concentration titration curves on (101) (red) and (001) (blue) facets. (d,e) Locations of product molecules on the (101) (red) and (100) (blue) facets. The black circles indicate UV irradiation areas. Panels a–e reprinted with permission from ref 205. Copyright 2011 American Chemical Society. (f,g) Spatial distributions of product molecules on the SEM images of individual (f) TiO_2 and (g) Au/TiO_2 nanoparticles. Panels f and g reprinted with permission from ref 211. Copyright 2011 American Chemical Society.

3.4.1. Active-Site/Facet Mapping. A traditional in situ study of photocatalysis with fluorescence imaging on individual ETS-10 zeolites suggested that the main photocatalytic active sites on ETS-10 are the crystal defects.[198] This observation was based on a comparison between the ensemble fluorescence intensities of the product molecules formed on the defects and those formed on other areas; however, ensemble fluorescence intensities can be influenced by the ambient environment and intermolecular interactions. To minimize this effect, a direct and effective method is to decrease the substrate concentration, observe catalytic events one by one on single nanocatalysts just as in single-enzyme and single-nanoparticle catalysis,[141,204] and then map the precise locations of the individual fluorescent spots. Majima and co-workers used this approach to study the crystal-facet-dependent photocatalytic behavior of single TiO_2 crystals based on a reduction reaction of boron dipyrromethene (BODIPY) derivatives (Figure 15a).[203,205] The individual fluorescent bursts could be located precisely and attributed to the well-defined crystal facets. Interestingly, as shown in Figure 15b, the lateral (101) facets of the crystal preferentially catalyzed the product formation (bright spots), indicating a significant facet-dependent photocatalytic activity. The crystal-facet-dependent catalytic kinetic parameters were derived using the Langmuir–Hinshelwood equation (Figure 15c). Furthermore, as shown in Figure 15d,e, when the (001) facet was irradiated with UV light, fluorescent product molecules could still be observed on the (101) facets without irradiation. In contrast, the (001) facet showed much lower catalytic activity when the (101) facet was UV-irradiated selectively. These observations suggest that the (101) facets could be reservoirs of photogenerated electrons.[205]

It is known that Au nanoparticles can enhance the surface photocatalytic activity of TiO_2 by the surface plasmon resonance (SPR) effect.[206,207] This has led to investigations of the effects of the size and shape of Au nanoparticles on their photocatalytic properties[202,208−210] and the SPR-induced photocatalytic mechanism.[206,207] The SPR-induced photocatalytic reaction sites of Au/TiO_2 were identified by super-resolution mapping using a water-soluble fluorescent probe molecule.[211] Interestingly, catalytic reactions were observed on the entire TiO_2 surface (Figure 15f). By contrast, as shown in Figure 15g, the individual Au/TiO_2 nanoparticles displayed very low activities, as indicated by the limited active centers. It was also observed that the locations of the reactive sites on some catalysts correlated spatially with the locations of Au nanoparticles. The plasmon-induced photochemical reactions were therefore confirmed by this quantitative super-resolution mapping.

DOI: 10.1021/acs.chemrev.6b00673
Chem. Rev. XXXX, XXX, XXX−XXX

3.4.2. Photogenerated Charge Separation. With the knowledge that Au nanoparticles can effectively enhance the activities of photocatalysts and have a significant effect on the product distribution,[211−213] many studies have focused on the photocatalysis of metal−semiconductor heterostructures at the ensemble level.[213−217] Catalytic mechanisms for metal-modified semiconductors have therefore been proposed.[206,207,218−223] Based on the hybrid heterostructure of Au−CdS,[224] two distinct mechanisms have been proposed for the photoinduced charge separation. As shown in Figure 16, mechanism A occurs when the Au nanoparticle is excited with a green laser at 532 nm and e^-−h^+ pairs form upon the decay of the surface plasmons in Au. Then, a large fraction of the hot electrons tunnel through the metal−semiconductor interface to the conduction band of CdS, thus inducing spatially separated electron−hole pairs (Figure 16a) and charging the Au positively and the CdS negatively. Mechanism B starts with the formation of e^-−h^+ pairs in the semiconductor upon excitation with a blue laser at 405 nm, and then the photoexcited electrons are transferred to the Au metal until its Fermi level matches the edge of the conduction band of CdS, thus charging the CdS positively and the Au negatively (Figure 16b). Obviously, the two mechanisms induce two distinctive Au−CdS species with opposite polarities.

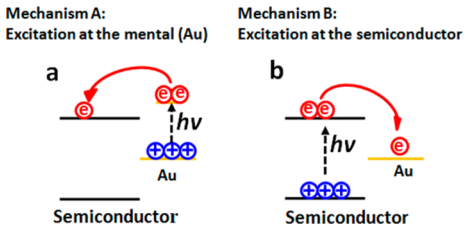

Figure 16. Different mechanisms of charge separation in Au−CdS: (a) mechanism A under the irradiation of a 532-nm laser and (b) mechanism B under the irradiation of a 405-nm laser.

Although super-resolution mapping was able to reveal the formation of the product molecules on or around the deposited Au nanoparticles (Figure 15g),[211] more accurate positions were hard to judge because the size of the Au nanoparticles was much smaller than the spatial resolution. Mechanism B has been confirmed widely on Au−CdS heterostructures.[215,223] To further investigate mechanism A, Fang and co-workers used the super-resolution imaging technique to map both the electron- and hole-induced reaction sites with one substrate but two different reaction pathways on individual Au−CdS heterostructures (Figure 17), thus determining the locations of the separated charges simultaneously.[224] Amplex Red, a nonfluorescent substrate, can react with $O_2^{\bullet-}$ produced from O_2 reduction by photoexcited electrons (e^-) or with $HO^\bullet$ produced from H_2O oxidation by photogenerated holes (h^+) to generate the same highly fluorescent product, resorufin.[225,226] Despite forming the same fluorescent product, the dissociation (on-time) kinetics were distinctly different because of the different interactions between the local environment and the product molecules. Therefore, the h^+ reactive sites and e^- reactive sites could be distinguished within the same fluorescence intensity trajectory.

To overcome the inadequate spatial resolution in mapping the h^+ and e^- reactive sites, a specially designed Au-tipped CdS heterostructure was synthesized (Figure 17a, bottom). Under the excitation of the green laser (532 nm), the h^+-based active sites were located only on the Au nanoparticles at the ends of the CdS nanorods, whereas the e^--based active sites were located only in the middle of the CdS nanorods (Figure 17c), further confirming the occurrence of mechanism A under these working conditions. On the other hand, when the photocatalysis proceeded under

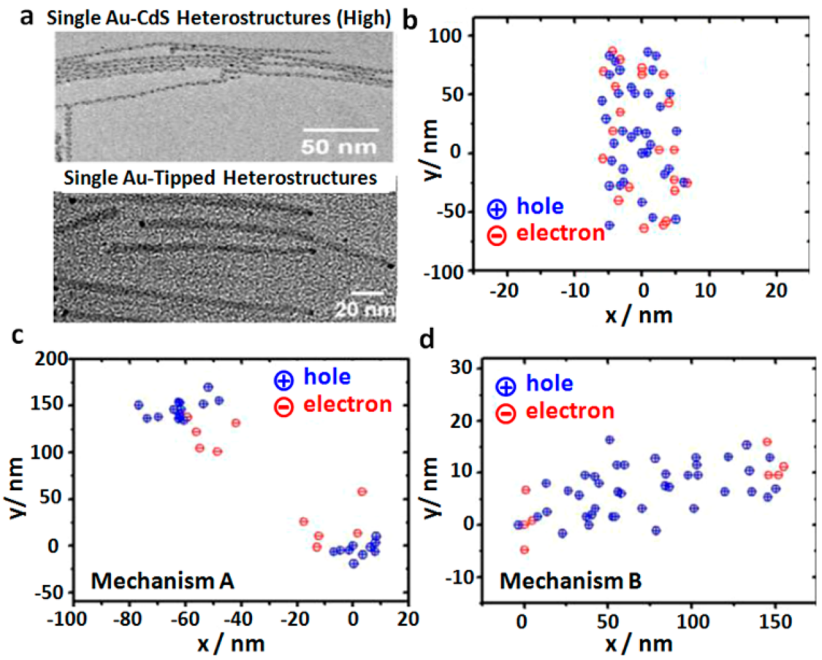

Figure 17. (a) TEM images of Au−CdS heterostructures with high (top) and low (bottom) Au loadings. (b) Superlocalization of h^+-based and e^--based active sites on a Au−CdS nanorod with a high Au loading under the excitation of a 532-nm laser. (c) Superlocalization of h^+-based and e^--based active sites on a Au-tipped CdS nanorod under the excitation of a 532-nm laser. (d) Superlocalization of h^+-based and e^--based active sites on a Au-tipped CdS nanorod under the excitation of a 405-nm laser. The 532-nm laser was still on to excite the product resorufin. Reprinted with permission from ref 224. Copyright 2014 American Chemical Society.

DOI: 10.1021/acs.chemrev.6b00673
Chem. Rev. XXXX, XXX, XXX−XXX

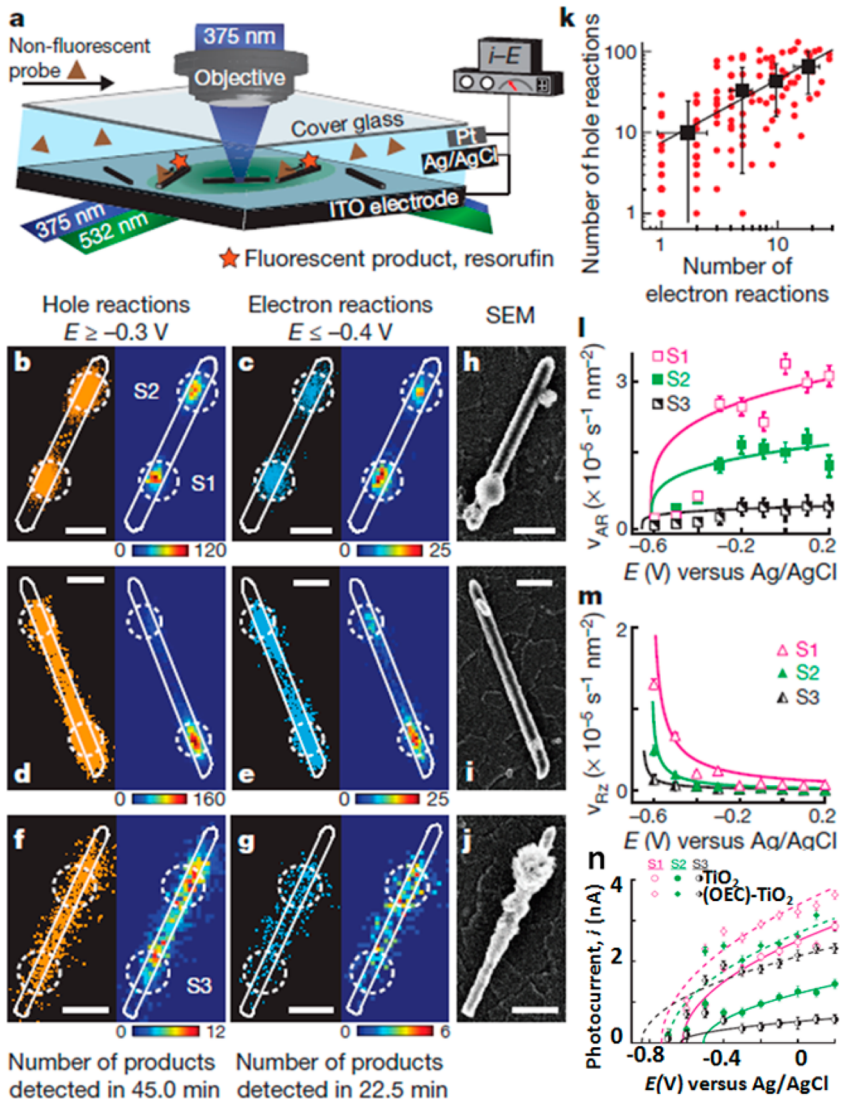

Figure 18. (a) Experimental setup for single-molecule photoelectronanocatalysis. (b) Scatter plot (left) and 2D mapping (right) of product molecules detected from h^+-based active sites on a single TiO_2 nanorod with $E \geq -0.3$ V. (c) Scatter plot (left) and 2D mapping (right) of multiple product molecules detected from e^--based active sites on a single TiO_2 nanorod with $E \leq -0.4$ V. (d–g) Similar to panels b and c but with (d,e) a single hot spot of h^+ reaction or (f,g) h^+ reactions delocalized. (h–j) Corresponding SEM images of the rods in panels b–g after deposition of the OEC. Scale bars: 400 nm. (k) Correlation analysis between the h^+ reaction and e^- reaction. (l,m) Effects of the potential on (l) v_{AR} and (m) v_{Rz}. (n) Current–potential curves of different spots before and after deposition of the OEC. Reprinted with permission from ref 227. Copyright 2016 Nature Publishing Group.

405-nm laser excitation (mechanism B), the h^+-based active sites were distributed along the entire CdS nanorods, and the e^--based active sites were located at the ends (Figure 17d). These two different charge-separation mechanisms revealed by super-resolution imaging are important for helping researchers design and develop better metal–semiconductor heterostructures through the engineering of the energy flows on semiconductor-based heterostructured nanomaterials.

3.4.3. Guide for Photo(electro)catalyst Design. Although super-resolution imaging studies on photonanocatalysis have revealed important information about the photocatalytic mechanism as discussed above, much more work still needs to be done to translate the information obtained from experiments into guidance for the rational design of new high-efficiency photocatalysts. Recently, on the basis of the combination of optical super-resolution imaging with photocurrent mapping on individual photocatalysts, Chen and co-workers proposed new strategies for the optimization of the catalyst-modified photoanode for the water-splitting reaction.[227]

Photoelectrochemical water splitting is limited by the low water-oxidation efficiency of photogenerated holes.[228−230] An oxygen evolution catalyst (OEC) can be used to modify the photoanode to achieve higher photocatalytic efficiency.[230−232] A deeper understanding of the OEC targeted-site effect is highly desirable to achieve the optimal site-selective deposition of the OEC on the photoanode. Using a microfluidic photoelectrochemical cell, Chen and co-workers mapped both the h^+- and e^--based active sites (30-nm resolution) based on the super-localization of the product molecules and measurements of the photocurrent of water oxidation by selective laser irradiation on single TiO_2 nanorods (Figure 18a).[227] Their experiments were carried out in three steps.

First, super-resolution imaging and SEM were combined to map the positions of photogenerated-hole- or photogenerated-electron-induced reactions with two fluorogenic reagents on

DOI: 10.1021/acs.chemrev.6b00673
Chem. Rev. XXXX, XXX, XXX−XXX

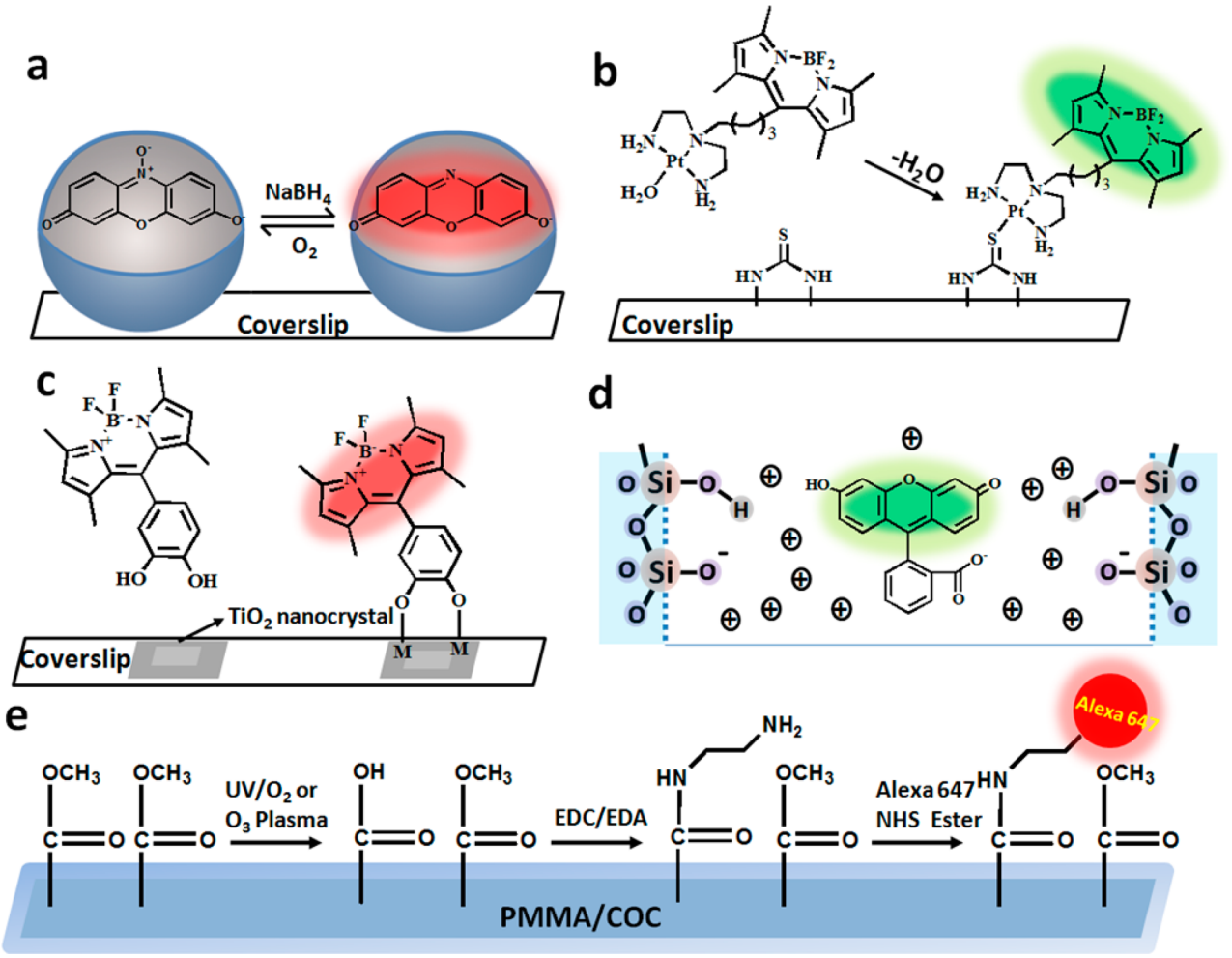

Figure 19. Chemical reactions used in super-resolution imaging studies.

individual TiO_2 nanorods (Figure 18b–j). When the applied potential was higher than −0.3 V, it was observed that the hole-induced oxidative domains were centered nonuniformly at some discrete "hot spots" on the surface of individual nanorods (Figure 18b,d,f). The same phenomena were observed on the electron-induced reductive domains when the applied potential was less than −0.4 V (Figure 18c,e,g). The heterogeneous distribution of the active sites indicates that the activities of surface structural defects are likely higher than that of the (100) facet sites. Interestingly, the hole-induced activity showed a spatial correlation with the electron-induced activity (Figure 18k). Furthermore, the hole-induced oxidation rate (ν_{AR}) and the electron-induced reduction rate (ν_{Rz}) of the hot spots (Figure 18b, spots S1 and S2) and low-activity spots (Figure 18f, spot S3) at different potentials could be determined (Figure 18l,m).

Second, a focused UV laser (375 nm) was used to induce the photocurrent (i) from water oxidation on different locations of a nanorod (Figure 18b–g, circles). On both the hot spots (Figure 18b, spots S1 and S2) and the low-activity spots (Figure 18f, spot S3), the anodic photocurrent i was always observed to scale with the applied potential (E) (Figure 18n). The onset potential ($E_{on,GB}$), the absorbed-photon-to-current water oxidation efficiency (η), and the effective rate constants of holes (k_h) and electrons (k_e) were obtained by fitting the i–E, ν_{AR}–E, and ν_{Rz}–E data with the Gärtner–Butler and Reichman models for each spot. Interestingly, η was found to be positively correlated with the surface hole and electron activities (k_h and k_e, respectively), indicating that the sites with high water oxidation efficiencies were also effective surface recombination sites.

Finally, a cobalt–borate OEC was deposited photoelectrochemically onto different spots (Figure 18h–j) to test its effect on the photocatalytic performance for water oxidation. Enhancements to i, $E_{on,GB}$, and η were observed in all cases. However, the optimal OEC deposition sites for enhancing i and $E_{on,GB}$ were not necessarily the same: the spots with the lowest h^+ and e^- activities were optimal for i, whereas the sites with the most positive $E_{on,GB}$ values were optimal for $E_{on,GB}$. Based on these critical experimental findings highlighting the challenges of engineering photoanodes, a block–deposit–remove strategy, based on the functions of materials rather than their structures, was proposed for catalyst design: Block some hot spots with protecting groups, then deposit the desired catalysts at the remaining sites, and finally remove the protecting groups to yield an optimal photoanode.

More recently, using the same approach, Chen and co-workers distinguished direct and indirect photoelectrocatalytic oxidation mechanisms on TiO_2 nanorods.[233]

3.5. Electrocatalysts

Electrochemical methods have been applied extensively in nanocatalysis.[234,235] Efforts to combine these methods with super-resolution imaging have gained momentum in recent years. Two detection schemes have been implemented using these methods. The first detection scheme monitors the

DOI: 10.1021/acs.chemrev.6b00673
Chem. Rev. XXXX, XXX, XXX–XXX

electrochemical current. Interested readers can consult the related reviews[137,234,236] and recent reports.[135,140,237−239] The second detection scheme is based on the variations of the optical signals of individual molecules occurring during electrochemical processes, and it has been used on polymer nanoparticles,[240−242] metal nanoparticles,[133,151,243,244] fluorescent redox-active molecules,[245,246] clay nanoparticles,[247] and carbon nanotubes.[248] As one of the earliest examples, Chen and co-workers studied the reduction reaction of resazurin electrocatalyzed by single-walled carbon nanotubes (SWCNTs).[248] Superlocalization of individual product molecules on the nanocubes revealed that the catalytic reactions were concentrated in the areas with diameters similar to the spatial resolution of ~20 nm, suggesting that the electrocatalytic sites on SWCNTs are discrete and nanometer-sized. Therefore, each reactive site in an SWCNT can act as an ultrasmall electrode for the further study of the electron-transfer kinetics of SWCNTs. Recently, Xu and co-workers reported a single-molecule fluorescence study of carbon-supported Pt (Pt/C) electrocatalysts that indirectly revealed the deactivation mechanism of Pt/C electrocatalysts for the hydrogen oxidation reaction.[151] As electrocatalysts play a prominent role in fuel cells, we look forward to further efforts to obtain new insights into electrocatalysis at the single-molecule and single-active-site levels, such as mapping the distributions of electrochemical active sites and revealing the electrodeactivation patterns.

4. SUPER-RESOLUTION IMAGING OF CHEMICAL REACTIONS

Single-molecule fluorescence studies have revealed many new insights into stoichiometric reactions.[62] These studies can be divided into two categories: One involves the study of the detailed mechanisms of fluorogenic reactions, such as the reversibility of some chemical reactions,[249−251] ion-/galvanic-exchange reaction kinetics,[252,253] and mechanisms of organic reactions;[254] the other involves the use of fluorescent probes to learn about the properties of different surfaces, such as thermoplastic surfaces,[255] functionalized glass surfaces,[256−258] metal oxide surfaces,[259] nanotube surfaces,[260,261] and nano-/microchannel surfaces.[262−264]

The choice of fluorescent probes is essential in designing single-molecule imaging experiments. Representative fluorescent probes and fluorogenic reactions are presented in Figure 19. Unlike heterogeneous catalytic reactions occurring mostly on the surfaces of catalysts, homogeneous reactions take place in solution, making it more challenging to capture fluorescence signals. To overcome this technical difficulty, fluorescent probes are usually fixed on the surface of functionalized supports or captured in nanocontainers (e.g., hollow SiO_2 nanoparticles or nanochannels). For further details, readers can consult a review of the development of fluorescent probes for single-molecule imaging experiments.[62]

4.1. Studies of Single-Molecule Fluorogenic Reactions

Individual turnover cycles have been observed directly at the single-molecule level upon addition of different reagents.[250,251] By tracking the reversible redox process of single fluorescent dye molecules in hollow SiO_2 nanoparticles (Figure 19a) and employing quantum chemical calculations, Xu and co-workers studied the kinetics and dynamics of elementary chemical reactions in the condensed phase.[249] The dynamic reactivity fluctuations of single molecules were observed during both the reduction and oxidation steps.

According to the scheme shown in Figure 20, two distance sequences in each trajectory (denoted as **D1** and **Dk**) were

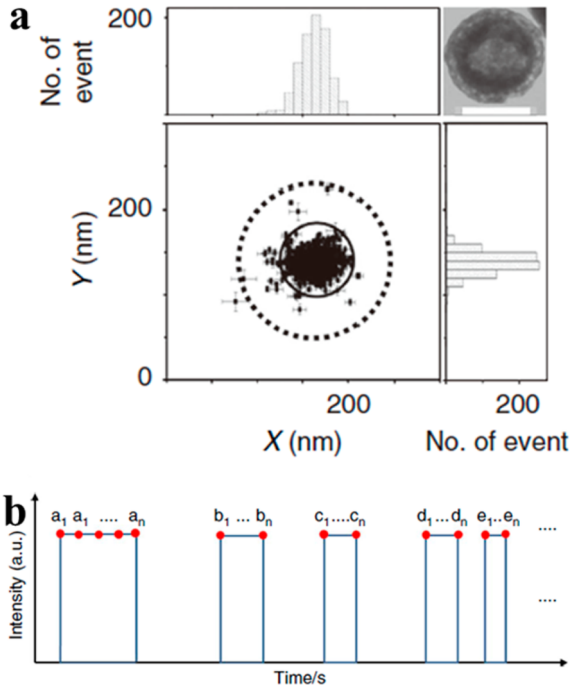

Figure 20. (a) Mapping of the Brownian motion of a fluorescent dye molecule inside a spherical hollow SiO_2 particle. (b) Calculation of two of the distance sequences (**D1** and **Dk**) from each trajectory. Reprinted with permission from ref 249. Copyright 2014 Nature Publishing Group.

calculated: The **D1** sequence (a_1a_2, a_2a_3, ..., $a_{n-1}a_n$, b_1b_2, b_2b_3, ..., $b_{n-1}b_n$, ...) contained the sequential distances of a molecule in two adjacent frames during the same on event, whereas the **Dk** sequence (a_nb_1, b_nc_1, ... d_ne_1, ...) contained the sequential distances of a molecule in two frames separated by an off event. The average value of **Dk** (36 ± 6 nm) was found to be much larger than that of **D1** (24 ± 4 nm), suggesting a divergent diffusion pattern. Furthermore, an autocorrelation analysis was carried out for both the **D1** and **Dk** data sets. The successive diffusion steps (the **D1** sequences) showed a decay behavior, confirming a memory effect or dynamic disorder, that usually occurs in enzyme and nanoparticle catalysis;[141,204] however, no autocorrelation or memory effect was found for the **Dk** sequences. Such diffusion-induced dynamic fluctuations, or memory effect, might contribute to the dynamic fluctuations of the reactivity of single dye molecules.

4.2. Single-Molecule Reactions on Different Surfaces

4.2.1. Silicon Dioxide Surfaces. Surface modification with silyloxy reagents is a common strategy for tethering metal complexes to silica surfaces.[265,266] Irregular surface features are often characterized by atomic force microscopy;[267] however, the correlation between static physical and chemical surface features and the surface's chemical reactivity is often elusive to find. Nevertheless, the super-resolution imaging approach allowed Blum and co-workers to connect the surface features with their dynamic chemical reactivities by mapping the precise distribution of reaction sites on a surface modified with triethoxysilane with a localization precision of ~11 nm.[256,258] This study relied on a fluorescent BODIPY-tagged (dien)-platinum complex that could rapidly bind to the surface thiourea groups through a

DOI: 10.1021/acs.chemrev.6b00673
Chem. Rev. XXXX, XXX, XXX−XXX

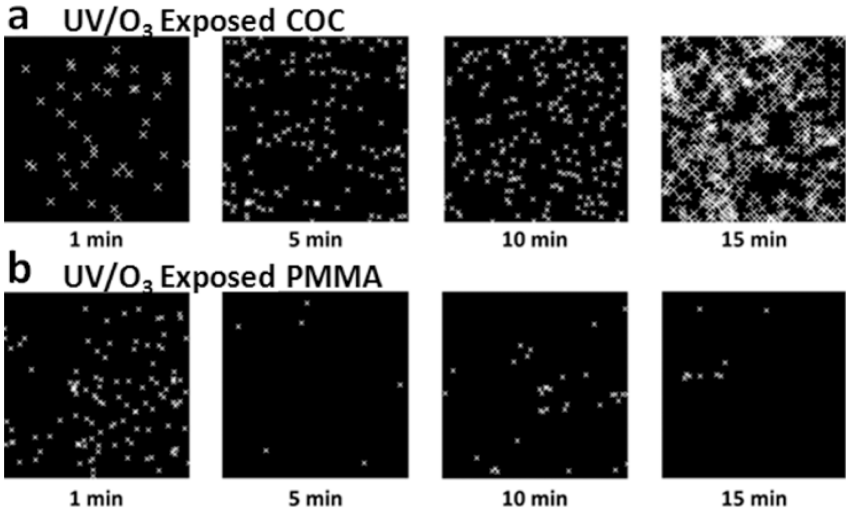

Figure 21. Representative STORM images of (a) cyclic olefin copolymer (COC) and (b) poly(methyl methacrylate) (PMMA) surfaces exposed to UV/O_3 radiation. Reprinted with permission from ref 255. Copyright 2016 American Chemical Society.

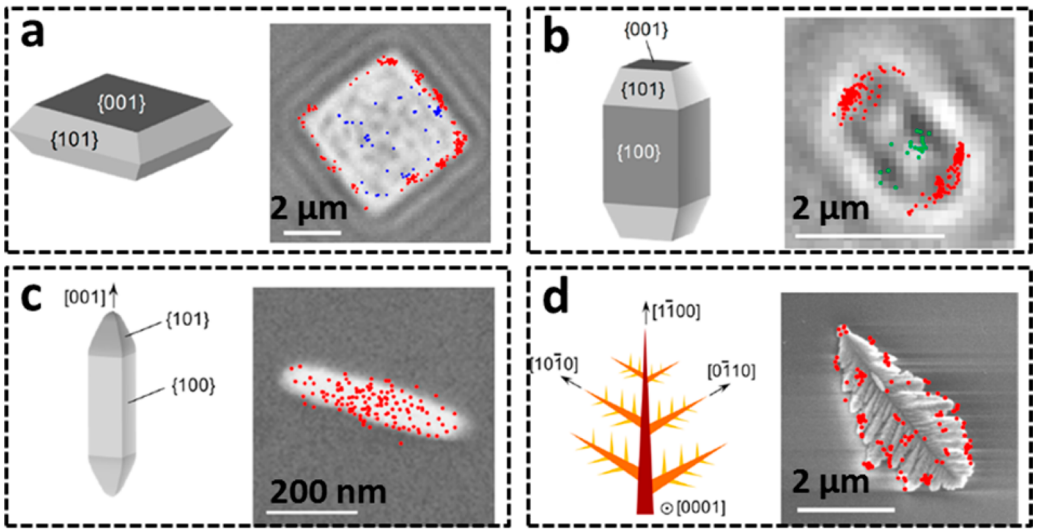

Figure 22. (a,b) Structure analysis of TiO_2 nanoplates (left) and active-site distributions on different surfaces [blue or green dots, (001); red dots, (101)] (right). (c) Structure analysis of TiO_2 nanorods in anatase (left) and active-site distribution (red dots) on the SEM image of a TiO_2 nanorod (right). (d) Growth directions of α-Fe_2O_3 micropins (left) and active-site distribution on the SEM image of an α-Fe_2O_3 micropin (right). Reprinted with permission from ref 259. Copyright 2013 American Chemical Society.

ligand-exchange reaction by forming platinum−sulfur covalent bonds (Figure 19b).[256,258] Position correlation analysis revealed uncorrelated individual chemical reactions occurring on the surface.

4.2.2. Thermoplastic Surfaces. Thermoplastics, as attractive materials for microfluidics and nanofluidics,[268,269] have the advantages of lower costs and simpler fabrication campared to glass-based devices.[270] To increase their surface wettability and charge density, thermoplastics are often surface-modified with carboxylic acid groups (−COOH) through exposure to UV/O_3 or O_2 plasma.[271,272] The heterogeneous distribution of the surface functional groups can profoundly affect the electrophoretic performance of micro- and nanofluidic devices. However, surface characterization has been hampered by ensemble measurements.[273]

Recently, using a commercial photoswitchable dye (Alexa Flour 647 NHS ester) label on the functional groups (Figure 19e), Soper and co-workers characterized these modified surfaces by STORM.[255] Their experiments revealed the surface densities and heterogeneous distributions of dye-labeled −COOH groups on different polymer surfaces (Figure 21a,b). The fluid flow profiles in the nanochannels were then reconstructed by COMSOL simulations based on the super-resolution mapping results. The simulations showed a distorted electroosmotic flow and regions of possible fluid recirculation, which were further confirmed by tracking the electrophoretic migration of single fluorescent polystyrene nanoparticles.

4.2.3. Metal Oxide Surfaces. Surfaces adsorption of molecules is usually a key step in chemical syntheses. Similarly to the probing of heterogeneous surface structures, the characterization of stochastic surface adsorption/desorption events is also highly challenging. Very little work has been done to explore the interfacial adsorption sites for substrate molecules or ions. Recently, Majima and co-workers used a catechol-modified boron dipyrromethene (CA-BODIPY) dye to identify the effective adsorption sites on different TiO_2 and

DOI: 10.1021/acs.chemrev.6b00673
Chem. Rev. XXXX, XXX, XXX−XXX

Fe_2O_3 surfaces through a chelating reaction (Figure 19c).[259] The nonfluorescent CA-BODIPY could be transformed into fluorescent chelating complexes when adsorbed on the TiO_2 surface. The adsorption locations of individual CA-BODIPY molecules were then determined by super-resolution imaging (Figure 22a–c). In this way, the crystal-facet-dependent adsorption ability of CA-BODIPY on the TiO_2 microcrystal surfaces in water was observed, namely, (101) > (001) ≈ (100). Interestingly, the order of the adsorption ability was reversed in an aprotic solvent. Furthermore, the nano-TiO_2 crystals were found to exhibit superior adsorptivity compared to micro-TiO_2 crystals and bulk TiO_2 surfaces because of the larger number of defects on the nanoparticles. Similarly, as shown in Figure 22d, the adsorption sites on Fe_2O_3 micropines were found to be mostly distributed on the top branches where the Fe cations were highly concentrated, indicating that the Fe sites facilitate molecular adsorption.

4.2.4. Ion Distribution in Extended Nanochannels. A space of 10–1000 nm above a surface is termed extended nanospace. Because of confinement effects, the behaviors of liquid molecules in such nanospaces and in the bulk are remarkably different.[274,275] Understanding the properties of liquids in the extended nanospace, especially protons in the electric double layer, is important for nanofluidics and nanochemistry.[276] Both experimental and theoretical efforts have been made to validate the electric double layer model.[277−279] However, it is still difficult to measure precisely the ion distributions on or near the surface owing to the lack of direct measurements.

Using a STED microscope and a proton-sensitive fluorescent pH indicator (Figure 19d), Kitamori and co-workers measured the distribution of ions in rectangular nanochannels with a width of 410 nm and a depth of 405 nm.[263] Following a calibration of the pH and fluorescence intensity, the proton distribution in the nanochannels was mapped with the STED microscope and found to show a strong correlation with the thickness of the electric double layer. Based on these results, numerical simulations of the electric double layer and proton/water distribution in the extended nanochannel were later implemented.[274] In principle, this method can be generalized for measuring other ion distributions with properly chosen fluorescence indicators.

5. OTHER APPLICATIONS OF SUPER-RESOLUTION IMAGING

The aim of this review article is to summarize the latest developments in the optical super-resolution imaging of catalytic reactions; however, as a powerful tool in the field of nanoscience, the application of optical super-resolution imaging is not limited to only the subjects mentioned above. Many other systems have also been studied, such as energy migration processes in conjugated polymers,[280−284] J-aggregates,[285] and perovskite nanocrystals;[286] mapping of nanostructures;[287−290] molecular diffusion and transport processes in porous materials;[291−308] imaging of quantum dots;[309,310] dynamics of polymers;[311−316] detection of the quenching centers of graphene,[317] and probing of plasmonic hot spots in metal nanoparticles.[318−328]

6. CONCLUDING REMARKS AND PERSPECTIVES

Optical super-resolution imaging has gained momentum in investigations of heterogeneous and homogeneous chemical reactions at the single-molecule level. Thanks to its exceptional spatial resolution and ability to monitor dynamic systems, much detailed information on single-molecule reaction/adsorption processes and single-particle catalytic processes has been revealed, including chemical kinetics and reaction dynamics; surface active-site distributions; and size-, shape-, and facet-dependent catalytic activities of individual nanocatalysts. Even with such extensive applications, optical super-resolution imaging techniques require further developments in the following areas for wider and deeper chemical imaging applications:

(i) In principle, the spatial resolution can be improved to 1 nm or even better as long as sufficiently high signal-to-noise (S/N) ratios can be achieved with a perfectly calibrated imaging system. However, because of the limitations of the present best photon detectors, available fluorescence probes, and often non-negligible background associated with functionalized surfaces or complex nanostructures, the S/N ratios in the reported in situ super-resolution imaging experiments typically provide a limited spatial resolution of a few tens of nanometers. As the current imaging detectors already approach the perfection of single photon counting with >95% quantum efficiency, the greatest gain in S/N ratio and resolution will likely come from the design and synthesis of brighter, more stable fluorescence probes, as well as clever sample design and meticulous sample preparation. Nanomaterials used in imaging experiments might require special designs that share several common traits, such as optical transparency, well-defined geometry, and ordered structural units that are larger than the resolution.

(ii) Coupling of optical microscopy imaging and electron microscopy has been practiced by many groups to correlate information at different spatial and temporal resolutions. However, none of these efforts were carried out in situ. Because of spontaneous or catalysis-induced surface reconstructions, obviously, the information obtained from such ex situ structure–reactivity correlation analyses still cannot reliably or precisely reflect the real structural dependence of the catalytic reactivities of individual nanocatalysts. To solve this problem, the in situ combination of optical super-resolution imaging with high resolution electron microscopy is highly desirable to reveal the real structure–reactivity relationships of surface or interfacial processes at the micro- and nanoscales.

(iii) In addition to the nanoscale, new challenges and opportunities also arise at the intermediate scales (namely, mesoscale) between nanoscale and traditional macroscale (bulk) materials. A fundamental challenge is to observe and characterize the inherent imperfections and statistical variations in mesoscale materials. The complexity of mesoscale materials increases significantly from that of atomic, molecular, or nanoscale building blocks. Super-resolution imaging techniques will have to adapt to the increased complexity to study chemical reactions at the mesoscale.

(iv) Super-resolution fluorescence microscopy enables real-time, high-throughput, single-turnover observations of nanocatalysis on various functional materials. However, several practically important catalytic reactions not involving highly fluorescent molecules cannot be investigated directly under a super-resolution microscope. To overcome this challenge, indirect detection methods, such as use of a subsequent fluorogenic reaction, need to be developed to detect non-fluorescent products in the reactions of interest.

(v) New fluorescence microscopy studies of surface chemical reactions by molecular catalysts continue to emerge. For example, Goldsmith and co-workers reported a study of the

DOI: 10.1021/acs.chemrev.6b00673
Chem. Rev. XXXX, XXX, XXX–XXX

initiation dynamics of a palladium cross-coupling catalyst supported at surfaces in which a large degree of heterogeneity was identified by Weibull analysis.[146] Blum and co-workers developed a new tool for elucidating the mechanistic roles of additives in the synthesis of organometallic reagents through direct metal insertion.[329] These developments in single-molecule and subensemble fluorescence imaging of chemical reactions represent new frontiers in which the concepts and techniques of super-resolution imaging might be helpful for extracting new information.

With the rapid development of modern science and technologies, these breakthroughs could be realized sooner than we expect. New chapters of molecular chemical measurement will certainly be written by in situ super-resolution chemical imaging.

AUTHOR INFORMATION

Corresponding Authors

* E-mail: shkang@khu.ac.kr.
* E-mail: jwha77@ulsan.ac.kr.
* E-mail: weilinxu@ciac.ac.cn.
* E-mail: nfang@gsu.edu.

ORCID

Ji Won Ha: 0000-0003-0566-8176
Weilin Xu: 0000-0001-7140-8060
Ning Fang: 0000-0003-4710-0984

Notes

The authors declare no competing financial interest.

Biographies

Tao Chen received his B.S. in Chemistry from Liaoning University, China, in 2012. He is currently a graduate student at University of Chinese Academy of Sciences under the supervision of Professor Weilin Xu. His research is on single-molecule studies of nanocatalysis.

Bin Dong received his B.S. in Chemistry from the Xiamen University, China, in 2011 and his Ph.D. in Chemistry from Iowa State University in the group of Prof. Ning Fang in 2015. He continues to work as a postdoctoral research associate in Prof. Fang's group at Georgia State University. His main research interests are studying biological and chemical systems at the single-molecule and single-particle levels by optical imaging methods.

Kuangcai Chen completed his B.S. in Chemistry at Shandong University, China, in 2009 and obtained his M.S. in analytical chemistry from Changwon National University, South Korea, in 2011. He received his Ph.D. in analytical chemistry from Iowa State University in 2015. He is currently a Postdoctoral Research Associate at Georgia State University under the supervision of Prof. Ning Fang. His research involves the development of novel optical imaging methods using single-particle tracking and super-resolution imaging for chemical and biophysical applications.

Fei Zhao received her B.S. in Chemistry from Nankai University, China, in 2012, and she is now a graduate student under the supervision of Prof. Ning Fang in the Department of Chemistry at Georgia State University. Her research focuses on single-molecule and single-particle imaging.

Xiaodong Cheng received his B.S. degree in 2008 from Hunan University of Science and Technology, China, and obtained his Ph.D. degree in Analytical Chemistry in 2014 under the cosupervision of Professor Yan He and Professor Edward S. Yeung in the Department of Chemistry at Hunan University. He is currently a postdoctoral fellow in the group of Prof. Ning Fang at Georgia State University. His current research focuses on optical sensing and single-particle imaging and their applications in biological research.

Changbei Ma received his B.S. from Hunan Normal University, China, in 2002 and his Ph.D. in analytical chemistry in 2007 from Hunan University. He was a Postdoctoral Associate at Iowa State University and Ames Laboratory, U.S. Department of Energy, with Prof. Edward S. Yeung from 2008 to 2011. He is currently an Associate Professor of Biochemistry at Central South University, China. His research interests are in chemical biology and bioanalytical chemistry.

Seungah Lee received her B.S., M.S., and Ph.D. degrees from Chonbuk National University, Republic of Korea, in the group of Professor Seong Ho Kang in 2003, 2006, and 2010, respectively. Currently, she is an Assistant Professor at Kyung Hee University, Republic of Korea. Her main research interest focuses on chemical/biological analysis on biochips at the single-molecule level using various detection systems.

Peng Zhang received his B.E. degree from the Institute of Materials Science and Engineering at Qilu University of Technology, China, in 2011. In 2012, he joined Prof. Seong Ho Kang's laboratory at Kyung Hee University, Republic of Korea, as a Ph.D. candidate. His research experiences include the analysis of biomolecules and nanomaterials with microfluidic systems and single-molecule detection techniques. His current research focuses on the development of single-particle-detection-based super-resolution microscopy and its uses in bio/nanotechnology.

Seong Ho Kang received his B.S. and M.S. degrees in Chemistry from Kyung Hee University, Republic of Korea, in 1987 and 1989, respectively. He worked as a Senior Researcher at Hanil Pharmaceutical Co. from 1989 to 1997. He received his Ph.D. degree in Chemistry from Seoul National University, Republic of Korea, in 1998. He was a Postdoctoral Research Associate Scholar at Iowa State University and Ames Laboratory, U.S. Department of Energy, with Dr. Edward S. Yeung from 1998 to 2000. He then served as a Senior Researcher at Samsung Advanced Institute of Science and Technology from 2000 to 2002 and then as a Professor of Chemistry at Chonbuk National University, Republic of Korea, from 2002 to 2010. He is currently a Professor at Kyung Hee University, a position he has held since 2010. His research interests include developments in various analytical systems and methods based on micro- and nanoseparation, single-molecule detection, and various nanobio fusion technologies.

Ji Won Ha received a Master's degree in Physical Chemistry from Rice University in 2010 under the direction of Prof. Stephan Link. In 2013, he received a Ph.D. degree in Analytical Chemistry from Iowa State University in the group of Prof. Ning Fang. He then moved to Northwestern University as a Postdoctoral Associate in the group of Prof. Teri W. Odom. He is currently an Assistant Professor of Chemistry at the University of Ulsan, Republic of Korea. His research interests include single plasmonic nanoparticle imaging and spectroscopy for biological, surface, and photocatalysis studies.

Weilin Xu is a Professor at Changchun Institute of Applied Chemistry (CIAC), Chinese Academy of Science. He received his B.S. degree in Chemistry in 2001 from Jilin University, China, and his Ph.D. degree from CIAC in 2006. He did postdoctoral research at Cornell University, UC Berkeley, and Lawrence Berkeley National Laboratory successively from 2007 to 2011, working on single-molecule nanocatalysis. In 2012, he returned to CIAC and became a Professor in physical chemistry performing work focusing on energy-related basic (from the single-molecule level) and practical (based on cheap and sustainable materials) research.

Ning Fang received his B.S. degree in Chemistry from Xiamen University, China, in 1998 and his Ph.D. degree from the University

DOI: 10.1021/acs.chemrev.6b00673
Chem. Rev. XXXX, XXX, XXX−XXX

of British Columbia, Canada, in the group of Prof. David D. Y. Chen in 2006, and he was a Postdoctoral Associate at Iowa State University and Ames Laboratory, U.S. Department of Energy, with Prof. Edward S. Yeung from 2006 to 2008. From 2008 to 2015, he was an Assistant Professor of Chemistry at Iowa State University and a Faculty Scientist at the U.S. Department of Energy, Ames Laboratory. In July 2015, he moved his laboratory to the Department of Chemistry at Georgia State University and became an Associate Professor. His research aims to open up new frontiers in chemical and biological discovery through the development and use of novel optical imaging platforms that provide subdiffraction-limited spatial resolution, high angular resolution, excellent detectability, and/or nanometer localization accuracy for single molecules and nanoparticles.

ACKNOWLEDGMENTS

B.D., K.C., F.Z., and N.F. were supported by the National Science Foundation (CHE-1609225/1607305). T.C. and W.X. were supported by the National Basic Research Program of China (973 Program 2014CB932700) and National Natural Science Foundation of China (21422307, U1601211, 21633008).

REFERENCES

(1) Schlögl, R. Heterogeneous Catalysis. *Angew. Chem., Int. Ed.* **2015**, *54* (11), 3465−3520.
(2) Dhara, K.; Sarkar, K.; Roy, P.; Nandi, M.; Bhaumik, A.; Banerjee, P. A Highly Enantioselective Chiral Schiff-Base Fluorescent Sensor for Mandelic Acid. *Tetrahedron* **2008**, *64* (14), 3153−3159.
(3) Jia, C.-J.; Schüth, F. Colloidal Metal Nanoparticles as a Component of Designed Catalyst. *Phys. Chem. Chem. Phys.* **2011**, *13* (7), 2457−2487.
(4) Li, Y.; Hong, X. M.; Collard, D. M.; El-Sayed, M. A. Suzuki Cross-Coupling Reactions Catalyzed by Palladium Nanoparticles in Aqueous Solution. *Org. Lett.* **2000**, *2* (15), 2385−2388.
(5) Crooks, R. M.; Zhao, M.; Sun, L.; Chechik, V.; Yeung, L. K. Dendrimer-Encapsulated Metal Nanoparticles: Synthesis, Characterization, and Applications to Catalysis. *Acc. Chem. Res.* **2001**, *34* (3), 181−190.
(6) Zope, B. N.; Hibbitts, D. D.; Neurock, M.; Davis, R. J. Reactivity of the Gold/Water Interface During Selective Oxidation Catalysis. *Science* **2010**, *330* (6000), 74−78.
(7) Somorjai, G. A.; Contreras, A. M.; Montano, M.; Rioux, R. M. Clusters, Surfaces, and Catalysis. *Proc. Natl. Acad. Sci. U. S. A.* **2006**, *103* (28), 10577−10583.
(8) Liu, X.; He, L.; Liu, Y.-M.; Cao, Y. Supported Gold Catalysis: From Small Molecule Activation to Green Chemical Synthesis. *Acc. Chem. Res.* **2014**, *47* (3), 793−804.
(9) Somorjai, G. A. Modern Surface Science and Surface Technologies: An Introduction. *Chem. Rev.* **1996**, *96* (4), 1223−1236.
(10) Burda, C.; Chen, X.; Narayanan, R.; El-Sayed, M. A. Chemistry and Properties of Nanocrystals of Different Shapes. *Chem. Rev.* **2005**, *105* (4), 1025−1102.
(11) Somorjai, G. A.; Li, Y. *Introduction to Surface Chemistry and Catalysis*, 2nd ed.; John Wiley & Sons: New York, 2010.
(12) De Cremer, G.; Sels, B. F.; De Vos, D. E.; Hofkens, J.; Roeffaers, M. B. J. NASCA Microscopy: Super-Resolution Mapping of Chemical Reaction Centers. In *Far-Field Optical Nanoscopy*; Tinnefeld, P., Eggeling, C., Hell, W. S., Eds.; Springer Series on Fluorescence; Springer: Berlin, 2015; Vol. 14, pp 245−261.
(13) Habuchi, S. Super-Resolution Molecular and Functional Imaging of Nanoscale Architectures in Life and Materials Science. *Front. Bioeng. Biotechnol.* **2014**, *2*, 20.
(14) Wang, W.; Gu, J.; He, T.; Shen, Y.; Xi, S.; Tian, L.; Li, F.; Li, H.; Yan, L.; Zhou, X. Optical Super-Resolution Microscopy and Its Applications in Nano-Catalysis. *Nano Res.* **2015**, *8* (2), 441−455.
(15) Whelan, D. R.; Bell, T. D. M. Super-Resolution Single-Molecule Localization Microscopy: Tricks of the Trade. *J. Phys. Chem. Lett.* **2015**, *6* (3), 374−382.
(16) Janssen, K. P. F.; De Cremer, G.; Neely, R. K.; Kubarev, A. V.; Van Loon, J.; Martens, J. A.; De Vos, D. E.; Roeffaers, M. B. J.; Hofkens, J. Single Molecule Methods for the Study of Catalysis: From Enzymes to Heterogeneous Catalysts. *Chem. Soc. Rev.* **2014**, *43*, 990−1006.
(17) Chen, P.; Zhou, X.; Andoy, N. M.; Han, K.-S.; Choudhary, E.; Zou, N.; Chen, G.; Shen, H. Spatiotemporal Catalytic Dynamics within Single Nanocatalysts Revealed by Single-Molecule Microscopy. *Chem. Soc. Rev.* **2014**, *43*, 1107−1117.
(18) Locquin, M.; Langeron, M. *Handbook of Microscopy*; Butterworth-Heinemann: Oxford, U.K., 1983.
(19) Pohl, D. W.; Denk, W.; Lanz, M. Optical Stethoscopy: Image Recording with Resolution $\lambda/20$. *Appl. Phys. Lett.* **1984**, *44* (7), 651−653.
(20) Masters, B. R. Handbook of Biological Confocal Microscopy, Second Edition, J. B. Pawley, Ed. *Opt. Eng.* **1996**, *35* (9), 2765−2766.
(21) Zipfel, W. R.; Williams, R. M.; Webb, W. W. Nonlinear Magic: Multiphoton Microscopy in the Biosciences. *Nat. Biotechnol.* **2003**, *21* (11), 1369−1377.
(22) Hell, S.; Stelzer, E. H. K. Fundamental Improvement of Resolution with a 4pi-Confocal Fluorescence Microscope Using Two-Photon Excitation. *Opt. Commun.* **1992**, *93* (5), 277−282.
(23) Gustafsson; Agard; Sedat. I^5M: 3D Widefield Light Microscopy with Better Than 100 nm Axial Resolution. *J. Microsc.* **1999**, *195* (1), 10−16.
(24) Bailey, B.; Farkas, D. L.; Taylor, D. L.; Lanni, F. Enhancement of Axial Resolution in Fluorescence Microscopy by Standing-Wave Excitation. *Nature* **1993**, *366* (6450), 44−48.
(25) Huang, B.; Bates, M.; Zhuang, X. Super Resolution Fluorescence Microscopy. *Annu. Rev. Biochem.* **2009**, *78*, 993−1016.
(26) Klar, T. A.; Hell, S. W. Subdiffraction Resolution in Far-Field Fluorescence Microscopy. *Opt. Lett.* **1999**, *24* (14), 954−956.
(27) Hell, S. W.; Kroug, M. Ground-State-Depletion Fluorscence Microscopy: A Concept for Breaking the Diffraction Resolution Limit. *Appl. Phys. B: Lasers Opt.* **1995**, *60* (5), 495−497.
(28) Hell, S. W. Strategy for Far-Field Optical Imaging and Writing without Diffraction Limit. *Phys. Lett. A* **2004**, *326* (1−2), 140−145.
(29) Rust, M. J.; Bates, M.; Zhuang, X. Sub-Diffraction-Limit Imaging by Stochastic Optical Reconstruction Microscopy (Storm). *Nat. Methods* **2006**, *3* (10), 793−796.
(30) Betzig, E.; Patterson, G. H.; Sougrat, R.; Lindwasser, O. W.; Olenych, S.; Bonifacino, J. S.; Davidson, M. W.; Lippincott-Schwartz, J.; Hess, H. F. Imaging Intracellular Fluorescent Proteins at Nanometer Resolution. *Science* **2006**, *313* (5793), 1642−1645.
(31) Hess, S. T.; Girirajan, T. P. K.; Mason, M. D. Ultra-High Resolution Imaging by Fluorescence Photoactivation Localization Microscopy. *Biophys. J.* **2006**, *91* (11), 4258−4272.
(32) Dertinger, T.; Colyer, R.; Iyer, G.; Weiss, S.; Enderlein, J. Fast, Background-Free, 3D Super-Resolution Optical Fluctuation Imaging (Sofi). *Proc. Natl. Acad. Sci. U. S. A.* **2009**, *106* (52), 22287−22292.
(33) Wolter, S.; Schüttpelz, M.; Tscherepanow, M.; Van De Linde, S.; Heilemann, M.; Sauer, M. Real-Time Computation of Subdiffraction-Resolution Fluorescence Images. *J. Microsc.* **2010**, *237* (1), 12−22.
(34) Heilemann, M.; van de Linde, S.; Schüttpelz, M.; Kasper, R.; Seefeldt, B.; Mukherjee, A.; Tinnefeld, P.; Sauer, M. Subdiffraction-Resolution Fluorescence Imaging with Conventional Fluorescent Probes. *Angew. Chem., Int. Ed.* **2008**, *47* (33), 6172−6176.
(35) Huang, B.; Babcock, H.; Zhuang, X. Breaking the Diffraction Barrier: Super-Resolution Imaging of Cells. *Cell* **2010**, *143* (7), 1047−1058.
(36) Heintzmann, R.; Gustafsson, M. G. L. Subdiffraction Resolution in Continuous Samples. *Nat. Photonics* **2009**, *3* (7), 362−364.
(37) Fernandez-Suarez, M.; Ting, A. Y. Fluorescent Probes for Super-Resolution Imaging in Living Cells. *Nat. Rev. Mol. Cell Biol.* **2008**, *9* (12), 929−943.
(38) Lippincott-Schwartz, J.; Patterson, G. H. Photoactivatable Fluorescent Proteins for Diffraction-Limited and Super-Resolution Imaging. *Trends Cell Biol.* **2009**, *19* (11), 555−565.
(39) Huang, B. Super-Resolution Optical Microscopy: Multiple Choices. *Curr. Opin. Chem. Biol.* **2010**, *14* (1), 10−14.

DOI: 10.1021/acs.chemrev.6b00673
Chem. Rev. XXXX, XXX, XXX−XXX

(40) Sydor, A. M.; Czymmek, K. J.; Puchner, E. M.; Mennella, V. Super-Resolution Microscopy: From Single Molecules to Supramolecular Assemblies. *Trends Cell Biol.* **2015**, *25* (12), 730−748.
(41) Hell, S. W.; Wichmann, J. Breaking the Diffraction Resolution Limit by Stimulated Emission: Stimulated-Emission-Depletion Fluorescence Microscopy. *Opt. Lett.* **1994**, *19* (11), 780−782.
(42) Gustafsson, M. G. L. Nonlinear Structured-Illumination Microscopy: Wide-Field Fluorescence Imaging with Theoretically Unlimited Resolution. *Proc. Natl. Acad. Sci. U. S. A.* **2005**, *102* (37), 13081−13086.
(43) Thompson, R. E.; Larson, D. R.; Webb, W. W. Precise Nanometer Localization Analysis for Individual Fluorescent Probes. *Biophys. J.* **2002**, *82* (5), 2775−2783.
(44) Pertsinidis, A.; Zhang, Y.; Chu, S. Subnanometre Single-Molecule Localization, Registration and Distance Measurements. *Nature* **2010**, *466* (7306), 647−651.
(45) Roeffaers, M. B. J.; De Cremer, G.; Libeert, J.; Ameloot, R.; Dedecker, P.; Bons, A.-J.; Bückins, M.; Martens, J. A.; Sels, B. F.; De Vos, D. E.; Hofkens, J. Super-Resolution Reactivity Mapping of Nanostructured Catalyst Particles. *Angew. Chem.* **2009**, *121* (49), 9449−9453.
(46) Ertl, G.; Knozinger, H.; Schüth, F.; Weitkamp, J., Eds. *Handbook of Heterogeneous Catalysis*, 2nd ed.; Wiley-VCH: Weinheim, Germany, 2008.
(47) Buurmans, I. L.; Weckhuysen, B. M. Heterogeneities of Individual Catalyst Particles in Space and Time as Monitored by Spectroscopy. *Nat. Chem.* **2012**, *4* (11), 873−886.
(48) Si, R.; Flytzani-Stephanopoulos, M. Shape and Crystal-Plane Effects of Nanoscale Ceria on the Activity of Au−CeO_2 Catalysts for the Water−Gas Shift Reaction. *Angew. Chem.* **2008**, *120* (15), 2926−2929.
(49) Crespo-Quesada, M.; Yarulin, A.; Jin, M.; Xia, Y.; Kiwi-Minsker, L. Structure Sensitivity of Alkynol Hydrogenation on Shape- and Size-Controlled Palladium Nanocrystals: Which Sites Are Most Active and Selective? *J. Am. Chem. Soc.* **2011**, *133* (32), 12787−12794.
(50) Collins, G.; Schmidt, M.; O'Dwyer, C.; Holmes, J. D.; McGlacken, G. P. The Origin of Shape Sensitivity in Palladium-Catalyzed Suzuki−Miyaura Cross Coupling Reactions. *Angew. Chem., Int. Ed.* **2014**, *53* (16), 4142−4145.
(51) Tao, F.; Grass, M. E.; Zhang, Y.; Butcher, D. R.; Renzas, J. R.; Liu, Z.; Chung, J. Y.; Mun, B. S.; Salmeron, M.; Somorjai, G. A. Reaction-Driven Restructuring of Rh-Pd and Pt-Pd Core-Shell Nanoparticles. *Science* **2008**, *322* (5903), 932−934.
(52) Somorjai, G. A. The Experimental Evidence of the Role of Surface Restructuring During Catalytic Reactions. *Catal. Lett.* **1992**, *12* (1−3), 17−34.
(53) Somorjai, G. A. Surface Reconstruction and Catalysis. *Annu. Rev. Phys. Chem.* **1994**, *45* (1), 721−751.
(54) Sambur, J. B.; Chen, P. Approaches to Single-Nanoparticle Catalysis. *Annu. Rev. Phys. Chem.* **2014**, *65* (1), 395−422.
(55) Chen, P.; Zhou, X.; Shen, H.; Andoy, N. M.; Choudhary, E.; Han, K.-S.; Liu, G.; Meng, W. Single-Molecule Fluorescence Imaging of Nanocatalytic Processes. *Chem. Soc. Rev.* **2010**, *39* (12), 4560−4570.
(56) Tachikawa, T.; Majima, T. Single-Molecule, Single-Particle Fluorescence Imaging of TiO_2-Based Pphotocatalytic Reactions. *Chem. Soc. Rev.* **2010**, *39* (12), 4802−4819.
(57) De Cremer, G.; Sels, B. F.; De Vos, D. E.; Hofkens, J.; Roeffaers, M. B. J. Fluorescence Micro(Spectro)Scopy as a Tool to Study Catalytic Materials in Action. *Chem. Soc. Rev.* **2010**, *39* (12), 4703−4717.
(58) Roeffaers, M. B.; De Cremer, G.; Uji-i, H.; Muls, B.; Sels, B. F.; Jacobs, P. A.; De Schryver, F. C.; De Vos, D. E.; Hofkens, J. Single-Molecule Fluorescence Spectroscopy in (Bio) Catalysis. *Proc. Natl. Acad. Sci. U. S. A.* **2007**, *104* (31), 12603−12609.
(59) Roeffaers, M. B. J.; Hofkens, J.; De Cremer, G.; De Schryver, F. C.; Jacobs, P. A.; De Vos, D. E.; Sels, B. F. Fluorescence Microscopy: Bridging the Phase Gap in Catalysis. *Catal. Today* **2007**, *126* (1−2), 44−53.
(60) Xu, S.-Y.; Ruan, Y.-B.; Luo, X.-X.; Gao, Y.-F.; Zhao, J.-S.; Shen, J.-S.; Jiang, Y.-B. Enhanced Saccharide Sensing Based on Simple Phenylboronic Acid Receptor by Coupling to Suzuki Homocoupling Reaction. *Chem. Commun.* **2010**, *46* (32), 5864−5866.
(61) Blum, S. A. Location Change Method for Imaging Chemical Reactivity and Catalysis with Single-Molecule and -Particle Fluorescence Microscopy. *Phys. Chem. Chem. Phys.* **2014**, *16* (31), 16333−16339.
(62) Cordes, T.; Blum, S. A. Opportunities and Challenges in Single-Molecule and Single-Particle Fluorescence Microscopy for Mechanistic Studies of Chemical Reactions. *Nat. Chem.* **2013**, *5* (12), 993−999.
(63) Rybina, A.; Wirtz, M.; Brox, D.; Krämer, R.; Jung, G.; Herten, D.-P. Toward Single-Molecule Catalysis. In *Molecular Catalysts: Structure and Functional Design*; Gade, L. H., Hofmann, P., Eds.; Wiley-VCH Verlag GmbH & Co. KGaA: Weinheim, Germany, 2014; Chapter 3, pp 53−80.
(64) De Cremer, G.; Bartholomeeusen, E.; Pescarmona, P. P.; Lin, K.; De Vos, D. E.; Hofkens, J.; Roeffaers, M. B. J.; Sels, B. F. The Influence of Diffusion Phenomena on Catalysis: A Study at the Single Particle Level Using Fluorescence Microscopy. *Catal. Today* **2010**, *157* (1−4), 236−242.
(65) Roeffaers, M. B. J.; Sels, B. F.; Loos, D.; Kohl, C.; Müllen, K.; Jacobs, P. A.; Hofkens, J.; De Vos, D. E. In Situ Space- and Time-Resolved Sorption Kinetics of Anionic Dyes on Individual Ldh Crystals. *ChemPhysChem* **2005**, *6* (11), 2295−2299.
(66) Sels, B. F.; De Vos, D. E.; Jacobs, P. A. Hydrotalcite-Like Anionic Clays in Catalytic Organic Reactions. *Catal. Rev.: Sci. Eng.* **2001**, *43* (4), 443−488.
(67) Lazaridis, N.; Karapantsios, T.; Georgantas, D. Kinetic Analysis for the Removal of a Reactive Dye from Aqueous Solution onto Hydrotalcite by Adsorption. *Water Res.* **2003**, *37* (12), 3023−3033.
(68) Hussein, M. Z.; Yahaya, A. H.; Ping, L. M. Dye-Interleaved Nanocomposite: Evan's Blue in the Lamella of Mg−Al-Layered Double Hydroxide. *Dyes Pigm.* **2004**, *63* (2), 135−140.
(69) Martínez, V. M. n.; Cremer, G. D.; Roeffaers, M. B. J.; Sliwa, M.; Baruah, M.; De Vos, D. E.; Hofkens, J.; Sels, B. F. Exploration of Single Molecule Events in a Haloperoxidase and Its Biomimic: Localization of Halogenation Activity. *J. Am. Chem. Soc.* **2008**, *130* (40), 13192−13193.
(70) Roeffaers, M. B. J.; Sels, B. F.; Uji-i, H.; De Schryver, F. C.; Jacobs, P. A.; De Vos, D. E.; Hofkens, J. Spatially Resolved Observation of Crystal-Face-Dependent Catalysis by Single Turnover Counting. *Nature* **2006**, *439* (7076), 572−575.
(71) Li, Y.; Yu, J. New Stories of Zeolite Structures: Their Descriptions, Determinations, Predictions, and Evaluations. *Chem. Rev.* **2014**, *114* (14), 7268−7316.
(72) Lee, C. S.; Park, T. J.; Lee, W. Y. Alkylation of Toluene over Double Structure ZSM-5 Type Catalysts Covered with a Silicalite Shell. *Appl. Catal., A* **1993**, *96* (2), 151−161.
(73) Jacobs, P. A.; van Santen, R. A., Eds. *Zeolites: Facts, Figures, Future. Proceedings of the 8th International Zeolite Conference, Amsterdam, The Netherlands, July 10−14, 1989*; Elsevier: Amsterdam, 1989; Vol. *49*.
(74) Rigutto, M. Cracking and Hydrocracking. In *Zeolites and Catalysis: Synthesis, Reactions and Applications*; Čejka, J., Corma, A., Zones, S., Eds.; Wiley-VCH: Weinheim, Germany, 2010; Vol. *2*, Chapter 18, pp 547−584.
(75) Stöcker, M. Methanol to Olefins (MTO) and Methanol to Gasoline (MTG). In *Zeolites and Catalysis: Synthesis, Reactions and Applications*; Čejka, J., Corma, A., Zones, S., Eds.; Wiley-VCH: Weinheim, Germany, 2010; Vol. *2*, Chapter 22, pp 687−712.
(76) Kerssens, M. M.; Sprung, C.; Whiting, G. T.; Weckhuysen, B. M. Selective Staining of Zeolite Acidity: Recent Progress and Future Perspectives on Fluorescence Microscopy. *Microporous Mesoporous Mater.* **2014**, *189*, 136−143.
(77) Pfenniger, M.; Calzaferri, G. Intrazeolite Diffusion Kinetics of Dye Molecules in the Nanochannels of Zeolite L, Monitored by Energy Transfer. *ChemPhysChem* **2000**, *1* (4), 211−217.
(78) Busby, M.; Blum, C.; Tibben, M.; Fibikar, S.; Calzaferri, G.; Subramaniam, V.; De Cola, L. Time, Space, and Spectrally Resolved Studies on J-Aggregate Interactions in Zeolite L Nanochannels. *J. Am. Chem. Soc.* **2008**, *130* (33), 10970−10976.
(79) Laeri, F., Schüth, F., Simon, U., Wark, M., Eds. *Host-Guest-Systems Based on Nanoporous Crystals*; Wiley-VCH: Weinheim, Germany, 2006.

DOI: 10.1021/acs.chemrev.6b00673
Chem. Rev. XXXX, XXX, XXX−XXX

(80) Seebacher, C.; Rau, J.; Deeg, F. W.; Bräuchle, C.; Altmaier, S.; Jäger, R.; Behrens, P. Visualization of Mesostructures and Organic Guest Inclusion in Molecular Sieves with Confocal Microscopy. *Adv. Mater.* **2001**, *13* (18), 1374−1377.
(81) Roeffaers, M. B.; Ameloot, R.; Baruah, M.; Uji-i, H.; Bulut, M.; De Cremer, G.; Müller, U.; Jacobs, P. A.; Hofkens, J.; Sels, B. F.; De Vos, D. E. Morphology of Large ZSM-5 Crystals Unraveled by Fluorescence Microscopy. *J. Am. Chem. Soc.* **2008**, *130* (17), 5763−5772.
(82) Kahr, B.; Gurney, R. W. Dyeing Crystals. *Chem. Rev.* **2001**, *101* (4), 893−952.
(83) Ameloot, R.; Vermoortele, F.; Hofkens, J.; De Schryver, F. C.; De Vos, D. E.; Roeffaers, M. B. J. Three-Dimensional Visualization of Defects Formed During the Synthesis of Metal−Organic Frameworks: A Fluorescence Microscopy Study. *Angew. Chem., Int. Ed.* **2013**, *52* (1), 401−405.
(84) Aramburo, L. R.; Ruiz-Martinez, J.; Hofmann, J. P.; Weckhuysen, B. M. Imaging the Effect of a Hydrothermal Treatment on the Pore Accessibility and Acidity of Large ZSM-5 Zeolite Crystals by Selective Staining. *Catal. Sci. Technol.* **2013**, *3* (5), 1208−1214.
(85) Geus, E. R.; Jansen, J. C.; van Bekkum, H. Calcination of Large Mfi-Type Single Crystals: Part 1. Evidence for the Occurrence of Consecutive Growth Forms and Possible Diffusion Barriers Arising Thereof. *Zeolites* **1994**, *14* (2), 82−88.
(86) Karwacki, L.; Stavitski, E.; Kox, M. H. F.; Kornatowski, J.; Weckhuysen, B. M. Intergrowth Structure of Zeolite Crystals as Determined by Optical and Fluorescence Microscopy of the Template-Removal Process. *Angew. Chem.* **2007**, *119* (38), 7366−7369.
(87) Karwacki, L.; Kox, M. H. F.; Matthijs de Winter, D. A.; Drury, M. R.; Meeldijk, J. D.; Stavitski, E.; Schmidt, W.; Mertens, M.; Cubillas, P.; John, N.; et al. Morphology-Dependent Zeolite Intergrowth Structures Leading to Distinct Internal and Outer-Surface Molecular Diffusion Barriers. *Nat. Mater.* **2009**, *8* (12), 959−965.
(88) Mores, D.; Stavitski, E.; Kox, M. H. F.; Kornatowski, J.; Olsbye, U.; Weckhuysen, B. M. Space- and Time-Resolved in-Situ Spectroscopy on the Coke Formation in Molecular Sieves: Methanol-to-Olefin Conversion over H-ZSM-5 and H-SAPO-34. *Chem. - Eur. J.* **2008**, *14* (36), 11320−11327.
(89) Parvulescu, A. N.; Mores, D.; Stavitski, E.; Teodorescu, C. M.; Bruijnincx, P. C. A.; Gebbink, R. J. M. K.; Weckhuysen, B. M. Chemical Imaging of Catalyst Deactivation During the Conversion of Renewables at the Single Particle Level: Etherification of Biomass-Based Polyols with Alkenes over H-Beta Zeolites. *J. Am. Chem. Soc.* **2010**, *132* (30), 10429−10439.
(90) Mores, D.; Stavitski, E.; Verkleij, S. P.; Lombard, A.; Cabiac, A.; Rouleau, L.; Patarin, J.; Simon-Masseron, A.; Weckhuysen, B. M. Core-Shell H-ZSM-5/Silicalite-1 Composites: Bronsted Acidity and Catalyst Deactivation at the Individual Particle Level. *Phys. Chem. Chem. Phys.* **2011**, *13* (35), 15985−15994.
(91) Cohen, B.; Sanchez, F.; Douhal, A. Mapping the Distribution of an Individual Chromophore Interacting with Silica-Based Nanomaterials. *J. Am. Chem. Soc.* **2010**, *132* (15), 5507−5514.
(92) Roeffaers, M. B. J.; Sels, B. F.; Uji-i, H.; Blanpain, B.; L'Hoëst, P.; Jacobs, P. A.; De Schryver, F. C.; Hofkens, J.; De Vos, D. E. Space- and Time-Resolved Visualization of Acid Catalysis in ZSM-5 Crystals by Fluorescence Microscopy. *Angew. Chem.* **2007**, *119* (10), 1736−1739.
(93) Kox, M. H. F.; Stavitski, E.; Weckhuysen, B. M. Nonuniform Catalytic Behavior of Zeolite Crystals as Revealed by in Situ Optical Microspectroscopy. *Angew. Chem., Int. Ed.* **2007**, *46* (20), 3652−3655.
(94) Stavitski, E.; Kox, M. H. F.; Weckhuysen, B. M. Revealing Shape Selectivity and Catalytic Activity Trends within the Pores of H-ZSM-5 Crystals by Time- and Space-Resolved Optical and Fluorescence Microspectroscopy. *Chem. - Eur. J.* **2007**, *13* (25), 7057−7065.
(95) Roeffaers, M. B. J.; Ameloot, R.; Bons, A.-J.; Mortier, W.; De Cremer, G.; de Kloe, R.; Hofkens, J.; De Vos, D. E.; Sels, B. F. Relating Pore Structure to Activity at the Subcrystal Level for ZSM-5: An Electron Backscattering Diffraction and Fluorescence Microscopy Study. *J. Am. Chem. Soc.* **2008**, *130* (41), 13516−13517.
(96) Stavitski, E.; Drury, M. R.; de Winter, D. A. M.; Kox, M. H. F.; Weckhuysen, B. M. Intergrowth Structure of Zeolite Crystals and Pore Orientation of Individual Subunits Revealed by Electron Backscatter Diffraction/Focused Ion Beam Experiments. *Angew. Chem., Int. Ed.* **2008**, *47* (30), 5637−5640.
(97) Kox, M. H. F.; Stavitski, E.; Groen, J. C.; Pérez-Ramírez, J.; Kapteijn, F.; Weckhuysen, B. M. Visualizing the Crystal Structure and Locating the Catalytic Activity of Micro- and Mesoporous ZSM-5 Zeolite Crystals by Using in Situ Optical and Fluorescence Microscopy. *Chem. - Eur. J.* **2008**, *14* (6), 1718−1725.
(98) Ruiz-Martínez, J.; Buurmans, I. L. C.; Knowles, W. V.; van der Beek, D.; Bergwerff, J. A.; Vogt, E. T. C.; Weckhuysen, B. M. Microspectroscopic Insight into the Deactivation Process of Individual Cracking Catalyst Particles with Basic Sulfur Components. *Appl. Catal., A* **2012**, *419*−*420*, 84−94.
(99) Buurmans, I. L. C.; Ruiz-Martínez, J.; van Leeuwen, S. L.; van der Beek, D.; Bergwerff, J. A.; Knowles, W. V.; Vogt, E. T. C.; Weckhuysen, B. M. Staining of Fluid-Catalytic-Cracking Catalysts: Localising Brønsted Acidity within a Single Catalyst Particle. *Chem. - Eur. J.* **2012**, *18* (4), 1094−1101.
(100) Buurmans, I. L. C.; Ruiz-Martínez, J.; Knowles, W. V.; van der Beek, D.; Bergwerff, J. A.; Vogt, E. T. C.; Weckhuysen, B. M. Catalytic Activity in Individual Cracking Catalyst Particles Imaged Throughout Different Life Stages by Selective Staining. *Nat. Chem.* **2011**, *3* (11), 862−867.
(101) Karreman, M. A.; Buurmans, I. L. C.; Geus, J. W.; Agronskaia, A. V.; Ruiz-Martínez, J.; Gerritsen, H. C.; Weckhuysen, B. M. Integrated Laser and Electron Microscopy Correlates Structure of Fluid Catalytic Cracking Particles to Brønsted Acidity. *Angew. Chem., Int. Ed.* **2012**, *51* (6), 1428−1431.
(102) Karreman, M. A.; Buurmans, I. L. C.; Agronskaia, A. V.; Geus, J. W.; Gerritsen, H. C.; Weckhuysen, B. M. Probing the Different Life Stages of a Fluid Catalytic Cracking Particle with Integrated Laser and Electron Microscopy. *Chem. - Eur. J.* **2013**, *19* (12), 3846−3859.
(103) Ruiz-Martínez, J.; Beale, A. M.; Deka, U.; O'Brien, M. G.; Quinn, P. D.; Mosselmans, J. F. W.; Weckhuysen, B. M. Correlating Metal Poisoning with Zeolite Deactivation in an Individual Catalyst Particle by Chemical and Phase-Sensitive X-ray Microscopy. *Angew. Chem., Int. Ed.* **2013**, *52* (23), 5983−5987.
(104) Sprung, C.; Weckhuysen, B. M. Dispersion and Orientation of Zeolite ZSM-5 Crystallites within a Fluid Catalytic Cracking Catalyst Particle. *Chem. - Eur. J.* **2014**, *20* (13), 3667−3677.
(105) Sprung, C.; Weckhuysen, B. M. Differences in the Location of Guest Molecules within Zeolite Pores as Revealed by Multilaser Excitation Confocal Fluorescence Microscopy: Which Molecule Is Where? *J. Am. Chem. Soc.* **2015**, *137* (5), 1916−1928.
(106) Sun, X.; Xie, J.; Xu, J.; Higgins, D. A.; Hohn, K. L. Single-Molecule Studies of Acidity Distributions in Mesoporous Aluminosilicate Thin Films. *Langmuir* **2015**, *31* (20), 5667−5675.
(107) De Cremer, G.; Roeffaers, M. B. J.; Bartholomeeusen, E.; Lin, K.; Dedecker, P.; Pescarmona, P. P.; Jacobs, P. A.; De Vos, D. E.; Hofkens, J.; Sels, B. F. High-Resolution Single-Turnover Mapping Reveals Intraparticle Diffusion Limitation in Ti-Mcm-41-Catalyzed Epoxidation. *Angew. Chem.* **2010**, *122* (5), 920−923.
(108) Liu, K.-L.; Kubarev, A. V.; Van Loon, J.; Uji-i, H.; De Vos, D. E.; Hofkens, J.; Roeffaers, M. B. J. Rationalizing Inter- and Intracrystal Heterogeneities in Dealuminated Acid Mordenite Zeolites by Stimulated Raman Scattering Microscopy Correlated with Super-Resolution Fluorescence Microscopy. *ACS Nano* **2014**, *8* (12), 12650−12659.
(109) Kubarev, A. V.; Janssen, K. P. F.; Roeffaers, M. B. J. Noninvasive Nanoscopy Uncovers the Impact of the Hierarchical Porous Structure on the Catalytic Activity of Single Dealuminated Mordenite Crystals. *ChemCatChem* **2015**, *7* (22), 3646−3650.
(110) Ristanović, Z.; Kerssens, M. M.; Kubarev, A. V.; Hendriks, F. C.; Dedecker, P.; Hofkens, J.; Roeffaers, M. B. J.; Weckhuysen, B. M. High-Resolution Single-Molecule Fluorescence Imaging of Zeolite Aggregates within Real-Life Fluid Catalytic Cracking Particles. *Angew. Chem., Int. Ed.* **2015**, *54* (6), 1836−1840.
(111) Ristanović, Z.; Hofmann, J. P.; De Cremer, G.; Kubarev, A. V.; Rohnke, M.; Meirer, F.; Hofkens, J.; Roeffaers, M. B. J.; Weckhuysen, B.

DOI: 10.1021/acs.chemrev.6b00673
Chem. Rev. XXXX, XXX, XXX−XXX

M. Quantitative 3D Fluorescence Imaging of Single Catalytic Turnovers Reveals Spatiotemporal Gradients in Reactivity of Zeolite H-ZSM-5 Crystals Upon Steaming. *J. Am. Chem. Soc.* **2015**, *137* (20), 6559−6568.
(112) Ristanović, Z.; Kubarev, A. V.; Hofkens, J.; Roeffaers, M. B. J.; Weckhuysen, B. M. Single Molecule Nanospectroscopy Visualizes Proton-Transfer Processes within a Zeolite Crystal. *J. Am. Chem. Soc.* **2016**, *138* (41), 13586−13596.
(113) Rao, C. N. R.; Kulkarni, G. U.; Thomas, P. J.; Edwards, P. P. Size-Dependent Chemistry: Properties of Nanocrystals. *Chem. - Eur. J.* **2002**, *8* (1), 28−35.
(114) Cheong, S.; Watt, J. D.; Tilley, R. D. Shape Control of Platinum and Palladium Nanoparticles for Catalysis. *Nanoscale* **2010**, *2* (10), 2045−2053.
(115) Zeng, J.; Zhang, Q.; Chen, J.; Xia, Y. A Comparison Study of the Catalytic Properties of Au-Based Nanocages, Nanoboxes, and Nanoparticles. *Nano Lett.* **2010**, *10* (1), 30−35.
(116) Gao, D.; Zhou, H.; Wang, J.; Miao, S.; Yang, F.; Wang, G.; Wang, J.; Bao, X. Size-Dependent Electrocatalytic Reduction of Co2 over Pd Nanoparticles. *J. Am. Chem. Soc.* **2015**, *137* (13), 4288−4291.
(117) Arán-Ais, R. M.; Yu, Y.; Hovden, R.; Solla-Gullón, J.; Herrero, E.; Feliu, J. M.; Abruña, H. D. Identical Location Transmission Electron Microscopy Imaging of Site-Selective Pt Nanocatalysts: Electrochemical Activation and Surface Disordering. *J. Am. Chem. Soc.* **2015**, *137* (47), 14992−14998.
(118) Goodman, D. W. Model Studies in Catalysis Using Surface Science Probes. *Chem. Rev.* **1995**, *95* (3), 523−536.
(119) Purser, S.; Moore, P. R.; Swallow, S.; Gouverneur, V. Fluorine in Medicinal Chemistry. *Chem. Soc. Rev.* **2008**, *37* (2), 320−330.
(120) Kim, H.; Kosuda, K. M.; Van Duyne, R. P.; Stair, P. C. Resonance Raman and Surface- and Tip-Enhanced Raman Spectroscopy Methods to Study Solid Catalysts and Heterogeneous Catalytic Reactions. *Chem. Soc. Rev.* **2010**, *39* (12), 4820−4844.
(121) Nilsson, A., Pettersson, L. G. M., Nørskov, J. K., Eds. *Chemical Bonding at Surfaces and Interfaces*; Elsevier: Amsterdam, 2011.
(122) Santen, R. A. v.; Neurock, M.; Shetty, S. G. Reactivity Theory of Transition-Metal Surfaces: A Brønsted−Evans−Polanyi Linear Activation Energy−Free-Energy Analysis. *Chem. Rev.* **2010**, *110* (4), 2005−2048.
(123) Zheng, H.; Smith, R. K.; Jun, Y.-w.; Kisielowski, C.; Dahmen, U.; Alivisatos, A. P. Observation of Single Colloidal Platinum Nanocrystal Growth Trajectories. *Science* **2009**, *324* (5932), 1309−1312.
(124) Zheng, H.; Rivest, J. B.; Miller, T. A.; Sadtler, B.; Lindenberg, A.; Toney, M. F.; Wang, L.-W.; Kisielowski, C.; Alivisatos, A. P. Observation of Transient Structural-Transformation Dynamics in a Cu2s Nanorod. *Science* **2011**, *333* (6039), 206−209.
(125) Lai, S. C. S.; Dudin, P. V.; Macpherson, J. V.; Unwin, P. R. Visualizing Zeptomole (Electro)Catalysis at Single Nanoparticles within an Ensemble. *J. Am. Chem. Soc.* **2011**, *133* (28), 10744−10747.
(126) Ebejer, N.; Schnippering, M.; Colburn, A. W.; Edwards, M. A.; Unwin, P. R. Localized High Resolution Electrochemistry and Multifunctional Imaging: Scanning Electrochemical Cell Microscopy. *Anal. Chem.* **2010**, *82* (22), 9141−9145.
(127) Hulsken, B.; Van Hameren, R.; Gerritsen, J. W.; Khoury, T.; Thordarson, P.; Crossley, M. J.; Rowan, A. E.; Nolte, R. J. M.; Elemans, J. A. A. W.; Speller, S. Real-Time Single-Molecule Imaging of Oxidation Catalysis at a Liquid-Solid Interface. *Nat. Nanotechnol.* **2007**, *2* (5), 285−289.
(128) Zheng, Z.; Tachikawa, T.; Majima, T. Single-Particle Study of Pt-Modified Au Nanorods for Plasmon-Enhanced Hydrogen Generation in Visible to near-Infrared Region. *J. Am. Chem. Soc.* **2014**, *136* (19), 6870−6873.
(129) Novo, C.; Funston, A. M.; Mulvaney, P. Direct Observation of Chemical Reactions on Single Gold Nanocrystals Using Surface Plasmon Spectroscopy. *Nat. Nanotechnol.* **2008**, *3* (10), 598−602.
(130) Tang, M. L.; Liu, N.; Dionne, J. A.; Alivisatos, A. P. Observations of Shape-Dependent Hydrogen Uptake Trajectories from Single Nanocrystals. *J. Am. Chem. Soc.* **2011**, *133* (34), 13220−13223.
(131) Liu, N.; Tang, M. L.; Hentschel, M.; Giessen, H.; Alivisatos, A. P. Nanoantenna-Enhanced Gas Sensing in a Aingle Tailored Nanofocus. *Nat. Mater.* **2011**, *10* (8), 631−636.
(132) Xiao, X.; Bard, A. J. Observing Single Nanoparticle Collisions at an Ultramicroelectrode by Electrocatalytic Amplification. *J. Am. Chem. Soc.* **2007**, *129* (31), 9610−9612.
(133) Xiao, X.; Fan, F.-R. F.; Zhou, J.; Bard, A. J. Current Transients in Single Nanoparticle Collision Events. *J. Am. Chem. Soc.* **2008**, *130* (49), 16669−16677.
(134) Kwon, S. J.; Fan, F.-R. F.; Bard, A. J. Observing Iridium Oxide (Irox) Single Nanoparticle Collisions at Ultramicroelectrodes. *J. Am. Chem. Soc.* **2010**, *132* (38), 13165−13167.
(135) Dick, J. E.; Bard, A. J. Recognizing Single Collisions of Ptcl62− at Femtomolar Concentrations on Ultramicroelectrodes by Nucleating Electrocatalytic Clusters. *J. Am. Chem. Soc.* **2015**, *137* (43), 13752−13755.
(136) Fan, F.-R. F.; Bard, A. J. Observing Single Nanoparticle Collisions by Electrogenerated Chemiluminescence Amplification. *Nano Lett.* **2008**, *8* (6), 1746−1749.
(137) Murray, R. W. Nanoelectrochemistry: Metal Nanoparticles, Nanoelectrodes, and Nanopores. *Chem. Rev.* **2008**, *108* (7), 2688−2720.
(138) Krapf, D.; Wu, M.-Y.; Smeets, R. M. M.; Zandbergen, H. W.; Dekker, C.; Lemay, S. G. Fabrication and Characterization of Nanopore-Based Electrodes with Radii Down to 2 Nm. *Nano Lett.* **2006**, *6* (1), 105−109.
(139) Li, Y.; Cox, J. T.; Zhang, B. Electrochemical Responses and Electrocatalysis at Single Au Nanoparticles. *J. Am. Chem. Soc.* **2010**, *132* (9), 3047−3054.
(140) Holt, L. R.; Plowman, B. J.; Young, N. P.; Tschulik, K.; Compton, R. G. The Electrochemical Characterization of Single Core−Shell Nanoparticles. *Angew. Chem., Int. Ed.* **2016**, *55* (1), 397−400.
(141) Xu, W.; Kong, J. S.; Yeh, Y.-T. E.; Chen, P. Single-Molecule Nanocatalysis Reveals Heterogeneous Reaction Pathways and Catalytic Dynamics. *Nat. Mater.* **2008**, *7* (12), 992−996.
(142) Han, K. S.; Liu, G.; Zhou, X.; Medina, R. E.; Chen, P. How Does a Single Pt Nanocatalyst Behave in Two Different Reactions? A Single-Molecule Study. *Nano Lett.* **2012**, *12* (3), 1253−1259.
(143) Xu, W.; Kong, J. S.; Chen, P. Probing the Catalytic Activity and Heterogeneity of Au-Nanoparticles at the Single-Molecule Level. *Phys. Chem. Chem. Phys.* **2009**, *11* (15), 2767−2778.
(144) Carrillo, A. I.; Stamplecoskie, K. G.; Marin, M. L.; Scaiano, J. C. 'From the Mole to the Molecule': Ruthenium Catalyzed Nitroarene Reduction Studied with 'Bench', High-Throughput and Single Molecule Fluorescence Techniques. *Catal. Sci. Technol.* **2014**, *4* (7), 1989−1996.
(145) Luisa Marin, M.; Hallett-Tapley, G. L.; Impellizzeri, S.; Fasciani, C.; Simoncelli, S.; Netto-Ferreira, J. C.; Scaiano, J. C. Synthesis, Acid Properties and Catalysis by Niobium Oxide Nanostructured Materials. *Catal. Sci. Technol.* **2014**, *4* (9), 3044−3052.
(146) Ng, J. D.; Upadhyay, S. P.; Marquard, A. N.; Lupo, K. M.; Hinton, D. A.; Padilla, N. A.; Bates, D. M.; Goldsmith, R. H. Single-Molecule Investigation of Initiation Dynamics of an Organometallic Catalyst. *J. Am. Chem. Soc.* **2016**, *138* (11), 3876−3883.
(147) Chen, T.; Zhang, Y.; Xu, W. Single-Molecule Nanocatalysis Reveals Catalytic Activation Energy of Single Nanocatalysts. *J. Am. Chem. Soc.* **2016**, *138* (38), 12414−12421.
(148) Xu, W.; Kong, J. S.; Chen, P. Single-Molecule Kinetic Theory of Heterogeneous and Enzyme Catalysis. *J. Phys. Chem. C* **2009**, *113* (6), 2393−2404.
(149) Zhou, X.; Xu, W.; Liu, G.; Panda, D.; Chen, P. Size-Dependent Catalytic Activity and Dynamics of Gold Nanoparticles at the Single-Molecule Level. *J. Am. Chem. Soc.* **2010**, *132* (1), 138−146.
(150) Chen, T.; Zhang, Y.; Xu, W. Size-Dependent Catalytic Kinetics and Dynamics of Pd Nanocubes: A Single-Particle Study. *Phys. Chem. Chem. Phys.* **2016**, *18* (32), 22494−22502.
(151) Zhang, Y.; Chen, T.; Alia, S.; Pivovar, B. S.; Xu, W. Single-Molecule Nanocatalysis Shows in Situ Deactivation of Pt/C Electrocatalysts During the Hydrogen-Oxidation Reaction. *Angew. Chem., Int. Ed.* **2016**, *55* (9), 3086−3090.

DOI: 10.1021/acs.chemrev.6b00673
Chem. Rev. XXXX, XXX, XXX−XXX

(152) Chen, T.; Chen, S.; Zhang, Y.; Qi, Y.; Zhao, Y.; Xu, W.; Zeng, J. Catalytic Kinetics of Different Types of Surface Atoms on Shaped Pd Nanocrystals. *Angew. Chem.* **2016**, *128* (5), 1871−1875.
(153) Hensle, E. M.; Blum, S. A. Phase Separation Polymerization of Dicyclopentadiene Characterized by in Operando Fluorescence Microscopy. *J. Am. Chem. Soc.* **2013**, *135* (33), 12324−12328.
(154) Hodgson, G. K.; Impellizzeri, S.; Scaiano, J. C. Dye Synthesis in the Pechmann Reaction: Catalytic Behaviour of Samarium Oxide Nanoparticles Studied Using Single Molecule Fluorescence Microscopy. *Chem. Sci.* **2016**, *7* (2), 1314−1321.
(155) Decan, M. R.; Impellizzeri, S.; Marin, M. L.; Scaiano, J. C. Copper Nanoparticle Heterogeneous Catalytic 'Click' Cycloaddition Confirmed by Single-Molecule Spectroscopy. *Nat. Commun.* **2014**, *5*, 4612.
(156) Esfandiari, N. M.; Blum, S. A. Homogeneous Vs Heterogeneous Polymerization Catalysis Revealed by Single-Particle Fluorescence Microscopy. *J. Am. Chem. Soc.* **2011**, *133* (45), 18145−18147.
(157) Zhou, X.; Choudhary, E.; Andoy, N. M.; Zou, N.; Chen, P. Scalable Parallel Screening of Catalyst Activity at the Single-Particle Level and Subdiffraction Resolution. *ACS Catal.* **2013**, *3* (7), 1448−1453.
(158) Zhou, X.; Andoy, N. M.; Liu, G.; Choudhary, E.; Han, K.-S.; Shen, H.; Chen, P. Quantitative Super-Resolution Imaging Uncovers Reactivity Patterns on Single Nanocatalysts. *Nat. Nanotechnol.* **2012**, *7* (4), 237−241.
(159) Andoy, N. M.; Zhou, X.; Choudhary, E.; Shen, H.; Liu, G.; Chen, P. Single-Molecule Catalysis Mapping Quantifies Site-Specific Activity and Uncovers Radial Activity Gradient on Single 2D Nanocrystals. *J. Am. Chem. Soc.* **2013**, *135* (5), 1845−1852.
(160) Zhang, Y.; Lucas, J. M.; Song, P.; Beberwyck, B.; Fu, Q.; Xu, W.; Alivisatos, A. P. Superresolution Fluorescence Mapping of Single-Nanoparticle Catalysts Reveals Spatiotemporal Variations in Surface Reactivity. *Proc. Natl. Acad. Sci. U. S. A.* **2015**, *112* (29), 8959−8964.
(161) Satterfield, C. N. *Heterogeneous Catalysis in Practice*; McGraw-Hill: New York, 1980.
(162) Gulati, A.; Liao, H.; Hafner, J. H. Monitoring Gold Nanorod Synthesis by Localized Surface Plasmon Resonance. *J. Phys. Chem. B* **2006**, *110* (45), 22323−22327.
(163) Shen, H.; Zhou, X.; Zou, N.; Chen, P. Single-Molecule Kinetics Reveals a Hidden Surface Reaction Intermediate in Single-Nanoparticle Catalysis. *J. Phys. Chem. C* **2014**, *118* (46), 26902−26911.
(164) Carbó-Argibay, E.; Rodríguez-González, B.; Gómez-Graña, S.; Guerrero-Martínez, A.; Pastoriza-Santos, I.; Pérez-Juste, J.; Liz-Marzán, L. M. The Crystalline Structure of Gold Nanorods Revisited: Evidence for Higher-Index Lateral Facets. *Angew. Chem.* **2010**, *122* (49), 9587−9590.
(165) Katz-Boon, H.; Rossouw, C. J.; Weyland, M.; Funston, A. M.; Mulvaney, P.; Etheridge, J. Three-Dimensional Morphology and Crystallography of Gold Nanorods. *Nano Lett.* **2011**, *11* (1), 273−278.
(166) Imbihl, R.; Ertl, G. Oscillatory Kinetics in Heterogeneous Catalysis. *Chem. Rev.* **1995**, *95* (3), 697−733.
(167) Krischer, K.; Eiswirth, M.; Ertl, G. Oscillatory Co Oxidation on Pt(110): Modeling of Temporal Self-Organization. *J. Chem. Phys.* **1992**, *96* (12), 9161−9172.
(168) Lee, A. F.; Ellis, C. V.; Naughton, J. N.; Newton, M. A.; Parlett, C. M. A.; Wilson, K. Reaction-Driven Surface Restructuring and Selectivity Control in Allylic Alcohol Catalytic Aerobic Oxidation over Pd. *J. Am. Chem. Soc.* **2011**, *133* (15), 5724−5727.
(169) Wunder, S.; Lu, Y.; Albrecht, M.; Ballauff, M. Catalytic Activity of Faceted Gold Nanoparticles Studied by a Model Reaction: Evidence for Substrate-Induced Surface Restructuring. *ACS Catal.* **2011**, *1* (8), 908−916.
(170) Xin, H. L.; Alayoglu, S.; Tao, R.; Genc, A.; Wang, C.-M.; Kovarik, L.; Stach, E. A.; Wang, L.-W.; Salmeron, M.; Somorjai, G. A.; et al. Revealing the Atomic Restructuring of Pt−Co Nanoparticles. *Nano Lett.* **2014**, *14* (6), 3203−3207.
(171) Bond, G. C. Supported Metal Catalysts: Some Unsolved Problems. *Chem. Soc. Rev.* **1991**, *20* (4), 441−475.
(172) Iglesias-Juez, A.; Beale, A. M.; Maaijen, K.; Weng, T. C.; Glatzel, P.; Weckhuysen, B. M. A Combined in Situ Time-Resolved UV−Vis, Raman and High-Energy Resolution X-ray Absorption Spectroscopy Study on the Deactivation Behavior of Pt and PtSn Propane Dehydrogenation Catalysts under Industrial Reaction Conditions. *J. Catal.* **2010**, *276* (2), 268−279.
(173) Barghi, B.; Fattahi, M.; Khorasheh, F. Kinetic Modeling of Propane Dehydrogenation over an Industrial Catalyst in the Presence of Oxygenated Compounds. *React. Kinet., Mech. Catal.* **2012**, *107* (1), 141−155.
(174) Wang, Y.-J.; Wilkinson, D. P.; Zhang, J. Noncarbon Support Materials for Polymer Electrolyte Membrane Fuel Cell Electrocatalysts. *Chem. Rev.* **2011**, *111* (12), 7625−7651.
(175) Decan, M. R.; Scaiano, J. C. Study of Single Catalytic Events at Copper-in-Charcoal: Localization of Click Activity through Subdiffraction Observation of Single Catalytic Events. *J. Phys. Chem. Lett.* **2015**, *6* (20), 4049−4053.
(176) Zečević, J.; van der Eerden, A. M. J.; Friedrich, H.; de Jongh, P. E.; de Jong, K. P. Heterogeneities of the Nanostructure of Platinum/Zeolite Y Catalysts Revealed by Electron Tomography. *ACS Nano* **2013**, *7* (4), 3698−3705.
(177) Ersen, O.; Werckmann, J.; Houllé, M.; Ledoux, M.-J.; Pham-Huu, C. 3D Electron Microscopy Study of Metal Particles inside Multiwalled Carbon Nanotubes. *Nano Lett.* **2007**, *7* (7), 1898−1907.
(178) Han, R.; Ha, J. W.; Xiao, C.; Pei, Y.; Qi, Z.; Dong, B.; Bormann, N. L.; Huang, W.; Fang, N. Geometry-Assisted Three-Dimensional Superlocalization Imaging of Single-Molecule Catalysis on Modular Multilayer Nanocatalysts. *Angew. Chem.* **2014**, *126* (47), 13079−13083.
(179) Ma, Y.; Wang, X.; Jia, Y.; Chen, X.; Han, H.; Li, C. Titanium Dioxide-Based Nanomaterials for Photocatalytic Fuel Generations. *Chem. Rev.* **2014**, *114* (19), 9987−10043.
(180) White, J. L.; Baruch, M. F.; Pander Iii, J. E.; Hu, Y.; Fortmeyer, I. C.; Park, J. E.; Zhang, T.; Liao, K.; Gu, J.; Yan, Y.; et al. Light-Driven Heterogeneous Reduction of Carbon Dioxide: Photocatalysts and Photoelectrodes. *Chem. Rev.* **2015**, *115* (23), 12888−12935.
(181) Serpone, N.; Lawless, D.; Khairutdinov, R. Size Effects on the Photophysical Properties of Colloidal Anatase TiO_2 Particles: Size Quantization Versus Direct Transitions in This Indirect Semiconductor? *J. Phys. Chem.* **1995**, *99* (45), 16646−16654.
(182) Schneider, J.; Matsuoka, M.; Takeuchi, M.; Zhang, J.; Horiuchi, Y.; Anpo, M.; Bahnemann, D. W. Understanding TiO_2 Photocatalysis: Mechanisms and Materials. *Chem. Rev.* **2014**, *114* (19), 9919−9986.
(183) Tachikawa, T.; Fujitsuka, M.; Majima, T. Mechanistic Insight into the TiO_2 Photocatalytic Reactions: Design of New Photocatalysts. *J. Phys. Chem. C* **2007**, *111* (14), 5259−5275.
(184) Naito, K.; Tachikawa, T.; Fujitsuka, M.; Majima, T. Single-Molecule Fluorescence Imaging of the Remote TiO_2 Photocatalytic Oxidation. *J. Phys. Chem. B* **2005**, *109* (49), 23138−23140.
(185) Naito, K.; Tachikawa, T.; Cui, S.-C.; Sugimoto, A.; Fujitsuka, M.; Majima, T. Single-Molecule Detection of Airborne Singlet Oxygen. *J. Am. Chem. Soc.* **2006**, *128* (51), 16430−16431.
(186) Naito, K.; Tachikawa, T.; Fujitsuka, M.; Majima, T. Single-Molecule Observation of Photocatalytic Reaction in TiO_2 Nanotube: Importance of Molecular Transport through Porous Structures. *J. Am. Chem. Soc.* **2009**, *131* (3), 934−936.
(187) Naito, K.; Tachikawa, T.; Fujitsuka, M.; Majima, T. Real-Time Single-Molecule Imaging of the Spatial and Temporal Distribution of Reactive Oxygen Species with Fluorescent Probes: Applications to TiO_2 Photocatalysts. *J. Phys. Chem. C* **2008**, *112* (4), 1048−1059.
(188) Würthner, F. Perylene Bisimide Dyes as Vversatile Building Blocks for Functional Supramolecular Architectures. *Chem. Commun.* **2004**, *40* (14), 1564−1579.
(189) De Schryver, F. C.; Vosch, T.; Cotlet, M.; Van der Auweraer, M.; Müllen, K.; Hofkens, J. Energy Dissipation in Multichromophoric Single Dendrimers. *Acc. Chem. Res.* **2005**, *38* (7), 514−522.
(190) Biju, V.; Micic, M.; Hu, D.; Lu, H. P. Intermittent Single-Molecule Interfacial Electron Transfer Dynamics. *J. Am. Chem. Soc.* **2004**, *126* (30), 9374−9381.

DOI: 10.1021/acs.chemrev.6b00673
Chem. Rev. XXXX, XXX, XXX−XXX

(191) Tachikawa, T.; Cui, S.-C.; Tojo, S.; Fujitsuka, M.; Majima, T. Nanoscopic Heterogeneities in Adsorption and Electron Transfer Processes of Perylene Diimide Dye on TiO_2 Nanoparticles Studied by Single-Molecule Fluorescence Spectroscopy. *Chem. Phys. Lett.* **2007**, *443* (4), 313−318.
(192) Wang, Y.; Wang, X.; Lu, H. P. Probing Single-Molecule Interfacial Geminate Electron−Cation Recombination Dynamics. *J. Am. Chem. Soc.* **2009**, *131* (25), 9020−9025.
(193) Guo, L.; Wang, Y.; Lu, H. P. Combined Single-Molecule Photon-Stamping Spectroscopy and Femtosecond Transient Absorption Spectroscopy Studies of Interfacial Electron Transfer Dynamics. *J. Am. Chem. Soc.* **2010**, *132* (6), 1999−2004.
(194) Tachikawa, T.; Cui, S.-C.; Fujitsuka, M.; Majima, T. Interfacial Electron Transfer Dynamics in Dye-Modified Graphene Oxide Nanosheets Studied by Single-Molecule Fluorescence Spectroscopy. *Phys. Chem. Chem. Phys.* **2012**, *14* (12), 4244−4249.
(195) Wang, Y.; Wang, X.; Ghosh, S. K.; Lu, H. P. Probing Single-Molecule Interfacial Electron Transfer Dynamics of Porphyrin on TiO_2 Nanoparticles. *J. Am. Chem. Soc.* **2009**, *131* (4), 1479−1487.
(196) Kim, W.; Tachikawa, T.; Moon, G.-h.; Majima, T.; Choi, W. Molecular-Level Understanding of the Photocatalytic Activity Difference between Anatase and Rutile Nanoparticles. *Angew. Chem.* **2014**, *126* (51), 14260−14265.
(197) Tachikawa, T.; Majima, T. Photocatalytic Oxidation Surfaces on Anatase TiO_2 Crystals Revealed by Single-Particle Chemiluminescence Imaging. *Chem. Commun.* **2012**, *48* (27), 3300−3302.
(198) Tachikawa, T.; Yamashita, S.; Majima, T. Probing Photocatalytic Active Sites on a Single Titanosilicate Zeolite with a Redox-Responsive Fluorescent Dye. *Angew. Chem., Int. Ed.* **2010**, *49* (2), 432−435.
(199) Tachikawa, T.; Zhang, P.; Bian, Z.; Majima, T. Efficient Charge Separation and Photooxidation on Cobalt Phosphate-Loaded TiO_2 Mesocrystal Superstructures. *J. Mater. Chem. A* **2014**, *2* (10), 3381−3388.
(200) Tachikawa, T.; Majima, T. Exploring the Spatial Distribution and Transport Behavior of Charge Carriers in a Single Titania Nanowire. *J. Am. Chem. Soc.* **2009**, *131* (24), 8485−8495.
(201) Xu, W.; Jain, P. K.; Beberwyck, B. J.; Alivisatos, A. P. Probing Redox Photocatalysis of Trapped Electrons and Holes on Single Sb-Doped Titania Nanorod Surfaces. *J. Am. Chem. Soc.* **2012**, *134* (9), 3946−3949.
(202) Wang, N.; Tachikawa, T.; Majima, T. Single-Molecule, Single-Particle Observation of Size-Dependent Photocatalytic Activity in Au/TiO_2 Nanocomposites. *Chem. Sci.* **2011**, *2* (5), 891−900.
(203) Tachikawa, T.; Wang, N.; Yamashita, S.; Cui, S.-C.; Majima, T. Design of a Highly Sensitive Fluorescent Probe for Interfacial Electron Transfer on a TiO_2 Surface. *Angew. Chem., Int. Ed.* **2010**, *49* (46), 8593−8597.
(204) Lu, H. P.; Xun, L.; Xie, X. S. Single-Molecule Enzymatic Dynamics. *Science* **1998**, *282* (5395), 1877−1882.
(205) Tachikawa, T.; Yamashita, S.; Majima, T. Evidence for Crystal-Face-Dependent TiO_2 Photocatalysis from Single-Molecule Imaging and Kinetic Analysis. *J. Am. Chem. Soc.* **2011**, *133* (18), 7197−7204.
(206) Gomes Silva, C.; Juárez, R.; Marino, T.; Molinari, R.; García, H. Influence of Excitation Wavelength (UV or Visible Light) on the Photocatalytic Activity of Titania Containing Gold Nanoparticles for the Generation of Hydrogen or Oxygen from Water. *J. Am. Chem. Soc.* **2011**, *133* (3), 595−602.
(207) Tian, Y.; Tatsuma, T. Mechanisms and Applications of Plasmon-Induced Charge Separation at TiO_2 Films Loaded with Gold Nanoparticles. *J. Am. Chem. Soc.* **2005**, *127* (20), 7632−7637.
(208) Tanaka, A.; Sakaguchi, S.; Hashimoto, K.; Kominami, H. Preparation of Au/TiO_2 Exhibiting Strong Surface Plasmon Resonance Effective for Photoinduced Hydrogen Formation from Organic and Inorganic Compounds under Irradiation of Visible Light. *Catal. Sci. Technol.* **2012**, *2* (5), 907−909.
(209) Kowalska, E.; Abe, R.; Ohtani, B. Visible Light-Induced Photocatalytic Reaction of Gold-Modified Titanium(Iv) Oxide Particles: Action Spectrum Analysis. *Chem. Commun.* **2009**, *45* (2), 241−243.
(210) Kowalska, E.; Mahaney, O. O. P.; Abe, R.; Ohtani, B. Visible-Light-Induced Photocatalysis through Surface Plasmon Excitation of Gold on Titania Surfaces. *Phys. Chem. Chem. Phys.* **2010**, *12* (10), 2344−2355.
(211) Tachikawa, T.; Yonezawa, T.; Majima, T. Super-Resolution Mapping of Reactive Sites on Titania-Based Nanoparticles with Water-Soluble Fluorogenic Probes. *ACS Nano* **2013**, *7* (1), 263−275.
(212) Bao, N.; Shen, L.; Takata, T.; Lu, D.; Domen, K. Highly Ordered Pt-Loaded Cds Nanowire Arrays for Photocatalytic Hydrogen Production under Visible Light. *Chem. Lett.* **2006**, *35* (3), 318−319.
(213) Amirav, L.; Alivisatos, A. P. Photocatalytic Hydrogen Production with Tunable Nanorod Heterostructures. *J. Phys. Chem. Lett.* **2010**, *1* (7), 1051−1054.
(214) Ruberu, T. P. A.; Nelson, N. C.; Slowing, I. I.; Vela, J. Selective Alcohol Dehydrogenation and Hydrogenolysis with Semiconductor-Metal Photocatalysts: Toward Solar-to-Chemical Energy Conversion of Biomass-Relevant Substrates. *J. Phys. Chem. Lett.* **2012**, *3* (19), 2798−2802.
(215) Berr, M.; Vaneski, A.; Susha, A. S.; Rodríguez-Fernández, J.; Döblinger, M.; Jäckel, F.; Rogach, A. L.; Feldmann, J. Colloidal Cds Nanorods Decorated with Subnanometer Sized Pt Clusters for Photocatalytic Hydrogen Generation. *Appl. Phys. Lett.* **2010**, *97* (9), 093108.
(216) Menagen, G.; Macdonald, J. E.; Shemesh, Y.; Popov, I.; Banin, U. Au Growth on Semiconductor Nanorods: Photoinduced Versus Thermal Growth Mechanisms. *J. Am. Chem. Soc.* **2009**, *131* (47), 17406−17411.
(217) Murdoch, M.; Waterhouse, G. I. N.; Nadeem, M. A.; Metson, J. B.; Keane, M. A.; Howe, R. F.; Llorca, J.; Idriss, H. The Effect of Gold Loading and Particle Size on Photocatalytic Hydrogen Production from Ethanol over Au/TiO_2 Nanoparticles. *Nat. Chem.* **2011**, *3* (6), 489−492.
(218) Du, L.; Furube, A.; Hara, K.; Katoh, R.; Tachiya, M. Ultrafast Plasmon Induced Electron Injection Mechanism in Gold−TiO_2 Nanoparticle System. *J. Photochem. Photobiol., C* **2013**, *15*, 21−30.
(219) Zhang, Z.; Yates, J. T. Band Bending in Semiconductors: Chemical and Physical Consequences at Surfaces and Interfaces. *Chem. Rev.* **2012**, *112* (10), 5520−5551.
(220) Mukherjee, S.; Libisch, F.; Large, N.; Neumann, O.; Brown, L. V.; Cheng, J.; Lassiter, J. B.; Carter, E. A.; Nordlander, P.; Halas, N. J. Hot Electrons Do the Impossible: Plasmon-Induced Dissociation of H2 on Au. *Nano Lett.* **2013**, *13* (1), 240−247.
(221) Moskovits, M. Hot Electrons Cross Boundaries. *Science* **2011**, *332* (6030), 676−677.
(222) Lee, J.; Mubeen, S.; Ji, X.; Stucky, G. D.; Moskovits, M. Plasmonic Photoanodes for Solar Water Splitting with Visible Light. *Nano Lett.* **2012**, *12* (9), 5014−5019.
(223) Cho, I. S.; Chen, Z.; Forman, A. J.; Kim, D. R.; Rao, P. M.; Jaramillo, T. F.; Zheng, X. Branched TiO_2 Nanorods for Photoelectrochemical Hydrogen Production. *Nano Lett.* **2011**, *11* (11), 4978−4984.
(224) Ha, J. W.; Ruberu, T. P. A.; Han, R.; Dong, B.; Vela, J.; Fang, N. Super-Resolution Mapping of Photogenerated Electron and Hole Separation in Single Metal−Semiconductor Nanocatalysts. *J. Am. Chem. Soc.* **2014**, *136* (4), 1398−1408.
(225) Chih, T.; Jao, H.-J.; Wang, C. M. Glucose Sensing Based on an Effective Conversion of O_2 and H_2o_2 into Superoxide Anion Radical with Clay Minerals. *J. Electroanal. Chem.* **2005**, *581* (2), 159−166.
(226) Gorris, H. H.; Walt, D. R. Mechanistic Aspects of Horseradish Peroxidase Elucidated through Single-Molecule Studies. *J. Am. Chem. Soc.* **2009**, *131* (17), 6277−6282.
(227) Sambur, J. B.; Chen, T.-Y.; Choudhary, E.; Chen, G.; Nissen, E. J.; Thomas, E. M.; Zou, N.; Chen, P. Sub-Particle Reaction and Photocurrent Mapping to Optimize Catalyst-Modified Photoanodes. *Nature* **2016**, *530* (7588), 77−80.
(228) Walter, M. G.; Warren, E. L.; McKone, J. R.; Boettcher, S. W.; Mi, Q.; Santori, E. A.; Lewis, N. S. Solar Water Splitting Cells. *Chem. Rev.* **2010**, *110* (11), 6446−6473.
(229) Fujishima, A.; Honda, K. Electrochemical Photolysis of Water at a Semiconductor Electrode. *Nature* **1972**, *238* (5358), 37−38.

DOI: 10.1021/acs.chemrev.6b00673
Chem. Rev. XXXX, XXX, XXX−XXX

(230) Yang, J.; Wang, D.; Han, H.; Li, C. Roles of Cocatalysts in Photocatalysis and Photoelectrocatalysis. *Acc. Chem. Res.* **2013**, *46* (8), 1900−1909.
(231) Carroll, G. M.; Zhong, D. K.; Gamelin, D. R. Mechanistic Insights into Solar Water Oxidation by Cobalt-Phosphate-Modified [Small Alpha]-Fe_2o_3 Photoanodes. *Energy Environ. Sci.* **2015**, *8* (2), 577−584.
(232) Wilson, R. H. A Model for the Current-Voltage Curve of Photoexcited Semiconductor Electrodes. *J. Appl. Phys.* **1977**, *48* (10), 4292−4297.
(233) Sambur, J. B.; Chen, P. Distinguishing Direct and Indirect Photoelectrocatalytic Oxidation Mechanisms Using Quantitative Single-Molecule Reaction Imaging and Photocurrent Measurements. *J. Phys. Chem. C* **2016**, *120* (37), 20668−20676.
(234) Bard, A. J.; Fan, F.-R. F. Electrochemical Detection of Single Molecules. *Acc. Chem. Res.* **1996**, *29* (12), 572−578.
(235) Mathwig, K.; Aartsma, T. J.; Canters, G. W.; Lemay, S. G. Nanoscale Methods for Single-Molecule Electrochemistry. *Annu. Rev. Anal. Chem.* **2014**, *7* (1), 383−404.
(236) Bard, A. J. Toward Single Enzyme Molecule Electrochemistry. *ACS Nano* **2008**, *2* (12), 2437−2440.
(237) Zhou, Y.-G.; Rees, N. V.; Compton, R. G. The Electrochemical Detection and Characterization of Silver Nanoparticles in Aqueous Solution. *Angew. Chem., Int. Ed.* **2011**, *50* (18), 4219−4221.
(238) Capozzi, B.; Chen, Q.; Darancet, P.; Kotiuga, M.; Buzzeo, M.; Neaton, J. B.; Nuckolls, C.; Venkataraman, L. Tunable Charge Transport in Single-Molecule Junctions via Electrolytic Gating. *Nano Lett.* **2014**, *14* (3), 1400−1404.
(239) Yu, Y.; Sun, T.; Mirkin, M. V. Scanning Electrochemical Microscopy of Single Spherical Nanoparticles: Theory and Particle Size Evaluation. *Anal. Chem.* **2015**, *87* (14), 7446−7453.
(240) Palacios, R. E.; Fan, F.-R. F.; Bard, A. J.; Barbara, P. F. Single-Molecule Spectroelectrochemistry (Sms-Ec). *J. Am. Chem. Soc.* **2006**, *128* (28), 9028−9029.
(241) Chang, Y.-L.; Palacios, R. E.; Fan, F.-R. F.; Bard, A. J.; Barbara, P. F. Electrogenerated Chemiluminescence of Single Conjugated Polymer Nanoparticles. *J. Am. Chem. Soc.* **2008**, *130* (28), 8906−8907.
(242) Palacios, R. E.; Fan, F.-R. F.; Grey, J. K.; Suk, J.; Bard, A. J.; Barbara, P. F. Charging and Discharging of Single Conjugated-Polymer Nanoparticles. *Nat. Mater.* **2007**, *6* (9), 680−685.
(243) Chirea, M.; Collins, S. S. E.; Wei, X.; Mulvaney, P. Spectroelectrochemistry of Silver Deposition on Single Gold Nanocrystals. *J. Phys. Chem. Lett.* **2014**, *5* (24), 4331−4335.
(244) Hill, C. M.; Pan, S. A Dark-Field Scattering Spectroelectrochemical Technique for Tracking the Electrodeposition of Single Silver Nanoparticles. *J. Am. Chem. Soc.* **2013**, *135* (46), 17250−17253.
(245) Liu, J.; Hill, C. M.; Pan, S.; Liu, H. Interfacial Charge Transfer Events of Bodipy Molecules: Single Molecule Spectroelectrochemistry and Substrate Effects. *Phys. Chem. Chem. Phys.* **2014**, *16* (42), 23150−23156.
(246) Lei, C.; Hu, D.; Ackerman, E. J. Single-Molecule Fluorescence Spectroelectrochemistry of Cresyl Violet. *Chem. Commun.* **2008**, *44* (43), 5490−5492.
(247) Lei, C.; Hu, D.; Ackerman, E. Clay Nanoparticle-Supported Single-Molecule Fluorescence Spectroelectrochemistry. *Nano Lett.* **2009**, *9* (2), 655−658.
(248) Xu, W.; Shen, H.; Kim, Y. J.; Zhou, X.; Liu, G.; Park, J.; Chen, P. Single-Molecule Electrocatalysis by Single-Walled Carbon Nanotubes. *Nano Lett.* **2009**, *9* (12), 3968−3973.
(249) Zhang, Y.; Song, P.; Fu, Q.; Ruan, M.; Xu, W. Single-Molecule Chemical Reaction Reveals Molecular Reaction Kinetics and Dynamics. *Nat. Commun.* **2014**, *5*, 4238.
(250) Rybina, A.; Thaler, B.; Krämer, R.; Herten, D.-P. Monitoring Hydroquinone−Quinone Redox Cycling by Single Molecule Fluorescence Spectroscopy. *Phys. Chem. Chem. Phys.* **2014**, *16* (36), 19550−19555.
(251) Ameloot, R.; Roeffaers, M.; Baruah, M.; De Cremer, G.; Sels, B.; De Vos, D.; Hofkens, J. Towards Direct Monitoring of Discrete Events in a Catalytic Cycle at the Single Molecule Level. *Photochem. Photobiol. Sci.* **2009**, *8* (4), 453−456.
(252) Routzahn, A. L.; Jain, P. K. Single-Nanocrystal Reaction Trajectories Reveal Sharp Cooperative Transitions. *Nano Lett.* **2014**, *14* (2), 987−992.
(253) Smith, J. G.; Yang, Q.; Jain, P. K. Identification of a Critical Intermediate in Galvanic Exchange Reactions by Single-Nanoparticle-Resolved Kinetics. *Angew. Chem., Int. Ed.* **2014**, *53*, 2867−2872.
(254) Rybina, A.; Lang, C.; Wirtz, M.; Grußmayer, K.; Kurz, A.; Maier, F.; Schmitt, A.; Trapp, O.; Jung, G.; Herten, D.-P. Distinguishing Alternative Reaction Pathways by Single-Molecule Fluorescence Spectroscopy. *Angew. Chem., Int. Ed.* **2013**, *52* (24), 6322−6325.
(255) Oneil, C. E.; Jackson, J. M.; Shim, S.-H.; Soper, S. A. Interrogating Surface Functional Group Heterogeneity of Activated Thermoplastics Using Super-Resolution Fluorescence Microscopy. *Anal. Chem.* **2016**, *88* (7), 3686−3696.
(256) Esfandiari, N. M.; Wang, Y.; McIntire, T. M.; Blum, S. A. Real-Time Imaging of Platinum−Sulfur Ligand Exchange Reactions at the Single-Molecule Level via a General Chemical Technique. *Organometallics* **2011**, *30* (11), 2901−2907.
(257) Canham, S. M.; Bass, J. Y.; Navarro, O.; Lim, S.-G.; Das, N.; Blum, S. A. Toward the Single-Molecule Investigation of Organometallic Reaction Mechanisms: Single-Molecule Imaging of Fluorophore-Tagged Palladium(Ii) Complexes. *Organometallics* **2008**, *27* (10), 2172−2175.
(258) Esfandiari, N. M.; Wang, Y.; Bass, J. Y.; Cornell, T. P.; Otte, D. A. L.; Cheng, M. H.; Hemminger, J. C.; McIntire, T. M.; Mandelshtam, V. A.; Blum, S. A. Single-Molecule Imaging of Platinum Ligand Exchange Reaction Reveals Reactivity Distribution. *J. Am. Chem. Soc.* **2010**, *132* (43), 15167−15169.
(259) Tachikawa, T.; Ohsaka, T.; Bian, Z.; Majima, T. Single-Molecule Fluorescence Detection of Effective Adsorption Sites at the Metal Oxide−Solution Interface. *J. Phys. Chem. C* **2013**, *117* (21), 11219−11228.
(260) Cognet, L.; Tsyboulski, D. A.; Rocha, J.-D. R.; Doyle, C. D.; Tour, J. M.; Weisman, R. B. Stepwise Quenching of Exciton Fluorescence in Carbon Nanotubes by Single-Molecule Reactions. *Science* **2007**, *316* (5830), 1465−1468.
(261) Siitonen, A. J.; Tsyboulski, D. A.; Bachilo, S. M.; Weisman, R. B. Surfactant-Dependent Exciton Mobility in Single-Walled Carbon Nanotubes Studied by Single-Molecule Reactions. *Nano Lett.* **2010**, *10* (5), 1595−1599.
(262) Kazoe, Y.; Sato, Y. Measurement of Zeta-Potential at Microchannel Wall by a Nanoscale Laser Induced Fluorescence Imaging. *J. Fluid Sci. Technol.* **2007**, *2* (2), 429−440.
(263) Kazoe, Y.; Mawatari, K.; Sugii, Y.; Kitamori, T. Development of a Measurement Technique for Ion Distribution in an Extended Nanochannel by Super-Resolution-Laser-Induced Fluorescence. *Anal. Chem.* **2011**, *83* (21), 8152−8157.
(264) Kazoe, Y.; Sato, Y. Effect of Ion Motion on Zeta-Potential Distribution at Microchannel Wall Obtained from Nanoscale Laser-Induced Fluorescence. *Anal. Chem.* **2007**, *79* (17), 6727−6733.
(265) Yin; Liebscher, J. Carbon−Carbon Coupling Reactions Catalyzed by Heterogeneous Palladium Catalysts. *Chem. Rev.* **2007**, *107* (1), 133−173.
(266) Blümel, J. Linkers and Catalysts Immobilized on Oxide Supports: New Insights by Solid-State Nmr Spectroscopy. *Coord. Chem. Rev.* **2008**, *252* (21−22), 2410−2423.
(267) Howarter, J. A.; Youngblood, J. P. Optimization of Silica Silanization by 3-Aminopropyltriethoxysilane. *Langmuir* **2006**, *22* (26), 11142−11147.
(268) Nunes, P. S.; Ohlsson, P. D.; Ordeig, O.; Kutter, J. P. Cyclic Olefin Polymers: Emerging Materials for Lab-on-a-Chip Applications. *Microfluid. Nanofluid.* **2010**, *9* (2), 145−161.
(269) Soper, S. A.; Ford, S. M.; Qi, S.; McCarley, R. L.; Kelly, K.; Murphy, M. C. Peer Reviewed: Polymeric Microelectromechanical Systems. *Anal. Chem.* **2000**, *72* (19), 642 A−651A.

DOI: 10.1021/acs.chemrev.6b00673
Chem. Rev. XXXX, XXX, XXX−XXX

(270) Liang, X.; Chou, S. Y. Nanogap Detector inside Nanofluidic Channel for Fast Real-Time Label-Free DNA Analysis. *Nano Lett.* **2008**, *8* (5), 1472−1476.
(271) Uba, F. I.; Pullagurla, S. R.; Sirasunthorn, N.; Wu, J.; Park, S.; Chantiwas, R.; Cho, Y.-K.; Shin, H.; Soper, S. A. Surface Charge, Electroosmotic Flow and DNA Extension in Chemically Modified Thermoplastic Nanoslits and Nanochannels. *Analyst* **2015**, *140* (1), 113−126.
(272) Chan, C. M.; Ko, T. M.; Hiraoka, H. Polymer Surface Modification by Plasmas and Photons. *Surf. Sci. Rep.* **1996**, *24* (1−2), 1−54.
(273) Jackson, J. M.; Witek, M. A.; Hupert, M. L.; Brady, C.; Pullagurla, S.; Kamande, J.; Aufforth, R. D.; Tignanelli, C. J.; Torphy, R. J.; Yeh, J. J.; et al. UV Activation of Polymeric High Aspect Ratio Microstructures: Ramifications in Antibody Surface Loading for Circulating Tumor Cell Selection. *Lab Chip* **2014**, *14* (1), 106−117.
(274) Chang, C.-C.; Kazoe, Y.; Morikawa, K.; Mawatari, K.; Yang, R.-J.; Kitamori, T. Numerical Simulation of Proton Distribution with Electric Double Layer in Extended Nanospaces. *Anal. Chem.* **2013**, *85* (9), 4468−4474.
(275) Tsukahara, T.; Mawatari, K.; Kitamori, T. Integrated Extended-Nano Chemical Systems on a Chip. *Chem. Soc. Rev.* **2010**, *39* (3), 1000−1013.
(276) Ren, C. L.; Li, D. Electroviscous Effects on Pressure-Driven Flow of Dilute Electrolyte Solutions in Small Microchannels. *J. Colloid Interface Sci.* **2004**, *274* (1), 319−330.
(277) Scales, P. J.; Grieser, F.; Healy, T. W.; White, L. R.; Chan, D. Y. C. Electrokinetics of the Silica-Solution Interface: A Flat Plate Streaming Potential Study. *Langmuir* **1992**, *8* (3), 965−974.
(278) Pennathur, S.; Santiago, J. G. Electrokinetic Transport in Nanochannels. 1. Theory. *Anal. Chem.* **2005**, *77* (21), 6772−6781.
(279) Pennathur, S.; Santiago, J. G. Electrokinetic Transport in Nanochannels. 2. Experiments. *Anal. Chem.* **2005**, *77*, 6782−6789.
(280) Thomsson, D.; Sforazzini, G.; Anderson, H. L.; Scheblykin, I. G. Excitation Polarization Provides Structural Resolution of Individual Non-Blinking Nano-Objects. *Nanoscale* **2013**, *5* (7), 3070−3077.
(281) Park, H.; Hoang, D. T.; Paeng, K.; Kaufman, L. J. Localizing Exciton Recombination Sites in Conformationally Distinct Single Conjugated Polymers by Super-Resolution Fluorescence Imaging. *ACS Nano* **2015**, *9* (3), 3151−3158.
(282) Habuchi, S.; Onda, S.; Vacha, M. Mapping the Emitting Sites within a Single Conjugated Polymer Molecule. *Chem. Commun.* **2009**, *45* (32), 4868−4870.
(283) Bolinger, J. C.; Traub, M. C.; Brazard, J.; Adachi, T.; Barbara, P. F.; Vanden Bout, D. A. Conformation and Energy Transfer in Single Conjugated Polymers. *Acc. Chem. Res.* **2012**, *45* (11), 1992−2001.
(284) Habuchi, S.; Onda, S.; Vacha, M. Molecular Weight Dependence of Emission Intensity and Emitting Sites Distribution within Single Conjugated Polymer Molecules. *Phys. Chem. Chem. Phys.* **2011**, *13* (5), 1743−1753.
(285) Merdasa, A.; Jiménez, Á. J.; Camacho, R.; Meyer, M.; Würthner, F.; Scheblykin, I. G. Single Lévy States−Disorder Induced Energy Funnels in Molecular Aggregates. *Nano Lett.* **2014**, *14* (12), 6774−6781.
(286) Tian, Y.; Merdasa, A.; Peter, M.; Abdellah, M.; Zheng, K.; Ponseca, C. S., Jr.; Pullerits, T.; Yartsev, A.; Sundstrom, V.; Scheblykin, I. G. Giant Photoluminescence Blinking of Perovskite Nanocrystals Reveals Single-Trap Control of Luminescence. *Nano Lett.* **2015**, *15* (3), 1603−1608.
(287) Aloi, A.; Vargas Jentzsch, A.; Vilanova, N.; Albertazzi, L.; Meijer, E. W.; Voets, I. K. Imaging Nanostructures by Single-Molecule Localization Microscopy in Organic Solvents. *J. Am. Chem. Soc.* **2016**, *138* (9), 2953−2956.
(288) Harke, B.; Ullal, C. K.; Keller, J.; Hell, S. W. Three-Dimensional Nanoscopy of Colloidal Crystals. *Nano Lett.* **2008**, *8* (5), 1309−1313.
(289) Friedemann, K.; Turshatov, A.; Landfester, K.; Crespy, D. Characterization via Two-Color Sted Microscopy of Nanostructured Materials Synthesized by Colloid Electrospinning. *Langmuir* **2011**, *27* (11), 7132−7139.
(290) Kisley, L.; Brunetti, R.; Tauzin, L. J.; Shuang, B.; Yi, X.; Kirkeminde, A. W.; Higgins, D. A.; Weiss, S.; Landes, C. F. Characterization of Porous Materials by Fluorescence Correlation Spectroscopy Super-Resolution Optical Fluctuation Imaging. *ACS Nano* **2015**, *9* (9), 9158−9166.
(291) Hellriegel, C.; Kirstein, J.; Bräuchle, C.; Latour, V.; Pigot, T.; Olivier, R.; Lacombe, S.; Brown, R.; Guieu, V.; Payrastre, C.; et al. Diffusion of Single Streptocyanine Molecules in the Nanoporous Network of Sol−Gel Glasses. *J. Phys. Chem. B* **2004**, *108* (38), 14699−14709.
(292) Kirstein, J.; Platschek, B.; Jung, C.; Brown, R.; Bein, T.; Brauchle, C. Exploration of Nanostructured Channel Systems with Single-Molecule Probes. *Nat. Mater.* **2007**, *6* (4), 303−310.
(293) Zurner, A.; Kirstein, J.; Doblinger, M.; Brauchle, C.; Bein, T. Visualizing Single-Molecule Siffusion in Mesoporous Materials. *Nature* **2007**, *450* (7170), 705−708.
(294) Michaelis, J.; Brauchle, C. Reporters in the Nanoworld: Diffusion of Single Molecules in Mmesoporous Materials. *Chem. Soc. Rev.* **2010**, *39* (12), 4731−4740.
(295) Feil, F.; Jung, C.; Kirstein, J.; Michaelis, J.; Li, C.; Nolde, F.; Müllen, K.; Bräuchle, C. Diffusional and Orientational Dynamics of Various Single Terylene Diimide Conjugates in Mesoporous Materials. *Microporous Mesoporous Mater.* **2009**, *125* (1−2), 70−78.
(296) Jung, C.; Kirstein, J.; Platschek, B.; Bein, T.; Budde, M.; Frank, I.; Müllen, K.; Michaelis, J.; Bräuchle, C. Diffusion of Oriented Single Molecules with Switchable Mobility in Networks of Long Unidimensional Nanochannels. *J. Am. Chem. Soc.* **2008**, *130* (5), 1638−1648.
(297) Jung, C.; Hellriegel, C.; Platschek, B.; Wöhrle, D.; Bein, T.; Michaelis, J.; Bräuchle, C. Simultaneous Measurement of Orientational and Spectral Dynamics of Single Molecules in Nanostructured Host−Guest Materials. *J. Am. Chem. Soc.* **2007**, *129* (17), 5570−5579.
(298) Lebold, T.; Mühlstein, L. A.; Blechinger, J.; Riederer, M.; Amenitsch, H.; Köhn, R.; Peneva, K.; Müllen, K.; Michaelis, J.; Bräuchle, C.; et al. Tuning Single-Molecule Dynamics in Functionalized Mesoporous Silica. *Chem. - Eur. J.* **2009**, *15* (7), 1661−1672.
(299) Davies, M.; Rühle, B.; Li, C.; Müllen, K.; Bein, T.; Bräuchle, C. Insights into Nanoscale Electrophoresis of Single Dye Molecules in Highly Oriented Mesoporous Silica Channels. *J. Phys. Chem. C* **2014**, *118* (41), 24013−24024.
(300) Rühle, B.; Davies, M.; Lebold, T.; Bräuchle, C.; Bein, T. Highly Oriented Mesoporous Silica Channels Synthesized in Microgrooves and Visualized with Single-Molecule Diffusion. *ACS Nano* **2012**, *6* (3), 1948−1960.
(301) Feil, F.; Cauda, V.; Bein, T.; Bräuchle, C. Direct Visualization of Dye and Oligonucleotide Diffusion in Silica Filaments with Collinear Mesopores. *Nano Lett.* **2012**, *12* (3), 1354−1361.
(302) Kumarasinghe, R.; Higgins, E. D.; Ito, T.; Higgins, D. A. Spectroscopic and Polarization-Dependent Single-Molecule Tracking Reveal the One-Dimensional Diffusion Pathways in Surfactant-Templated Mesoporous Silica. *J. Phys. Chem. C* **2016**, *120* (1), 715−723.
(303) Giri, D.; Ashraf, K. M.; Collinson, M. M.; Higgins, D. A. Single-Molecule Perspective on Mass Transport in Condensed Water Layers over Gradient Self-Assembled Monolayers. *J. Phys. Chem. C* **2015**, *119* (17), 9418−9428.
(304) Robben, K. C.; Tran-Ba, K.-H.; Ito, T.; Higgins, D. A. Trajectory-Profile-Guided Single Molecule Tracking for Assignment of One-Dimensional Diffusion Trajectories. *Anal. Chem.* **2014**, *86* (21), 10820−10827.
(305) Higgins, D. A.; Tran-Ba, K.-H.; Ito, T. Following Single Molecules to a Better Understanding of Self-Assembled One-Dimensional Nanostructures. *J. Phys. Chem. Lett.* **2013**, *4* (18), 3095−3103.
(306) Jung, C.; Hellriegel, C.; Michaelis, J.; Bräuchle, C. Single-Molecule Traffic in Mesoporous Materials: Translational, Orientational, and Spectral Dynamics. *Adv. Mater.* **2007**, *19* (7), 956−960.
(307) Feil, F.; Naumov, S.; Michaelis, J.; Valiullin, R.; Enke, D.; Kärger, J.; Bräuchle, C. Single-Particle and Ensemble Diffusivities—Test of Ergodicity. *Angew. Chem., Int. Ed.* **2012**, *51* (5), 1152−1155.
(308) Higgins, D. A.; Park, S. C.; Tran-Ba, K.-H.; Ito, T. Single-Molecule Investigations of Morphology and Mass Transport Dynamics

DOI: 10.1021/acs.chemrev.6b00673
Chem. Rev. XXXX, XXX, XXX−XXX

in Nanostructured Materials. *Annu. Rev. Anal. Chem.* **2015**, *8* (1), 193−216.
(309) Wang, Y.; Fruhwirth, G.; Cai, E.; Ng, T.; Selvin, P. R. 3D Super-Resolution Imaging with Blinking Quantum Dots. *Nano Lett.* **2013**, *13* (11), 5233−5241.
(310) Lidke, K. A.; Rieger, B.; Jovin, T. M.; Heintzmann, R. Superresolution by Localization of Quantum Dots Using Blinking Statistics. *Opt. Express* **2005**, *13* (18), 7052−7062.
(311) Dedecker, P.; Muls, B.; Deres, A.; Uji-i, H.; Hotta, J.-i.; Sliwa, M.; Soumillion, J.-P.; Müllen, K.; Enderlein, J.; Hofkens, J. Defocused Wide-Field Imaging Unravels Structural and Temporal Heterogeneity in Complex Systems. *Adv. Mater.* **2009**, *21* (10−11), 1079−1090.
(312) Wöll, D.; Uji-i, H.; Schnitzler, T.; Hotta, J.-i.; Dedecker, P.; Herrmann, A.; De Schryver, F. C.; Müllen, K.; Hofkens, J. Radical Polymerization Tracked by Single Molecule Spectroscopy. *Angew. Chem., Int. Ed.* **2008**, *47* (4), 783−787.
(313) Woll, D.; Braeken, E.; Deres, A.; De Schryver, F. C.; Uji-i, H.; Hofkens, J. Polymers and Single Molecule Fluorescence Spectroscopy, What Can We Learn? *Chem. Soc. Rev.* **2009**, *38* (2), 313−328.
(314) Muls, B.; Uji-i, H.; Melnikov, S.; Moussa, A.; Verheijen, W.; Soumillion, J.-P.; Josemon, J.; Müllen, K.; Hofkens, J. Direct Measurement of the End-to-End Distance of Individual Polyfluorene Polymer Chains. *ChemPhysChem* **2005**, *6* (11), 2286−2294.
(315) Kulzer, F.; Xia, T.; Orrit, M. Single Molecules as Optical Nanoprobes for Soft and Complex Matter. *Angew. Chem., Int. Ed.* **2010**, *49* (5), 854−866.
(316) Albertazzi, L.; van der Zwaag, D.; Leenders, C. M. A.; Fitzner, R.; van der Hofstad, R. W.; Meijer, E. W. Probing Exchange Pathways in One-Dimensional Aggregates with Super-Resolution Microscopy. *Science* **2014**, *344* (6183), 491−495.
(317) Stöhr, R. J.; Kolesov, R.; Xia, K.; Reuter, R.; Meijer, J.; Logvenov, G.; Wrachtrup, J. Super-Resolution Fluorescence Quenching Microscopy of Graphene. *ACS Nano* **2012**, *6* (10), 9175−9181.
(318) Cang, H.; Labno, A.; Lu, C.; Yin, X.; Liu, M.; Gladden, C.; Liu, Y.; Zhang, X. Probing the Electromagnetic Field of a 15-Nanometre Hotspot by Single Molecule Imaging. *Nature* **2011**, *469* (7330), 385−388.
(319) Su, L.; Lu, G.; Kenens, B.; Rocha, S.; Fron, E.; Yuan, H.; Chen, C.; Van Dorpe, P.; Roeffaers, M. B. J.; Mizuno, H. Visualization of Molecular Fluorescence Point Spread Functions via Remote Excitation Switching Fluorescence Microscopy. *Nat. Commun.* **2015**, *6*, 6287.
(320) Wertz, E.; Isaacoff, B. P.; Flynn, J. D.; Biteen, J. S. Single-Molecule Super-Resolution Microscopy Reveals How Light Couples to a Plasmonic Nanoantenna on the Nanometer Scale. *Nano Lett.* **2015**, *15* (4), 2662−2670.
(321) Simoncelli, S.; Roberti, M. J.; Araoz, B.; Bossi, M. L.; Aramendía, P. F. Mapping the Fluorescence Performance of a Photochromic−Fluorescent System Coupled with Gold Nanoparticles at the Single Molecule−Single Particle Level. *J. Am. Chem. Soc.* **2014**, *136* (19), 6878−6880.
(322) Khatua, S.; Orrit, M. Probing, Sensing, and Fluorescence Enhancement with Single Gold Nanorods. *J. Phys. Chem. Lett.* **2014**, *5* (17), 3000−3006.
(323) Blythe, K. L.; Titus, E. J.; Willets, K. A. Comparing the Accuracy of Reconstructed Image Size in Super-Resolution Imaging of Fluorophore-Labeled Gold Nanorods Using Different Fit Models. *J. Phys. Chem. C* **2015**, *119* (33), 19333−19343.
(324) Lin, H.; Centeno, S. P.; Su, L.; Kenens, B.; Rocha, S.; Sliwa, M.; Hofkens, J.; Uji-i, H. Mapping of Surface-Enhanced Fluorescence on Metal Nanoparticles Using Super-Resolution Photoactivation Localization Microscopy. *ChemPhysChem* **2012**, *13* (4), 973−981.
(325) Blythe, K. L.; Titus, E. J.; Willets, K. A. Triplet-State-Mediated Super-Resolution Imaging of Fluorophore-Labeled Gold Nanorods. *ChemPhysChem* **2014**, *15* (4), 784−793.
(326) Yuan, H.; Khatua, S.; Zijlstra, P.; Yorulmaz, M.; Orrit, M. Thousand-Fold Enhancement of Single-Molecule Fluorescence near a Single Gold Nanorod. *Angew. Chem., Int. Ed.* **2013**, *52* (4), 1217−1221.
(327) Su, L.; Yuan, H.; Lu, G.; Rocha, S.; Orrit, M.; Hofkens, J.; Uji-i, H. Super-Resolution Localization and Defocused Fluorescence Microscopy on Resonantly Coupled Single-Molecule, Single-Nanorod Hybrids. *ACS Nano* **2016**, *10* (2), 2455−2466.
(328) Weber, M. L.; Litz, J. P.; Masiello, D. J.; Willets, K. A. Super-Resolution Imaging Reveals a Difference between Sers and Luminescence Centroids. *ACS Nano* **2012**, *6* (2), 1839−1848.
(329) Feng, C.; Cunningham, D. W.; Easter, Q. T.; Blum, S. A. Role of Licl in Generating Soluble Organozinc Reagents. *J. Am. Chem. Soc.* **2016**, *138* (35), 11156−11159.

DOI: 10.1021/acs.chemrev.6b00673
Chem. Rev. XXXX, XXX, XXX−XXX